

https://dspace.org/

Geophysical characterisation of orthomagmatic nickel-copper sulphide satellites around Madziwa Mine, Zimbabwe

Cranswick, Russell Vos

2025-10

University of the Witwatersrand, Johannesburg

https://hdl.handle.net/10539/50204

Cranswick, Russell Vos. (2025). Geophysical characterisation of orthomagmatic nickel-copper sulphide satellites around Madziwa Mine, Zimbabwe. [Master's dissertation, University of the Witwatersrand, Johannesburg]. WIReDSpace.

Downloaded from a DSpace repository. https://dspace.org/



Geophysical characterisation of orthomagmatic nickel-copper sulphide satellites around Madziwa Mine, Zimbabwe

By

Russell Cranswick
682429

Research Report
Submitted in partial fulfillment of the requirements for the degree
Master of Science
in
Economic Geology
in the Faculty of Science, University of the Witwatersrand, Johannesburg, South Africa

Supervisor: Dr Stephanie Sheiber

October2025

DECLARATION

I declare that this research report is my own, unaided work. It is being submitted for the Degree of Master of Science at the University of the Witwatersrand, Johannesburg. It has not been submitted before for any degree or examination at any other University.



_____

(Signature of candidate)

31st day of October 2025 at Port Alfred, South Africa

Acknowledgements

This Research Report was made possible by the ground geophysical surveys sponsored and executed by Associated African Nickel Resources PLC as part of the exploration programme at their Madziwa tenements in Zimbabwe. AANR is acknowledged and thanked for its resources and support.

I also express my gratitude to Mr Mhaka Ushendibaba for his contribution in the design, oversight and evaluation of the ground geophysical surveys at Madziwa, and for his guidance in data handling and processing.

Dr Martin Prendergast's work and contribution to the understanding of Madziwa's geology is also acknowledged. Extensive use has been made of his mapping, reporting and insights into the ore forming processes at Madziwa.

The University of the Witwatersrand is thanked for the use of their MPP-E2S multi parameter probe.

Finally, thanks are owed to Dr Stephanie Sheiber for her freely available series of educational videos on YouTube dealing with geophysical data processing, manipulation and presentation on Geosoft's Oasis Montaj software, as well as her guidance and input as Supervisor in the writing of this Research Report.

Table of Contents

1. Introduction: Madziwa and the application of geophysical methods to renewed exploration 1
2. The geology and exploration history of the Madziwa Igneous Complex 3
3. Methods and measurements 6
   - 3.1 Physical Property measurements on drill core from Madziwa 6
   - 3.2 Canadian International Development Agency Airborne Magnetic Survey 6
   - 3.3 Ground Magnetic Survey 9
   - 3.4 Moving Loop Ground Electromagnetic Survey 12
4. Results 13
   - 4.1 Physical Property Measurements – Magnetic Susceptibility and Conductivity 13
   - 4.2 Ground magnetic survey results 16
   - 4.3 Magnetic Profile Lines 20
   - 4.4 Moving Loop EM Results 24
5. Discussion and interpretation 34
6. Conclusion 42
7. Bibliography 43

List Of Figures

Figure 1: Stidolph, P. A., 1978. Reproduced from 1:100 000 Geological Map of Rhodesia Geological Survey Bulletin No. 78, The Geology of the Country around Shamva. 4

Figure 2: Simplified geology map of the Madziwa Complex with Aeromagnetic Contours; A=Amms, E=Ely, SH=Sulphide Hill, Th=Thyrza, Ph=Phoebus, SD=Slimes Dam, Sf=Sulphide Fault. Reproduced from Prendergast and Wilson (2015) 5

Figure 3: Hypothesized structural model for the Madziwa Igneous Complex. Diagrammatic and not to scale. The interpreted structural relationships of the principal rock types, and of the two main lower dike and upper lopolithic components, are depicted in section, together with the apparent north-south lithological zonation of the Madziwa Igneous Complex observed at present erosion levels. The structure shown in the central inset is modelled on that seen at Phoebus (Prendergast and Wilson, 2015). 7

Figure 4: Geology of the Ely prospect area at Madziwa (Stidolph, 1977). 8

Figure 5: Soil geochemical anomalies and sample lines in (a) mapped by Anglo-American around the Ely prospect for nickel in soil; (b) shows the 1:1000 map of adjacent E1/E2 and E3/E4 anomalies along with diamond drilling significant intersections; (c) shows the 1:1000 map of E5 anomaly with the yellow zone representing >3000ppm Ni, as well as trenches and diamond drilling with significant intersections; and (d) shows the 1:1000 Anglo-American maps georeferenced on the B78 geology map after field locating the drill collars. 3

Figure 6: (a) Prospecting Ventures simplified and annotated geology of the Ely area overlaid on the B78 geology map; (b) the same simplified geology plan with black square showing location of zoomed in plan of E5 area in (c); (c) plan view of the E5 prospect at Ely and (d) section view of the E5 prospect and mineralised zone based on the drilling completed there in the 1960s and 1990s (Prendergast and Wilson, 2015). 5

Figure 7: MPP-EM2S Multi Parameter Probe used for physical property measurements of drill core samples collected from Madziwa (GDD Instruments website, 2024). 6

Figure 8: Details of the Canadian International Development Agency sponsored airborne magnetic survey flown over Zimbabwe in the early 1980s, as published in the 1731 B1 Aeromagnetic Map of Bushu, obtained from the Zimbabwe Geological Survey in Harare. 7

Figure 9: CIDA aeromag TMI for whole 1731 B1 Survey Block (a) ; (b) CIDA aeromag TMI plotted over the magnetic contours as published in the 1731 B1 hard copy map from the Zimbabwe Geological Survey; (c) CIDA aeromag TMI plotted over the Bulletin 78 Geology Map for the Madziwa area. 9

Figure 10: (a) ground magnetic data collection at Ely in 2021; (b) GEM Systems GSM-19 Overhauser Magnetometer used as the rover for data collection. 10

Figure 11: (a) spatial extent of the Ely ground magnetic grid over B78 geology with GPS track recorded walklines over B78 geology; and (b) the walklines over geology as mapped by Prospecting Ventures at Ely. 11

Figure 12: Spatial extent and position of the ground Moving Loop EM survey carried out in 2022 at Ely, relative to the B78 geology. 12

Figure 13: (a) gneiss; (b) norite; (c) mineralised pyroxenite with massive sulphides; (d) mineralised pyroxenite with combination of net textured and disseminated sulphides; (e) unmineralised (barren) pyroxenite; (f) dolerite; and (g) leuconorite. 16

Figure 14: Profile showing base station data over the course of the ground magnetic survey. Note the small range of values on the y-axis showing stable diurnal variations of between 5 nT and 20 nT over the course of a day's survey. 17

Figure 15: (a) TMI with track recorded walk lines shown after decorrugation and 15m upward contuation with a geometric colour scale applied; (b) the TMI with a linear colour scale applied. 18

Figure 16: Ely TMI shown in (a), RTP (b), AS (c) and 1VD (d) filter products or enhancements with annotations showing relevant features. 20

Figure 17: Magnetic profile lines over (a) CIDA aeromagnetic TMI with extent of the ground magnetic survey grid shown; and (b) the same profile lines over CIDA aeromagnetic TMI with the groundmag TMI superimposed for reference. 21

Figure 18: Magnetic profile lines of TMI for Profile 1 of (a) CIDA TMI; (b) of ground magnetic TMI with noise spike from the powerline deliberately kept in the data; and (c) of the ground magnetic TMI with the noise spike from the powerline cleaned from the data. Note that the red arrows on (a) indicate the start and end points of the profile extent for the ground magnetic TMI shown in (b) and (c). 22

Figure 19: Profile 2 results showing the TMI magnetic profiles for CIDA TMI (a) and ground magnetics TMI (b) at Ely. 23

Figure 20: Profile 3 results for TMI magnetic data (a) of the CIDA TMI and (b) of the ground magnetic survey TMI. 24

Figure 21: Location map of MLEM survey grid overlaid on the TMI map for reference 25

Figure 22: Location map showing the positions of the two modelled lines of MLEM data at the Ely survey grid. 29

Figure 23: Comparison of magnetic Profile 1 with modelling results for Line 1150 and comparison with TMI magnetic profile: (a) shows the TMI magnetic profile over the coincident negative magnetic anomaly at E1/E2; (b) shows the modelled EM plate dipping at 67° to the northwest, with the top of the conductor at a depth of about 26m; and (c) shows the measured EM response traces in black and the modelled EM response in red for the three components Z, X and Y respectively. Note the magnetic profile line and the MLEM survey line are not oriented in the same direction. 31

Figure 24: Modelling results for Line 1250 and comparison with TMI magnetic profile: (a) shows the TMI magnetic profile over the coincident negative magnetic anomaly at E3/E4; (b) shows the modelled EM plate view from the south; and (c) depicts the measured EM response traces in black and the modelled EM response in red for the three components Z, X and Y. 33

Figure 25: RTP map of Ely with anotations showing the powerline, interpreted faults and outlines of significant magnetic bodies. 35

Figure 26: Annotated RTP map (a) showing position of zoomed in area in (b); (b) zoomed in RTP with transparent overlay of georeferenced 1:1000 historical geochemsitry and drilling map from Anglo American reports with anomalies coinciding well with the distinct negative magnetic anomalies registered by the 2021 ground magnetic survey results. Note that the colour scale is the same as for (a). 37

Figure 27: (a) Annotated RTP map with black box outline showing the extent of the RTP map in (b); (b) RTP image zoomed in over E5 zone with georeferenced map of soil geochemistry and drilled

mineralisation at E5 from historical Anglo American reports. Note that the RTP colour scale is the same as for Figure 26 (a). 38

Figure 28: Gridded results of MLEM overlaid on RTP map showing (a) Channel 25Z, (b) Channel 30Z and (c) Channel 39Z. Note the strong spatial correlation of EM conductors with the annotated outlines of negative magnetic anomalies in RTP map. 41

List of Tables

Table 1: Results table for physical property measurements of selected drill core samples from various lithologies at Madziwa 13

Table 2: Summary table of EM gridded images for Channels 15Z through 39Z, from early time responses to late time responses of the bedrock conductors at E1/E2 and E3/E4 MLEM survey grid 26

List of Symbols

nT: nanoTesla

S/m: siemens per meter

SI: international system of units

1. Introduction: Madziwa and the application of geophysical methods to renewed exploration

Discovery rates for all deposit types, including nickel-copper-PGE sulphide deposits, reflect a declining trend over the past two decades (Davies et al, 2021). Attempting to address this dearth of recent discoveries, explorers are increasingly driven to adopt novel technologies like Artificial Intelligence, big data analysis and new conceptual frameworks to improve the odds of discovery. These are often touted as a silver bullet solution to overcoming challenges relating to declining grades, thicker cover and increasing depth of new targets. This study seeks to demonstrate that the application of standard geophysical methods still has the potential to reveal previously overlooked orebodies in terrains where these methods have not been effectively applied. The Archean granite-greenstone craton of Zimbabwe is an example of a fertile crustal region that exhibits fundamental geological similarities to analogous, better explored areas like those in Western Australia. The orthomagmatic nickel sulphide deposits of the Yilgarn Craton represent a class of relatively well explored deposit with a substantial body of published literature documenting the geophysical survey methods successfully applied there and the results that contributed to new discoveries in that jurisdiction (Dentith et al., 1994). Rather than (or in addition to) resorting to novel exploration approaches, simply replicating successful geophysical surveys from analogous geological settings continues to offer excellent scope for finding new orebodies.

The focus area of this study is the Madziwa Igneous Complex in northeastern Zimbabwe. A group of mafic to ultramafic igneous intrusions within a gneissic terrain that were found to host orthomagmatic nickel-copper sulphide orebodies, Madziwa was mined by Anglo American and then Bindura Nickel Corporation between 1969 and 2000. The historical exploration approach consisted primarily of comprehensive geochemistry surveys, with subsequent trenching and drilling of resultant anomalies. Where geophysical surveys were carried out at Madziwa, these were either not systematically applied to all anomalies or the relevant data, results and reports have not survived to inform current exploration initiatives. This left an obvious gap in the exploration knowledge base of the Madziwa area, which is otherwise well mapped and characterized by soil geochemistry, as well as having its orebodies relatively well understood after thirty years of mining.

The physical properties common to nickel sulphide deposits and the suite of rocks that typically host them make them particularly well suited to geophysical survey methods (King, 2007). These methods include gravity, magnetics and the electrical methods of conductivity and chargeability, relying respectively on density, magnetic susceptibility and electrical conductivity or resistivity properties (McCall et al., 1995). In contrast to northeastern Zimbabwe, much of Western Australia is covered by deeply weathered regolith profiles with calcrete and iron-rich lateritic layers that are responsible for high frequency noise in magnetic surveys, while saline ground water produces near surface conductivity responses that may mask deeper signals from metal sulphide accumulations in electrical surveys (Dentith et al., 1994). Despite these difficulties, airborne and ground-based magnetics and electromagnetic surveys have proven remarkably successful in identifying anomalies which led to new discoveries or extensions of known deposits, even in well-explored districts (Peters and Buck, 2000).

Could well-informed and well executed geophysical surveys using more sensitive modern instruments and computer processing, twenty years after previous exploration efforts in the area had ceased, help to define targets that were previously overlooked? Assessing the potential of applying standard

modern geophysical methods to brownfields settings such as Madziwa, using the lessons and findings of similar surveys in the Yilgarn Craton, is the aim of this study.

The geology and historical exploration of the Madziwa area, and the Ely prospect specifically, are described in detail in Chapter 2. This background provides important context for the evaluation of the design and results of ground geophysical surveys executed during the recent exploration campaign. The survey designs and instruments used in the geophysical surveys employed at Madziwa are detailed in Chapter 3 under methods and measurement. The results of these surveys are presented in Chapter 4 and are evaluated and discussed in Chapter 5. Conclusions and implications for exploration strategy in similar brownfields settings are presented in Chapter 6.

2. The geology and exploration history of the Madziwa Igneous Complex

The Madziwa Igneous Complex in Zimbabwe is a suite of mafic-ultramafic rocks intruded into the Archean gneissic terrain of the Madziwa batholith, and is surrounded to the south, west and north by the Shamva, Bindura and Mt Darwin Archean greenstone belts respectively (Stidolph, 1977). The Complex is situated approximately 110km northeast of the capital city of Harare, and immediately west of the Umfurudzi Safari Area. The area was mapped between 1968 and 1972 by P.A. Stidolph of the Rhodesian Geological Survey and described in Bulletin No. 78 (1977). The area surrounding the mine was additionally mapped at various scales by authors including Gewald (1974), Birch (1985) and Prendergast (1996).

The Madziwa Igneous Complex intrusive bodies are composed of amphibolitised pyroxenite, norite, leuconorite and ferro-diorite which are oriented in lenses roughly parallel to the fabric of the gneissic country rock along a northwesterly trend as shown in Figure 1 (Stidolph, 1977). The intrusive bodies in the central part of the complex are host to multiple bodies of nickel-copper sulphide mineralization, interpreted to be the result of sulphide segregation from mafic-ultramafic magmas (Birch, 1986). Anglo-American, and later Bindura Nickel Corporation, mined these ore bodies at Madziwa between 1969 and 2000 when the mine was finally closed (Prendergast and Wilson, 2015). The age of the pyroxenite suite in the Madziwa Complex has been calculated, using U-Pb dating of zircons from these rocks, at 2684 Ma (Prendergast and Wilson, 2015).

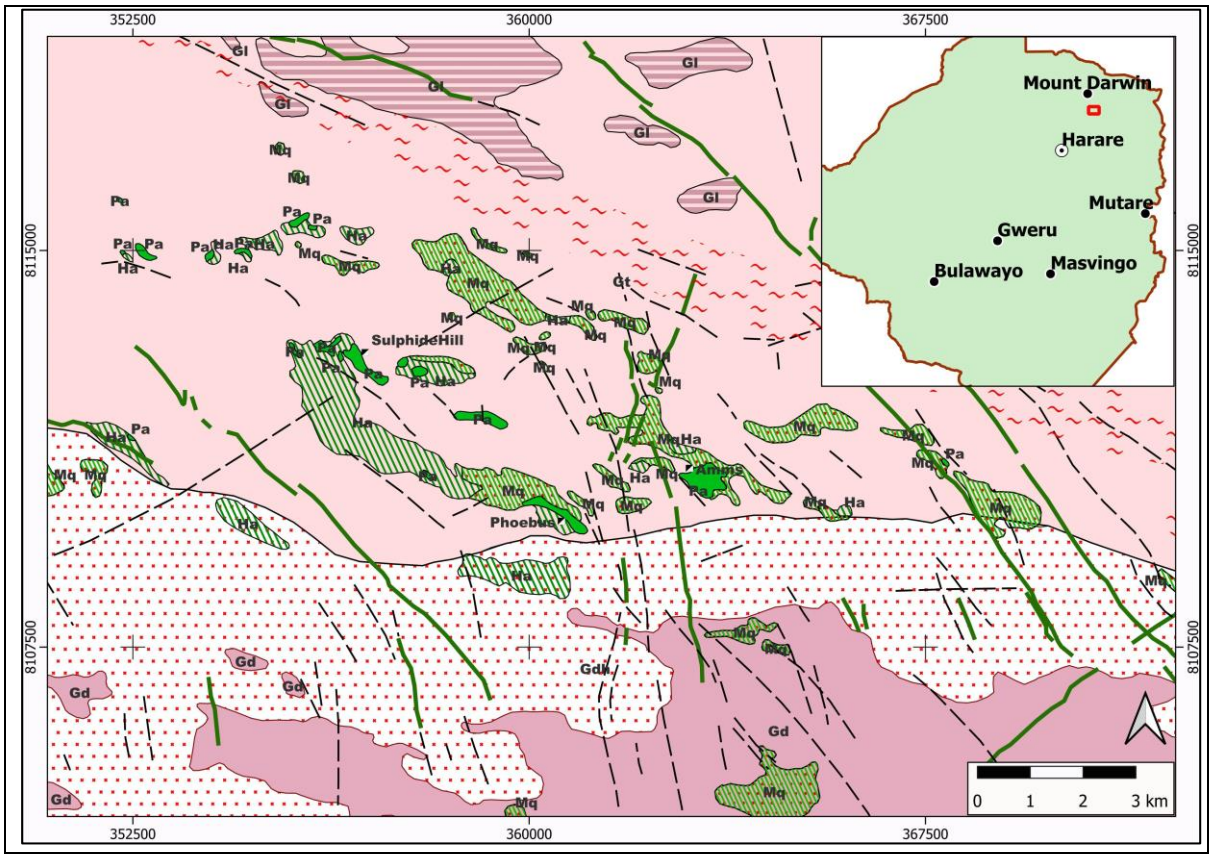

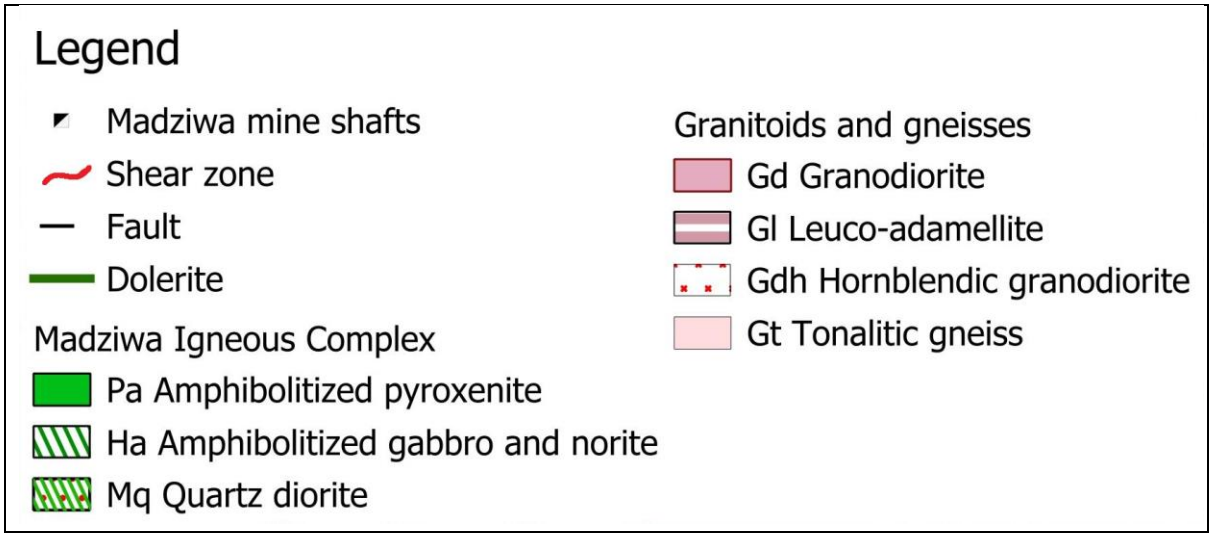

Figure 1: Stidolph, P. A., 1977. Digitized and simplified from 1:100 000 Geological Map of Rhodesia Geological Survey Bulletin No. 78, The Geology of the Country around Shamva.

The intrusive bodies are arranged in elongated pods, from one hundred meters up to several kilometres in strike length and are cross-cut by multiple pegmatites, aplites and veins of granitic rock (Stidolph, 1977). The contacts of the intrusive bodies with the surrounding gneissic rock are generally sub-vertical to vertical, with the southern contacts dipping steeply southwards (Prendergast and Wilson, 2015). Contacts are described as sharp to gradational over a few meters to tens of meters with interlayering of leucocratic and melanocratic bands and inter-fingering of gneissic rock with the mafic intrusive rock near the contacts (Birch, 1985). The overall WNW-ESE trend of the Madziwa intrusions' long axes is parallel to that of the gneissic banding within the Madziwa batholith (Prendergast and Wilson, 2015). Later major faults striking NNW-SSE disrupt and dismember the intrusive bodies throughout the complex with dextral offsets of up to a few hundred meters, as depicted in the simplified geology map of Madziwa in Figure 2 (Prendergast and Wilson, 2015).

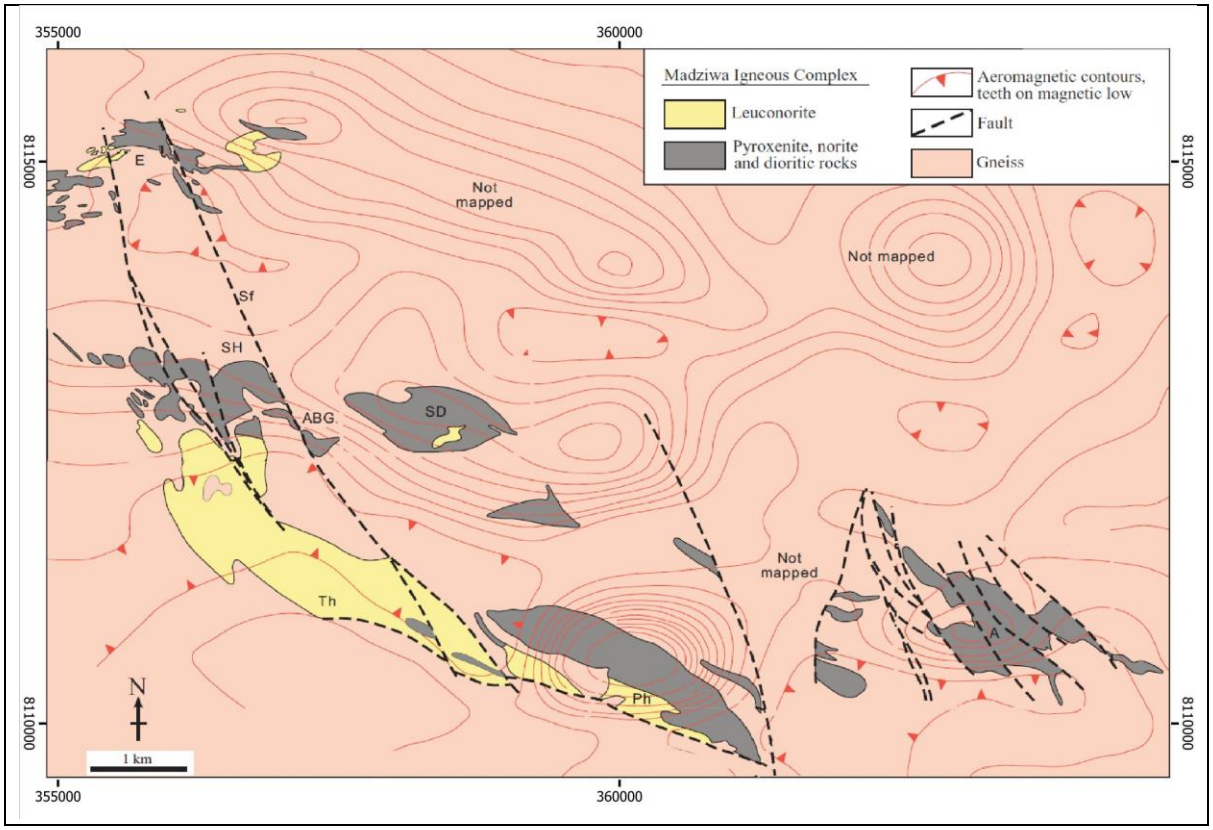

Figure 2: Simplified geology map of the Madziwa Complex with Aeromagnetic Contours; A=Amms, E=Ely, SH=Sulphide Hill, Th=Thyrza, Ph=Phoebus, SD=Slimes Dam, Sf=Sulphide Fault. Reproduced from Prendergast and Wilson (2015)

The petrology of the Madziwa intrusive bodies is characterized by lenses of pyroxenite (also termed "Bronzitites" in the historical descriptions) which is generally altered to amphibolite, and surrounding and internal lenses of norites and leuconorites, with some peripheral gabbroic rocks and ferro-diorites (Prendergast and Wilson, 2015). Leuconorites in the central portion of the largest intrusive lens are characterized by abundant plagioclase and minor hornblende, and have been suggested to represent a later, separate magma pulse with transgressive contacts to the pyroxenites and norites (Prendergast and Wilson, 2015). Wall rock assimilation into the intrusive bodies near their contacts and distinct changes in the characteristics of the banded tonalities near the contacts suggest that magmatic intrusion may have taken place at deep crustal levels and that wall rock contamination likely induced the segregation of the sulphides into economic horizons (Birch, 1985). However, sharp contacts and sheared contacts with pegmatitic veins were also noted in mine excavations at various depths and suggest some degree of low-grade metamorphism and tectonic disruption from the original intrusive orientation (Birch, 1985, and Gewald, 1974).

The Sulphide Hill and Amms ore bodies were the primary producers of the estimated 12 million tonnes of sulphide ore that was mined over Madziwa's mine life (Prendergast and Wilson, 2015). In 1995, Phoebus Shaft was commissioned and contributed to production during a period when Amms shaft was approaching closure. Sulphide mineralization at the various ore bodies is generally disseminated, with local remobilization into coarse disseminations and veined massive ore, with no primary massive ores recognized anywhere (Prendergast and Wilson, 2015). Disseminated orebodies are typically sub-vertical lenses of up to 200m long, up to 800m in depth extent and vary from 5m to 40m in width (Prendergast and Wilson, 2015). Massive sulphides associated with veins and faults are comparatively rare and occur in stringers and veins up to 15cm thick, surrounded by halos of

disseminated ore (Birch, 1985). The main sulphide mineral species in the Madziwa ore bodies are made up of roughly 40% pyrrhotite, 25% pentlandite and 25% chalcopyrite (Gewald, 1974). No characterization of the pyrrhotite as either monoclinic or hexagonal is available I the literature on Madziwa and this represents a topic where further research would be valuable. Contained nickel grades varied between 0.5% Ni and 0.7% Ni in the disseminated ores, with a nickel to copper ratio of between 2.5:1 and 5:1 (Chimimba, 1986). Ore bodies are generally located at the interface between pyroxenites and internal norite bodies, with no ores recognized in association with any of the leuconorite or ferro-diorite bodies. The ore body morphologies and orientations are ubiquitously vertical to sub-vertical and parallel or overlapping the lithological contacts between pyroxenites and norites (Prendergast and Wilson, 2015). Another notable feature of the Madziwa ores is their distinct lack of significant platinum group element (PGE) concentrations (Prendergast and Wilson, 2015).

There is some disagreement over the genesis and tectonic history of the Madziwa Igneous Complex. Birch (1985), Gewald (1974) and Stidolph (1977) contended that the various lenses of the complex were once part of a single continuous sill-like body with gravitational settling representing the primary mechanism for sulphides accumulating in discrete layers near the base of the intrusion. Subsequent tectonism deformed, fragmented and folded the complex into its present morphology (Birch, 1985; Gewald, 1974; and Stidolph, 1977). Prendergast and Wilson (2015) hold a contrasting view, namely that the Madziwa IC represents a 2-stage intrusive event, with the earlier intrusion of narrow vertical dikes of pyroxenite and norite into the gneissic terrain, followed by the intrusion of a larger lopolith or sill-like body of leuconorite which overlies and cross-cuts the earlier dikes (Prendergast and Wilson, 2015). Their contention is that the intrusive bodies are essentially in their original intrusive orientations with only minor deformation and alteration, and that structural evidence does not point to large scale displacement or folding. Refuting the mechanism of gravitational settling into horizontal layers that were later folded into upright orientations, they assert that the sulphide mineralization accumulated in the observed vertical orebodies driven by wall rock assimilation, silica contamination and the migration of immiscible sulphides ahead of a plagioclase crystallization front within the narrow pyroxenite bodies (Prendergast and Wilson, 2015).

Prendergast and Wilson (2015) present a genetic model of the Madziwa Igneous Complex graphically depicted in Figure 3, where the pods and lenses are remnants of dike-like intrusions, all approximately in their original vertical intrusive orientations within the gneissic Madziwa Batholith, and with the separate lithologies representing discrete pulses of magma with different compositions - pyroxenitic, noritic, and dioritic. These separate pulses are hypothesized to have originated from a deeper staging chamber, and once emplaced, the sulphides segregated into discrete mineralised zones ahead of a crystallisation front forming the presently oriented sub-vertical ore bodies. This process would have been characterised by relatively rapid cooling within the narrow dikes and sulphide immiscibility the result of contamination and assimilation of felsic country rock, as there is no evidence of a proximal sulphur source (Prendergast and Wilson, 2015). The leuconorite, according to Prendergast and Wilson (2015), represents a later pulse which transgresses the earlier lenses of pyroxenite and norite and forms a lopolith-type geometry.

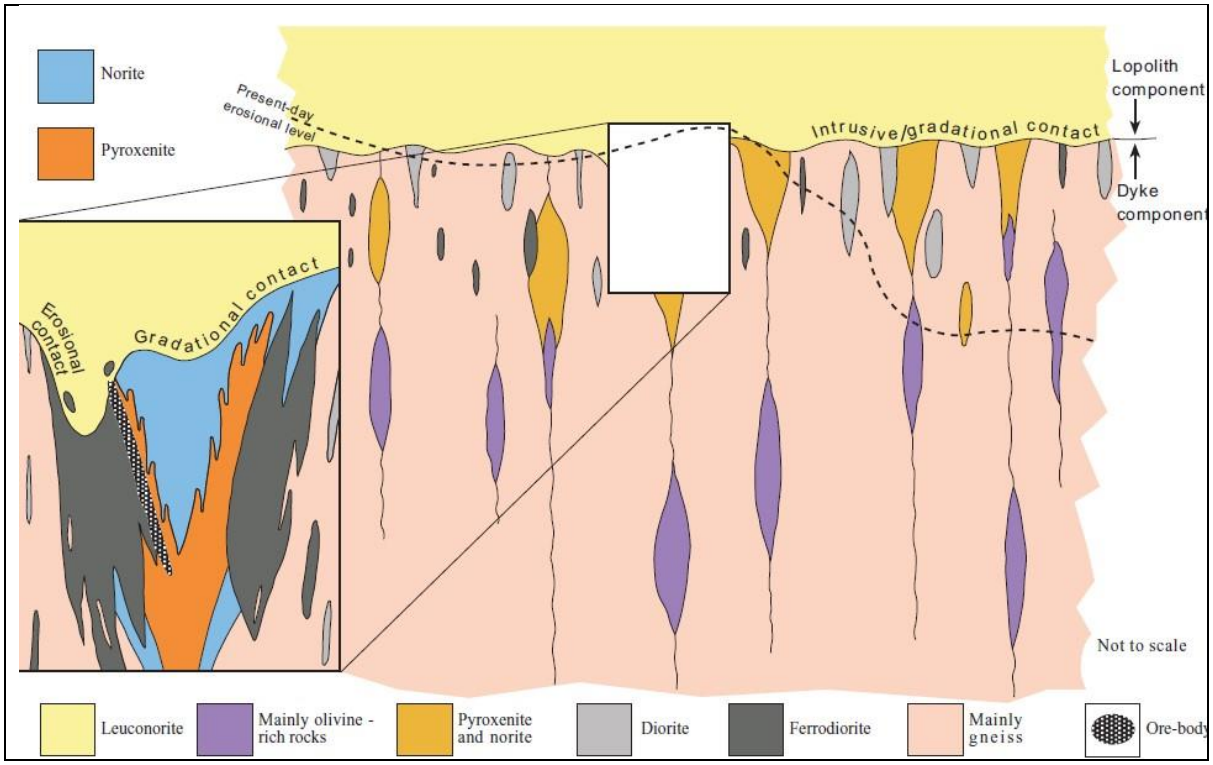

Figure 3: Hypothesized structural model for the Madziwa Igneous Complex. Schematicand not to scale. The interpreted structural relationships of the principal rock types, and of the two main lower dike and upper lopolithic components, are depicted in section, together with the apparent north-south lithological zonation of the Madziwa Igneous Complex observed at present erosion levels. The structure shown in the central inset is modelled on that seen at Phoebus (Prendergast and Wilson, 2015).

Regardless of the genetic origin and subsequent deformational history of the sulphide mineralisation in the Madziwa orebodies, their commonly sub-vertical orientations and limited strike lengths and widths make them challenging to detect using geophysical methods. Any mineralisation present at the Ely prospect is likely to produce a relatively small geophysical footprint, in the order of 100m to 200m in diameter, for direct detection using geophysical methods. This anticipated difficulty may be offset by the expected physical property contrasts between the gneissic host rock and pyroxenite and norite lithologies, the contacts of which are important controls for nickel sulphide mineralisation at Madziwa.

The magnetic susceptibility of mafic and ultramafic rock units can vary substantially depending on the type of alteration these units have been subjected to, with serpentinization resulting in secondary magnetite (increasing susceptibility) and talc chlorite alteration reducing magnetic susceptibility (McCall et al., 1994). In the fertile Kambalda area of the Yilgarn Craton, magnetic surveys are unable to directly detect orebodies because of surrounding noise by voluminously dominant magnetic host rocks but are instrumental in mapping and locating favourable lithologies and structural settings for mineralisation (Trench and Williams, 1994). At Madziwa it was anticipated that the gneissic host rock would be relatively resistive and muted in its magnetic character, and that significant physical property contrasts would likely characterise the ultramafic and mafic intrusive lithologies.

2.1 Ely Satellite Prospect

The Ely prospect is a group of smaller pyroxenite and norite bodies approximately 3km to northwest of the main Sulphide Shaft of the Madziwa Mining Complex shown in Figure 4. This area was identified as prospective by Anglo-American in the early 1960s based on the results of their regional stream sediment sampling campaign, followed up by a tenement wide soil geochemistry grid. Five distinct nickel and copper soil anomalies were identified and labelled E1 to E5 (Prospecting Ventures Report, 1968).

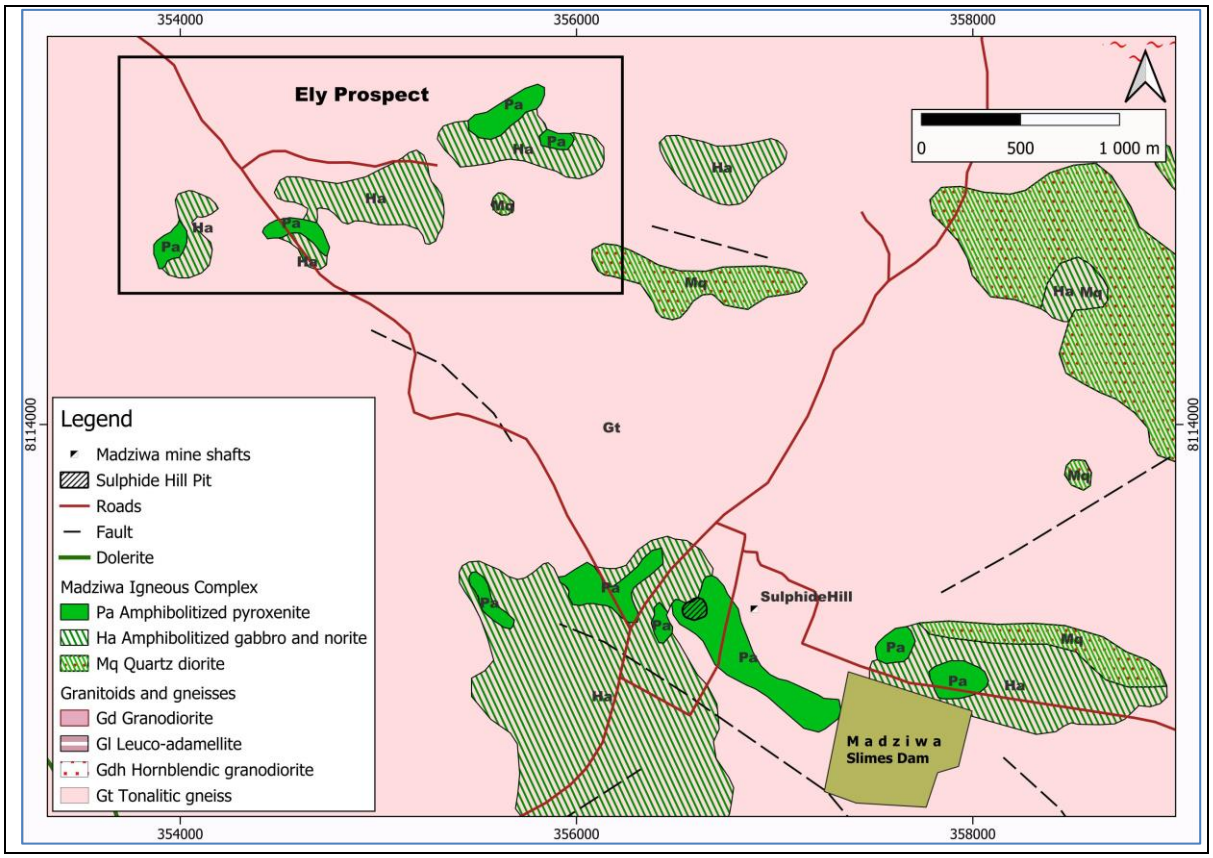

Figure 4: Geology of the Ely prospect area at Madziwa (Stidolph, 1977).

Soil anomalies for nickel and copper were defined on contours of 500ppm to 999ppm Ni for C-zone soil anomalies, 1000ppm to 2000ppm Ni for B-zone anomalies, and >2000ppm for A-zone anomalies. These are shown in Figure 5 (a). Background values of nickel and copper in soil were generally low where underlain by the Madziwa batholith gneisses, and so soil anomalies were treated as reliable indicators of sulphide mineralization beneath the residual soil profile. Unfortunately, the maps were plotted using a local survey grid which was not defined in the reports available, making georeferencing a challenge. This limits the accuracy that is possible for georeferencing in QGIS software. However, drill collars were found and marked by handheld GPS in the field, and their spatial pattern was used to geo-reference the smaller-scale maps showing anomalies, trenching and drilling depicted in Figures 5 (b), (c) and (d).

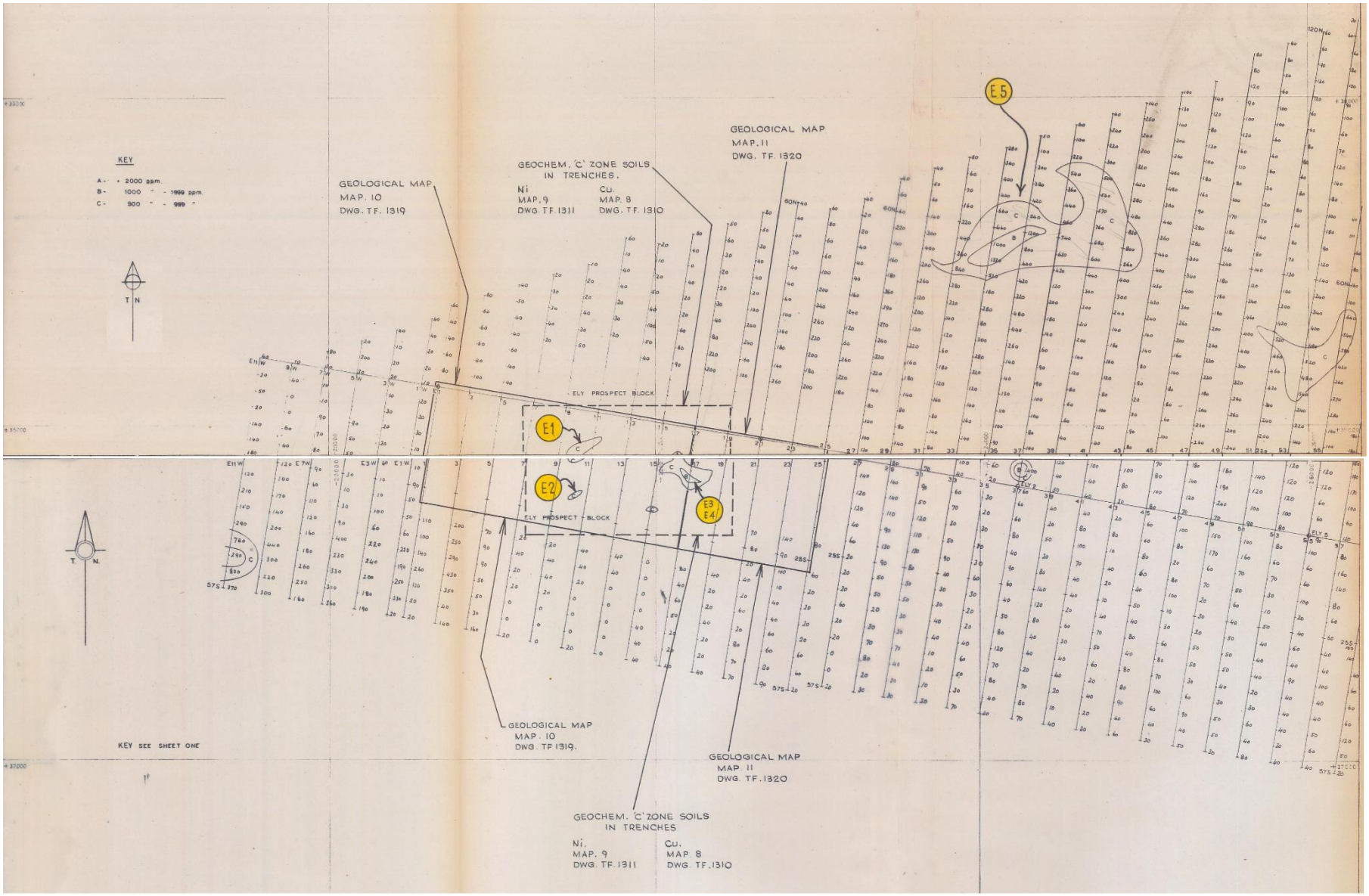
KEY
A- + 2000 ppm.
B- 1000 " - 1999 ppm.
C- 500 " - 999 "
T N
GEOLOGICAL MAP
MAP. 10
DWG. TF. 1319
GEOCHEM. 'C' ZONE SOILS
IN TRENCHES.
Ni
MAP. 9
DWG. TF. 1311
Cu.
MAP. 8
DWG. TF. 1310
GEOLOGICAL MAP
MAP. 11
DWG. TF. 1320
E5
E1
E2
E3
E4
ELY PROSPECT BLOCK
ELY PROSPECT - BLOCK
T. N.
KEY SEE SHEET ONE
GEOLOGICAL MAP
MAP. 10
DWG. TF 1319.
GEOLOGICAL MAP
MAP. 11
DWG. TF. 1320
GEOCHEM. 'C' ZONE SOILS
IN TRENCHES
Ni.
MAP. 9
DWG. TF. 1311
Cu.
MAP. 8
DWG. TF. 1310

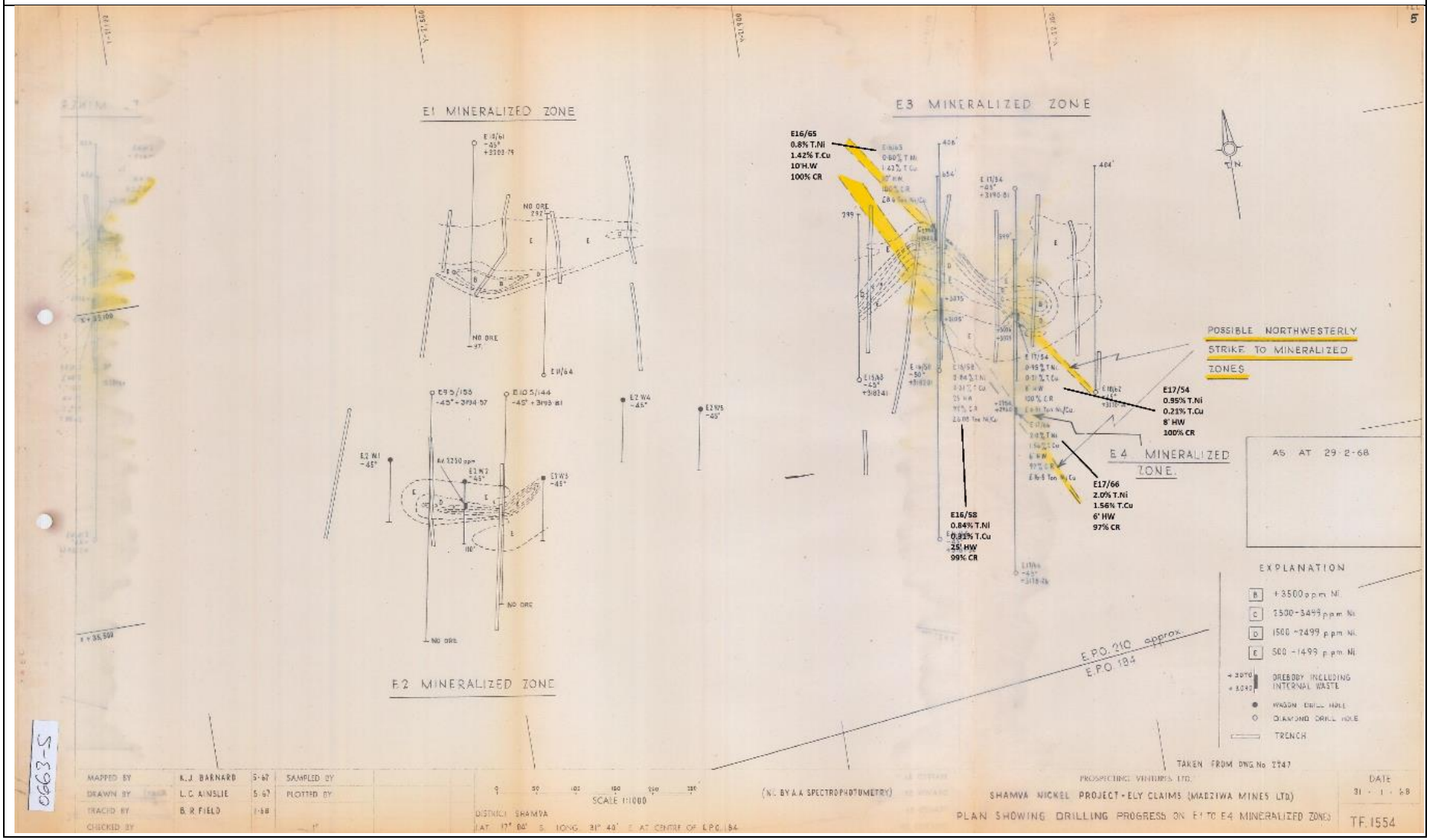
E1 MINERALIZED ZONE
E3 MINERALIZED ZONE
E2 MINERALIZED ZONE
E4 MINERALIZED ZONE.
E16/65
0.8% T.Ni
1.42% T.Cu
10'H.W
100% CR
E17/54
0.55% T.Ni
0.21% T.Cu
8' HW
100% CR
E17/66
2.0% T.Ni
1.56% T.Cu
6' HW
97% CR
E16/58
0.84% T.Ni
0.31% T.Cu
25' HW
99% CR
POSSIBLE NORTHWESTERLY STRIKE TO MINERALIZED ZONES
AS AT 29-2-68
EXPLANATION
B +3500 p.p.m. Ni
C 2500-3499 p.p.m. Ni
D 1500-2499 p.p.m. Ni
E 500-1499 p.p.m. Ni
OREBODY INCLUDING INTERNAL WASTE
WAGON DRILL HOLE
DIAMOND DRILL HOLE
TRENCH
E.P.O. 210 approx.
E.P.O. 184
NO ORE
TAKEN FROM DWG No 2747
MAPPED BY K.J. BARNARD 5-67
DRAWN BY L.C. AINSLIE 5-67
TRACED BY B.R. FIELD 1-68
CHECKED BY
SAMPLED BY
PLOTTED BY
SCALE 1:1000
(Ni BY A.A. SPECTROPHOTOMETRY)
DISTRICT SHAMVA
LAT. 17° 04' S. LONG. 31° 40' E. AT CENTRE OF E.P.O. 184
PROSPECTING VENTURES LTD.
SHAMVA NICKEL PROJECT - ELY CLAIMS (MAIZIWA MINES LTD.)
PLAN SHOWING DRILLING PROGRESS ON E1 TO E4 MINERALIZED ZONES
DATE 31-1-68
TF.1554
S-3690

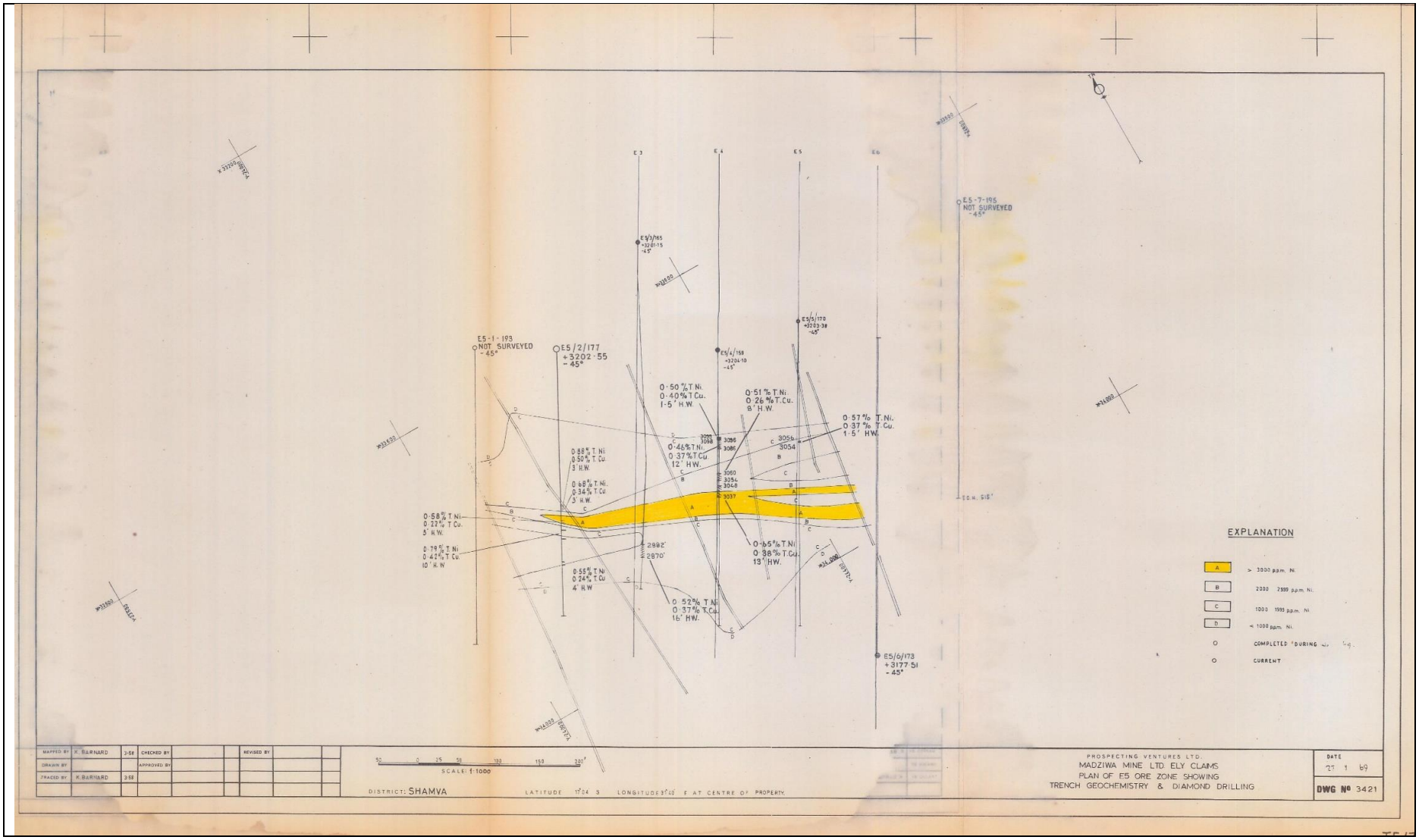
E5-1-193
NOT SURVEYED
-45°
E5/2/177
+3202·55
-45°
E5/3/165
+3201·15
-45°
E5/4/159
+3204·10
-45°
E5/5/170
+3203·38
-45°
E5-7-195
NOT SURVEYED
-45°
E5/6/173
+3177·51
-45°
0·50% T.Ni.
0·40% T.Cu.
1·5' H.W.
0·51% T.Ni.
0·26% T.Cu.
8' H.W.
0·57% T.Ni.
0·37% T.Cu.
1·5' HW.
0·46% T.Ni.
0·37% T.Cu.
12' HW.
0·88% T.Ni.
0·50% T.Cu.
3' H.W.
0·68% T.Ni.
0·34% T.Cu.
3' H.W.
0·58% T.Ni.
0·22% T.Cu.
5' H.W.
0·79% T.Ni.
0·42% T.Cu.
10' H.W.
0·55% T.Ni.
0·24% T.Cu.
4' H.W.
0·52% T.Ni.
0·37% T.Cu.
16' HW.
0·65% T.Ni.
0·38% T.Cu.
13' HW.
2882'
2870'
3056
3054
3060
3054
3048
3037
EXPLANATION
A > 3000 p.p.m. Ni.
B 2000 2999 p.p.m. Ni.
C 1000 1999 p.p.m. Ni.
D < 1000 p.p.m. Ni.
COMPLETED DURING
CURRENT
MAPPED BY K. BARNARD 3-58
DRAWN BY
TRACED BY K. BARNARD 3-58
CHECKED BY
APPROVED BY
REVISED BY
SCALE: 1:1000
DISTRICT: SHAMVA
LATITUDE 17°04' S LONGITUDE 31°40' E AT CENTRE OF PROPERTY.
PROSPECTING VENTURES LTD.
MADZIWA MINE LTD. ELY CLAIMS
PLAN OF E5 ORE ZONE SHOWING
TRENCH GEOCHEMISTRY & DIAMOND DRILLING
DATE
DWG No 3421

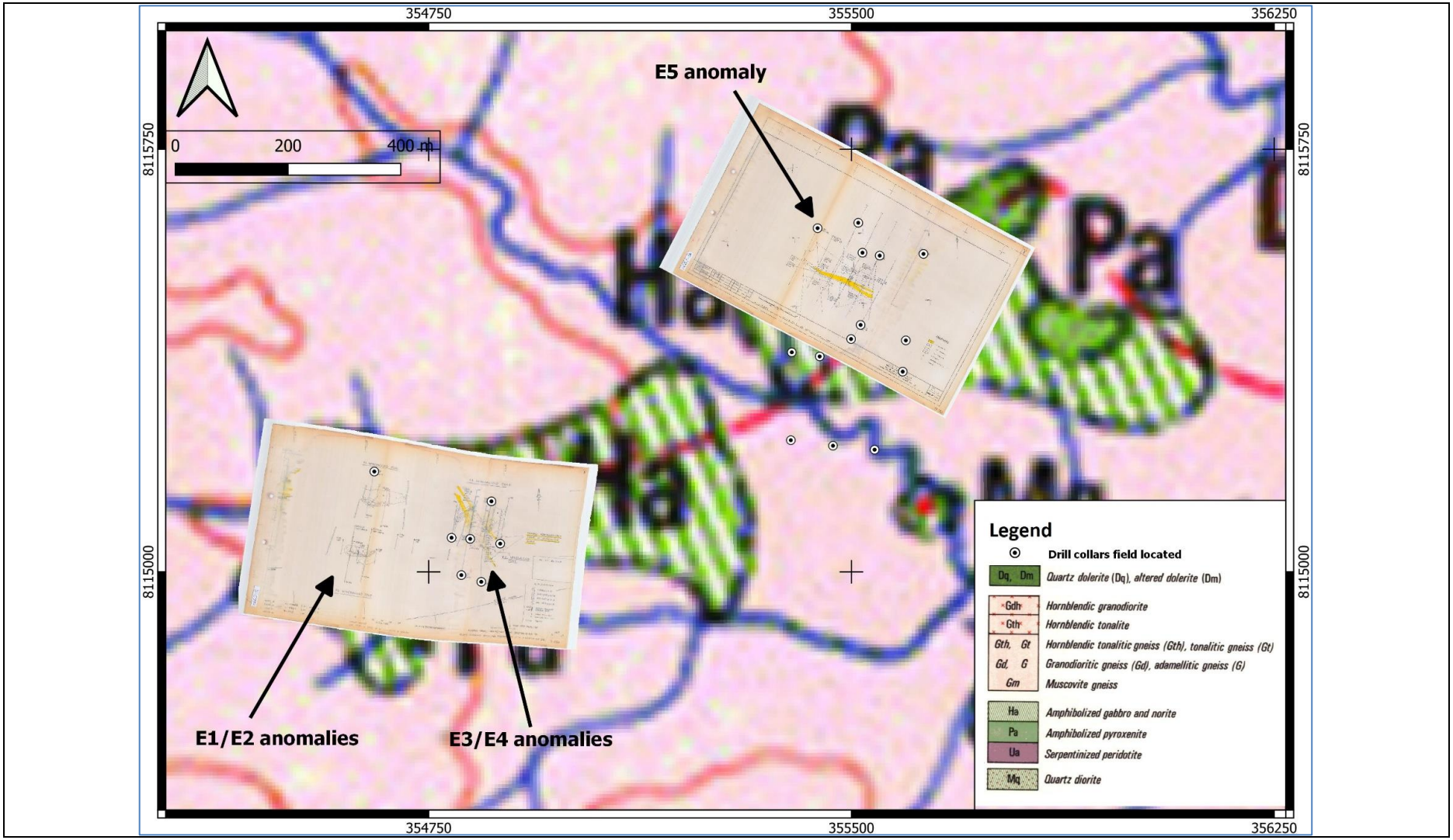

Figure 5: Soil geochemical anomalies and sample lines in (a) mapped by Anglo-American around the Ely prospect for nickel in soil; (b) shows the 1:1000 map of adjacent E1/E2 and E3/E4 anomalies along with diamond drilling significant intersections; (c) shows the 1:1000 map of E5 anomaly with the yellow zone representing >3000ppm Ni, as well as trenches and diamond drilling with significant intersections; and (d) shows the 1:1000 Anglo-American maps georeferenced on the B78 geology map after field locating the drill collars

These soil anomalies were trenched and drilled in two separate exploration campaigns, with the first campaign taking place in 1963 and a subsequent round of work carried out in 1995 and 1996, when Madziwa was running out of minable reserves and was under pressure to extend its resource. While showing narrow intercepts (>3m horizontal width) of steeply southwards dipping sulphide mineralization of up to 2% nickel and 1.5% copper, no further work was carried out at anomalies E1 through E4 after the 1960s round of exploration work. The E5 anomaly was subject to further drill testing in 1995 and 1996, with Prospecting Ventures ultimately abandoning it despite delineating a vertically oriented mineralized zone of low grade disseminated sulphides approximately 120m in length and averaging 12m in width (Prospecting Ventures Reports, 1996).

Prospecting Venture's mapping of the Ely group of intrusive bodies, as depicted in Prendergast and Wilson (2015), is more detailed and considered to be more accurate than the Bulletin 78 geology map as it was carried out at prospect scale. It shows the pyroxenite and norite bodies forming a collection of pods and lenses with small norite pods included within the pyroxenite lenses, all surrounded by the host tonalitic gneiss (Prendergast and Wilson, 2015). Two prominent, approximately north-south trending faults cut across and partially displace the Ely group of lenses (Gewald, 1974). The eastern fault is named the Sulphide Fault and extends 3km southwards to dislocate the historical orebody at Sulphide Hill and is shown in Figures 6 (a), (b) and (c). According to the available Prospecting Ventures reports (1996), the mineralisation at E5 ultimately proved not to be of sufficient grade and width to justify development at the time, and no further exploration work was carried out at Ely until 2021.

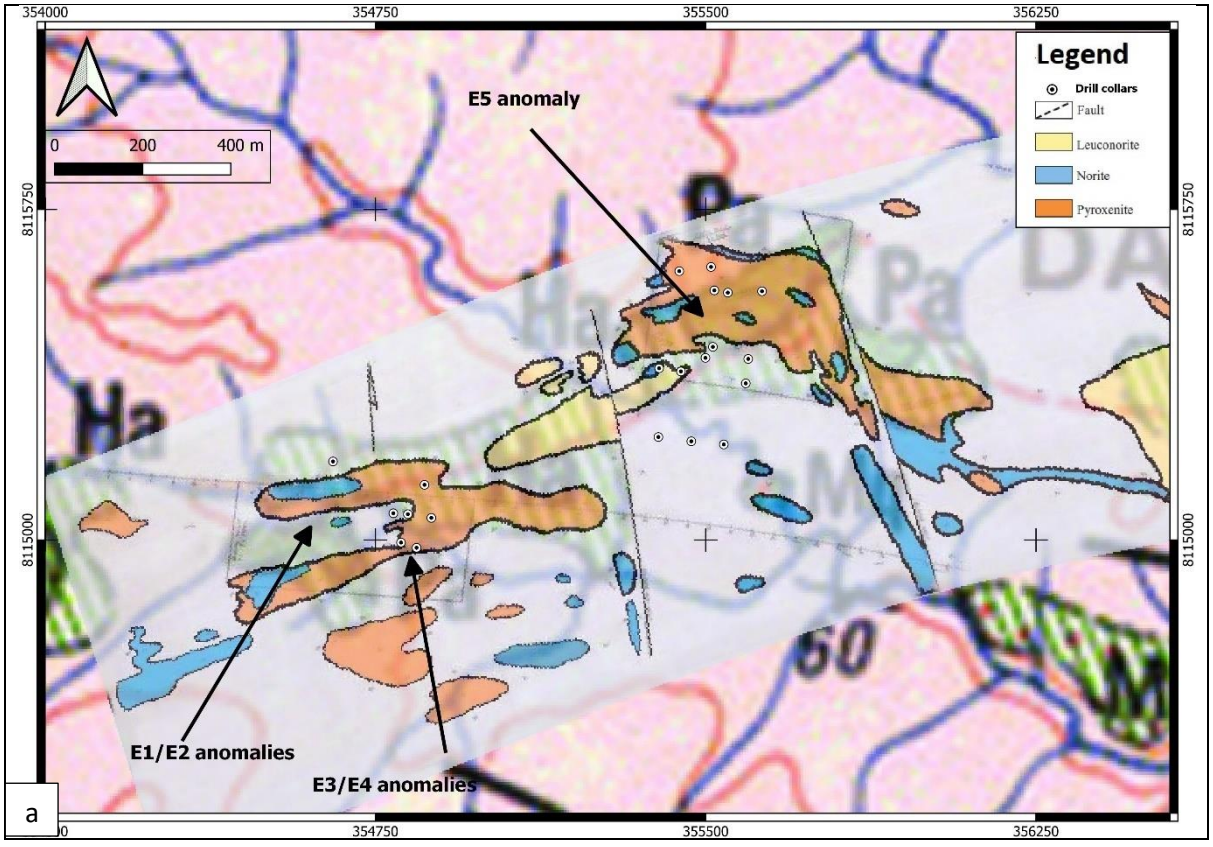

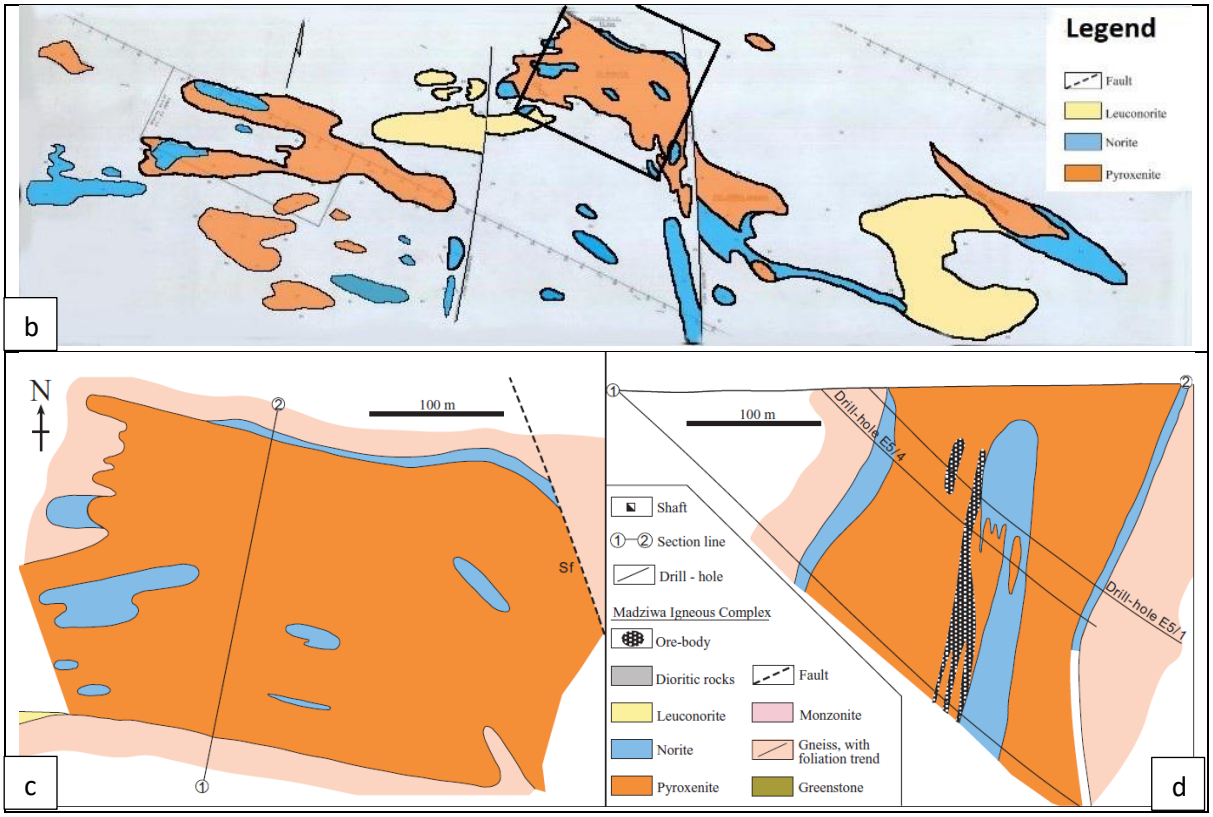

Figure 6: (a) Prospecting Ventures simplified and annotated geology of the Ely area overlaid on the B78 geology map; (b) the same simplified geology plan with black square showing location of zoomed in plan of E5 area in (c); (c) plan view of the E5 prospect at Ely and (d) section view of the E5 prospect and mineralised zone based on the drilling completed there in the 1960s and 1990s (Prendergast and Wilson, 2015).

3. Methods and measurements

3.1 Physical Property measurements on drill core from Madziwa

Representative samples of drill core for each of the major lithology types at Madziwa were collected from a site near the main Sulphide Shaft where a very large quantity of drill core had been discarded. Presumably the drill core had been kept in the Madziwa core storage sheds and, lamentably, was discarded in the bush upon closure of the mine. One sample per lithology was collected for physical property measurements. Samples were selected for their relative homogeneity and the degree to which they (subjectively) represent each of the main lithologies described by Prendergast and Wilson (2015). An MPP-EM2S Multi Parameter Probe belonging to the University of the Witwatersrand, made by GDD Instruments and depicted in Figure 7, was used to measure magnetic susceptibility and conductivity on each of the samples.

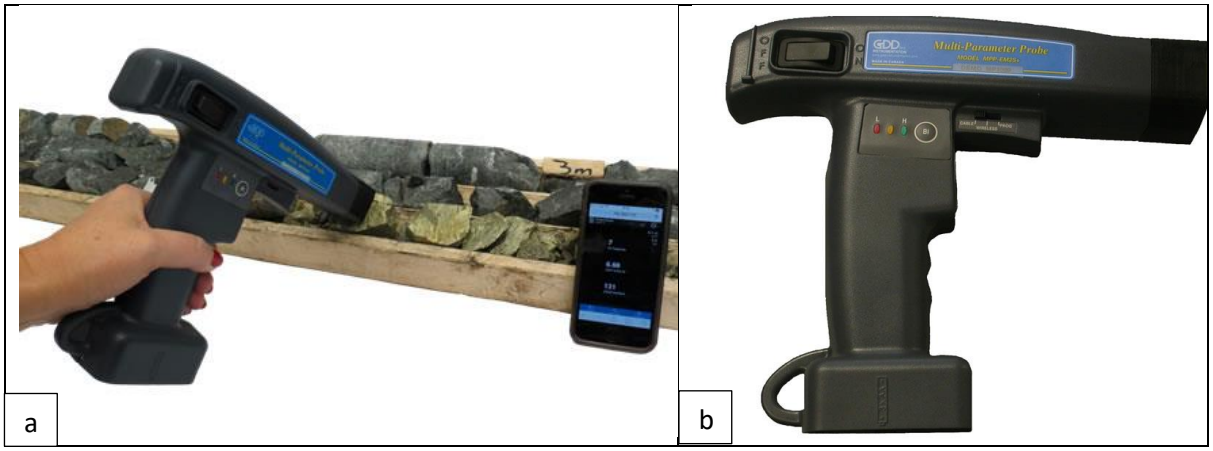

Figure 7: MPP-EM2S Multi Parameter Probe used for physical property measurements of drill core samples collected from Madziwa (GDD Instruments website, 2024).

A minimum of four readings were taken per sample from different points around the circumference of each core cylinder and measurements for magnetic susceptibility and conductivity were recorded. For the single half-core sample, the instrument settings were duly adjusted. All samples were photographed and are displayed in the results section.

3.2 Canadian International Development Agency Airborne Magnetic Survey

From 1983 to 1992 a multi-year airborne magnetics survey was flown using a line spacing of 1km and 305m ground clearance. This country-wide survey was sponsored by the Canadian International Development Agency (CIDA) to facilitate and promote exploration in Zimbabwe post-independence and covered approximately 70% of the country, as shown in Figure 8. Over the Madziwa area, flight lines were oriented east-west, while the predominant orientation trend of the intrusive bodies and tectonic fabric is northwest to southeast. The survey flight line direction and spacing was thus sub-optimal for delineating the magnetic signature of the intrusive igneous bodies, though it was almost orthogonal to one of the dominant structural trends, that of the Muda-Chipoli fault system and its subordinate structures, which are responsible for off-setting parts of the Madziwa Igneous Complex.

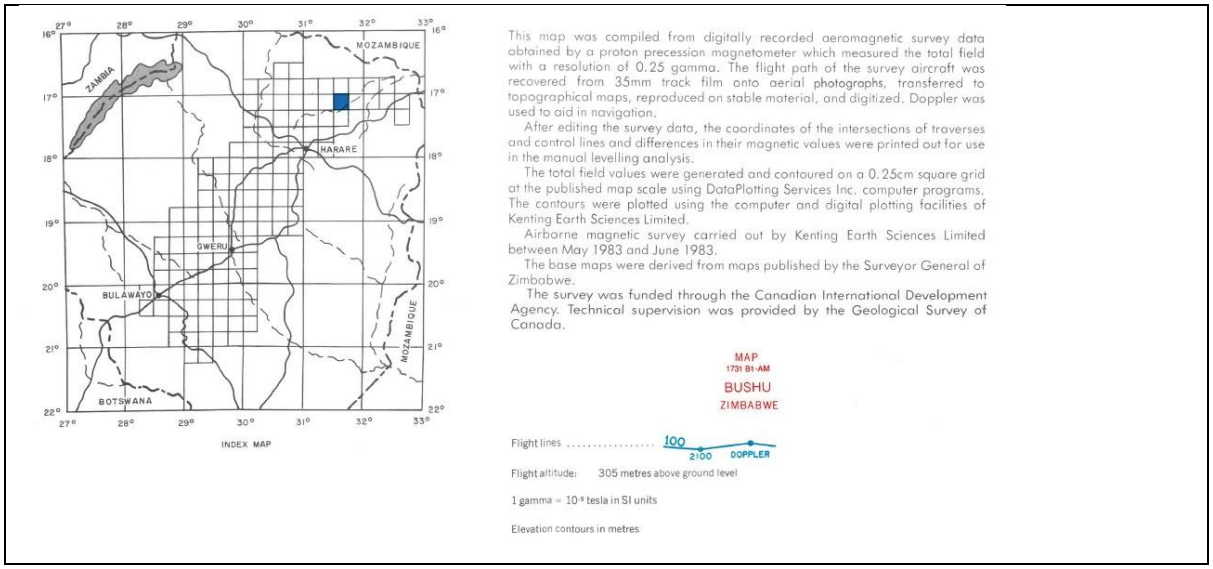

Figure 8: Details of the Canadian International Development Agency sponsored airborne magnetic survey flown over Zimbabwe in the early 1980s, as published in the 1731 B1 Aeromagnetic Map of Bushu, obtained from the Zimbabwe Geological Survey in Harare.

The CIDA aeromagnetic survey results were purchased from the Zimbabwe Geological Survey. This included a hard copy map of the 1731 B1 survey block at 1:50,000 scale with TMI contours over topography and flight lines shown. It also included gridded data files. Unfortunately, no raw data files were available for reprocessing and analysis. Flown at an average line spacing of 1km and ground clearance of 305m, the resolution of the TMI over the Madziwa area, while useful in showing up regional trends, is relatively coarse and not suitable to mapping prospect-scale features from their magnetic signatures. Figure 9 shows the CIDA aeromagnetic TMI map gridded in Geosoft Oasis Montaj for the whole B 1731 Block (a), as well as zoomed in plan of the Madziwa area with TMI contours shown beneath the transparent TMI colour grid (b), and the same TMI overlaid on the B78 geology map in (c).

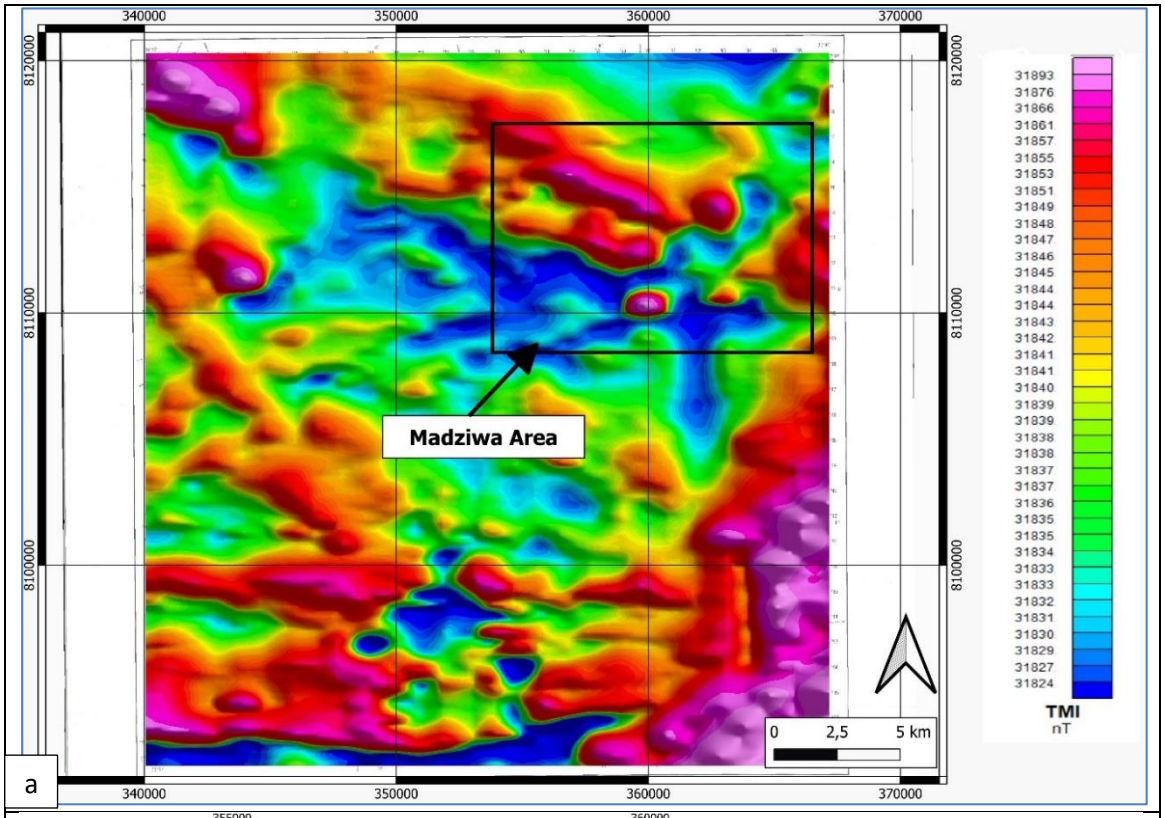
340000
350000
360000
370000
8120000
8110000
8100000
Madziwa Area
0
2,5
5 km
31893
31876
31866
31861
31857
31855
31853
31851
31849
31848
31847
31846
31845
31844
31844
31843
31842
31841
31841
31840
31839
31839
31838
31838
31837
31837
31836
31835
31835
31834
31833
31833
31832
31831
31830
31829
31827
31824
TMI
nT
a

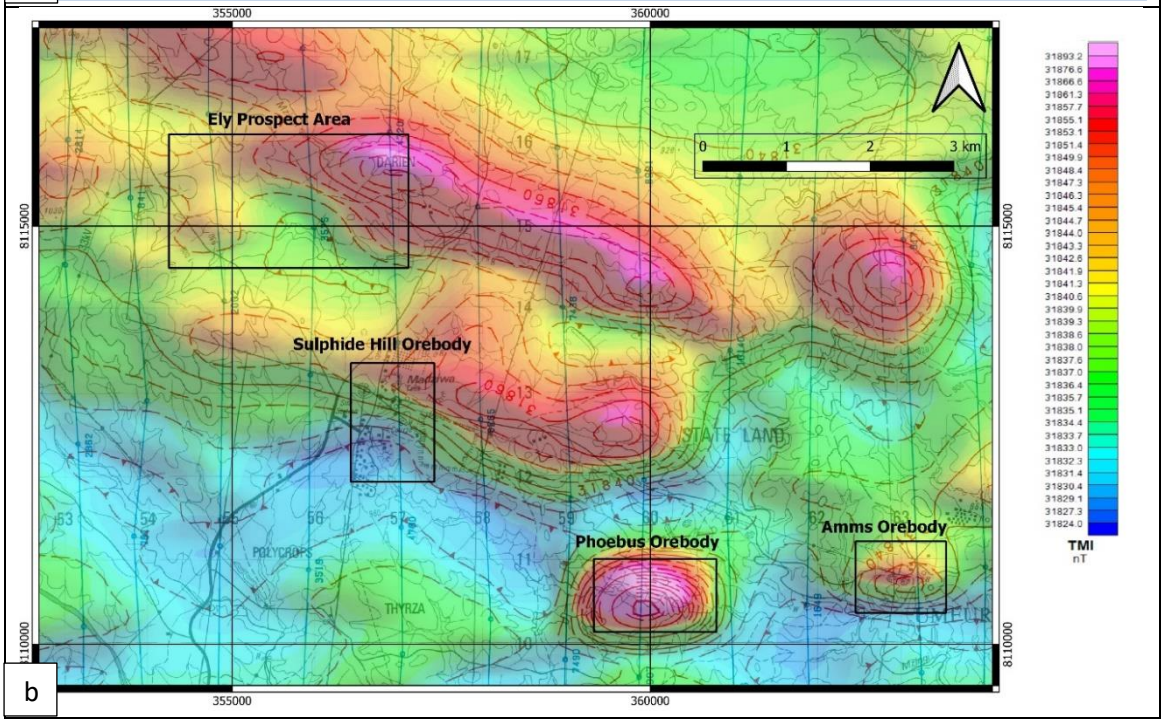
355000
360000
8115000
8110000
Ely Prospect Area
Sulphide Hill Orebody
Phoebus Orebody
Amms Orebody
0
1
2
3 km
TMI
nT
b

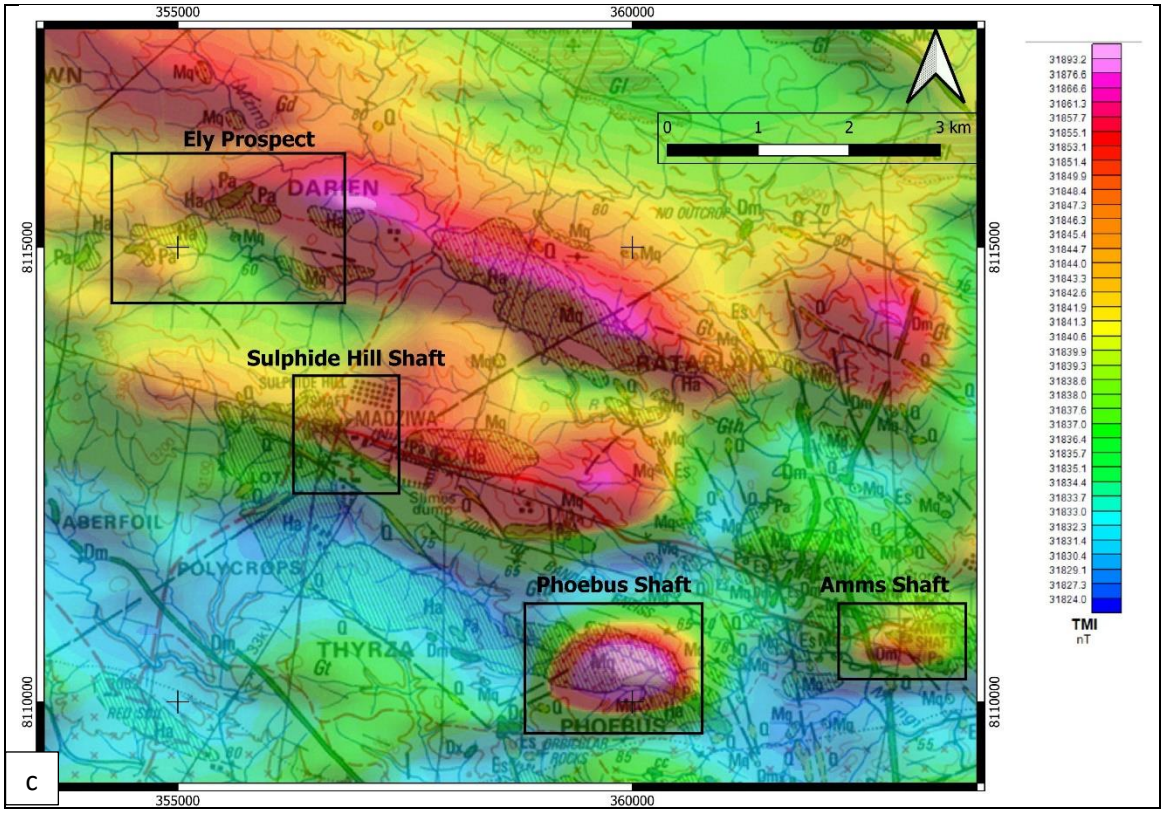

Figure 9: CIDA aeromag TMI for whole 1731 B1 Survey Block (a) ; (b) CIDA aeromag TMI plotted over the magnetic contours as published in the 1731 B1 hard copy map from the Zimbabwe Geological Survey; (c) CIDA aeromag TMI plotted over the Bulletin 78 Geology Map for the Madziwa area.

Note that the regional field (IGRF) was not subtracted from the TMI grid and that the results are presented in concordance with those shown on the hard copy B 1731 map of magnetic contours. The CIDA TMI shows a set of positive magnetic anomalies broadly coincident with the mapped positions and orientations of the Madziwa intrusive bodies of pyroxenite and norite. There is a distinct trend of positive anomaly magnetic "ridges" with their long axes oriented in a WNW to ESE direction associated with the intrusive bodies which host the Sulphide Hill and Ely mineralisation. Both of these known mineralised zones occur on the western edges of the positive magnetic ridges associated with their respective intrusive lenses, while circular positive magnetic anomalies are associated with the Phoebus and Amms orebodies.

3.3 Ground Magnetic Survey

A ground magnetic survey was carried out in 2021 during renewed brownfields exploration at the Ely prospect under the tenure of Associated African Nickel Resources PLC. This survey covered an area of 485 Ha and 110 line km at a line spacing of 25m and then 50m. A GSM-19 Overhauser Magnetometer, shown in Figure 10, was used as the rover and a GSM-19 Proton Precession Magnetometer as the base. The rover was set to automatically collect readings every second and a hand-held Garmin GPS synchronised to both the rover and the base magnetometers was used for navigation and tracking the walk lines marking waypoints every 5 seconds. The base station magnetometer was set up to monitor the diurnal variations collecting readings every 10 seconds. Sources of potential cultural noise such as

fences, powerlines, and homesteads were marked during data collection using the hand-held Garmin GPS.

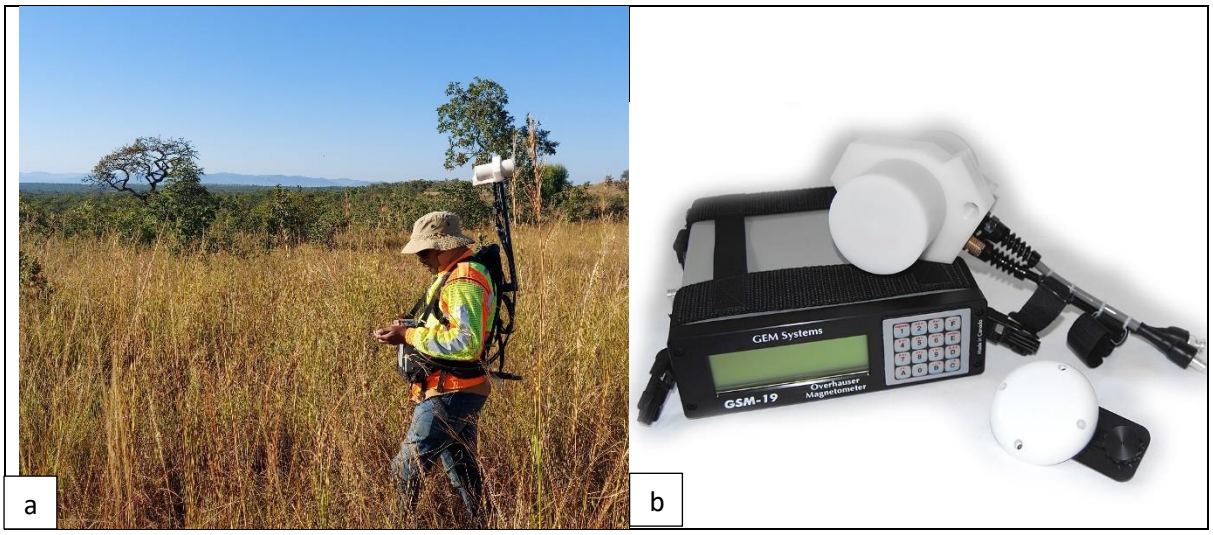

Figure 10: (a) ground magnetic data collection at Ely in 2021; (b) GEM Systems GSM-19 Overhauser Magnetometer used as the rover for data collection.

The ground magnetic survey grid was designed to cover the historical soil geochemistry anomalies and drill targets, as well as the surrounding mapped mafic and ultramafic intrusive bodies at Ely Prospect, ensuring sufficient coverage of surrounding gneissic country rock for collection of representative background readings. The ground magnetics survey at Ely was completed in 8 days.

Initially, a total of 136 survey lines, 1400m long were planned at 25m line spacing to ensure adequate resolution. Progressing from west to east, the first 78 lines which covered the known Ely anomalies and mineralised zones were surveyed at the planned line spacing of 25m. The line spacing was later increased to 50m for the remaining part of the grid. This translates to approximately 80% of the grid surveyed at 25m line spacing with the remaining 20% on the eastern side surveyed at 50m line spacing. This decision was taken after careful analysis of the data collected over the first 78 lines and post processing removal of alternating 25m spaced lines. This indicated that increasing the line spacing to 50m would not significantly detract from the final product resolution and would allow for earlier survey completion. Figure 11 (a) shows the spatial extent of the ground magnetic survey grid at Ely covering the historical anomalies with GPS track recorded walk lines plotted over the Bulletin 78 geology map, and (b) shows the same walk lines over the prospect-scale map from Prospecting Ventures reports showing change in line spacing and deviations due to human settlement obstacles. Note that in two areas, indicated in Figure 11 (b), deviations around small settlements and fenced gardens were unavoidable.

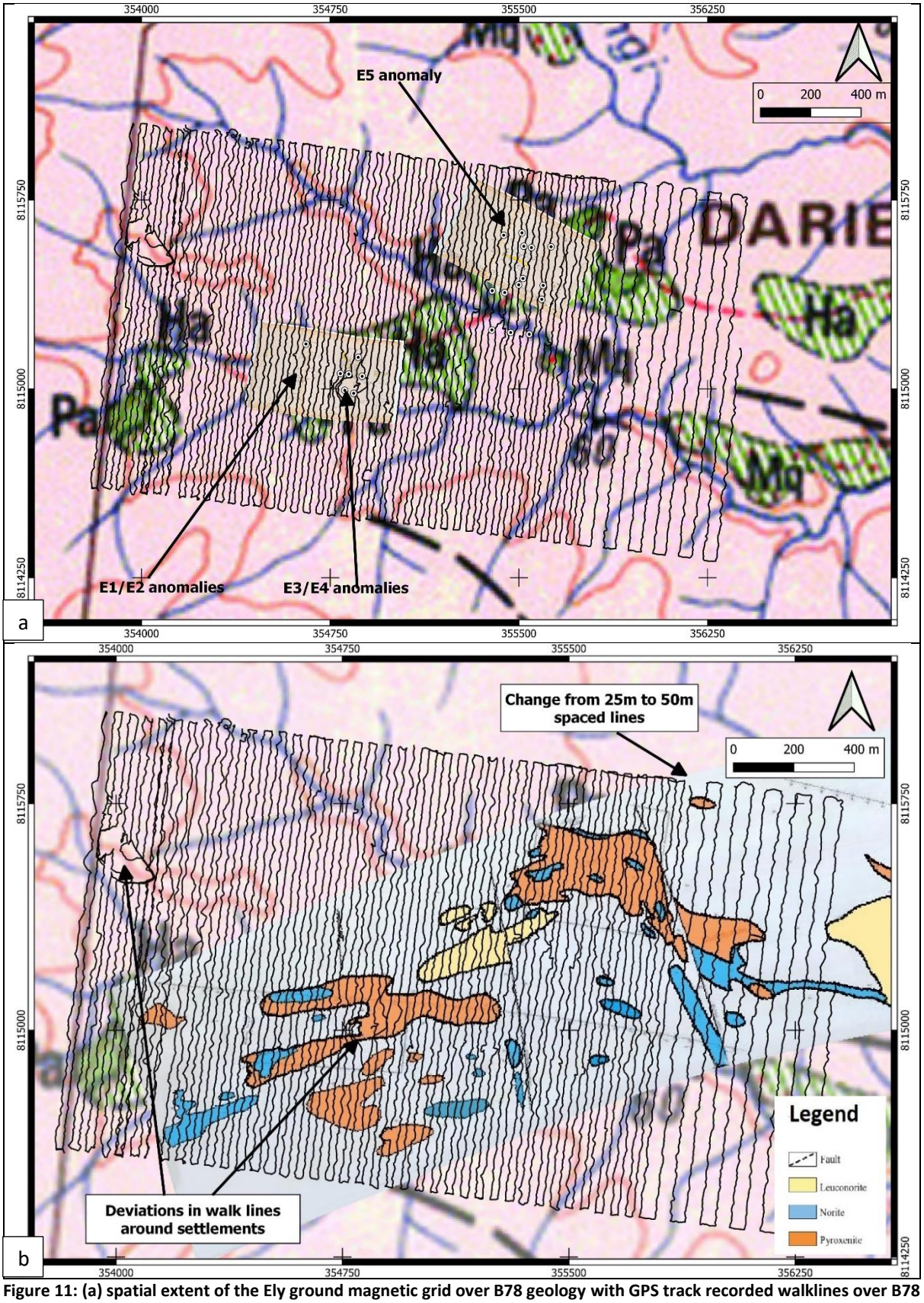

Figure 11: (a) spatial extent of the Ely ground magnetic grid over B78 geology with GPS track recorded walklines over B78 geology; and (b) the walklines over geology as mapped by Prospecting Ventures at Ely.

3.4 Moving Loop Ground Electromagnetic Survey

A detailed Moving Loop Time Domain Electromagnetic (MLEM) survey, the location of which is shown in Figure 12, was carried out at Ely over the E1/E2 and E3/E4 anomalies in July 2022. A total of 8 lines were surveyed at 50m line spacing and 25m station spacing. The target was justified by the historical soil geochemical anomalies, drilled mineralization, surface gossan occurrences, and the negative magnetic anomalies from the recent ground magnetic survey that appeared to be spatially correlated with the known anomalies.

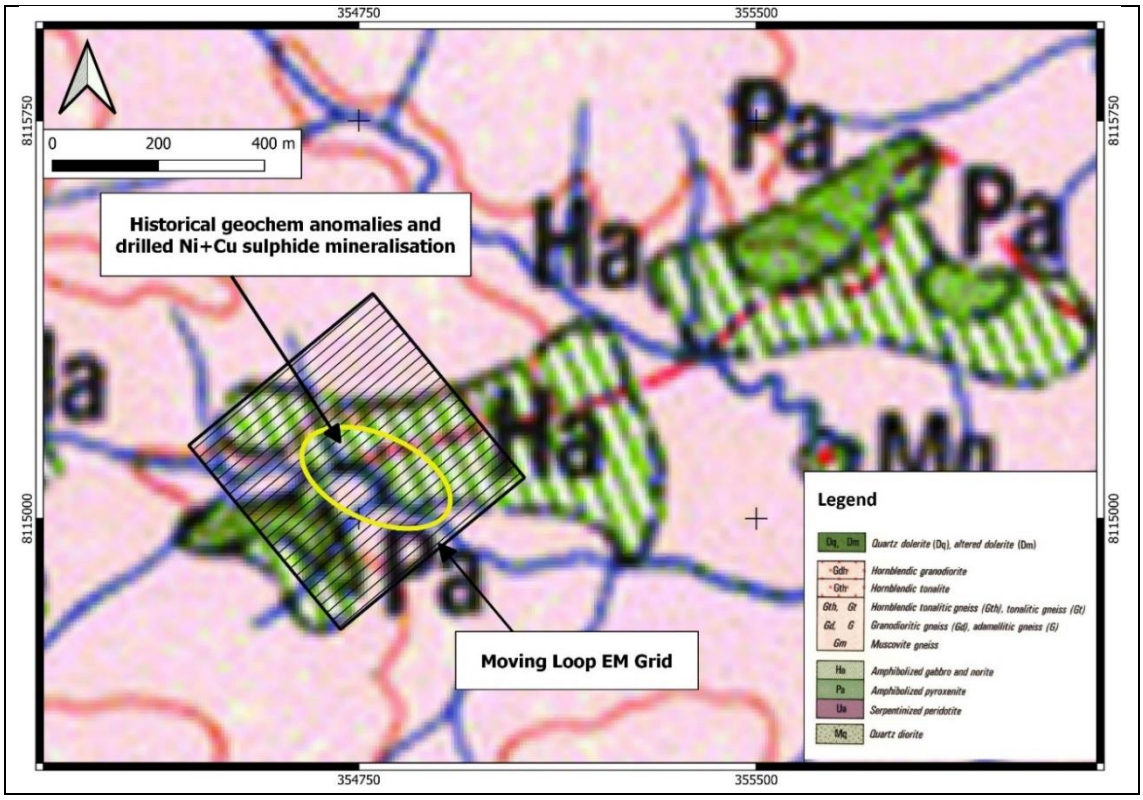

Figure 12: Spatial extent and position of the ground Moving Loop EM survey carried out in 2022 at Ely, relative to the B78 geology.

3.5 Survey Instrumentation

The ground EM survey was conducted with 100m square moving loops and EMIT's SMARTem24 receiver with a Smart Fluxgate magnetometer connected as sensor. A fluxgate is a B-field sensor that measures the time-integral of impulse response, which is called a "step response". This time integral serves to filter measured signal and attenuates faster decays, which are generally attributable to weaker conductors, in preference to slower decays which are more characteristic of strong conductors. This facilitates distinguishing and identifying the response from a good bedrock conductor which may otherwise be masked by the presence of weaker conductors, such as conductive overburden or adjacent bedrock features with innate but lower conductivity (Ushendibaba, 2016).

The data was acquired with a ZT30 transmitter supplying between 25A and 28A into a 100m x 100m moving transmitter loop at a base frequency of 0.5Hz. Three components X, Y, Z were measured at each station. By convention, X points along the survey line positive to the north, Y points perpendicular to the survey line positive to the west while Z is positive up.

4. Results

4.1 Physical Property Measurements – Magnetic Susceptibility and Conductivity

Physical property measurements on the Madziwa diamond drill core samples of selected lithologies produced a set of magnetic susceptibility values with a combination of expected and somewhat surprising results compared to published ranges for the rock types concerned. These are displayed in Table 1. Conductivity readings for the various lithologies were in line with expectations. The pyroxenite mineralised with massive sulphides displayed markedly stronger responses in terms of both magnetic susceptibility, with a mean of 68 SI x 10^{-3}, and electrical conductivity with a mean of 6001 S/m. This is unsurprising given the ferrimagnetic magnetic nature of pyrrhotite as the dominant sulphide species, and the conductive nature of sulphide grains that are interconnected in a massive sulphide dominated rock sample. The pyroxenite with disseminated sulphide mineralisation displayed slightly higher magnetic susceptibility than barren pyroxenite, but no conductivity response. This is also in line with the anticipated response in view of the relatively low abundance of sulphide in the rock with disseminated mineralisation and the degree to which sulphide grains are isolated within the rock matrix.

Table 1: Results table for physical property measurements of selected drill core samples (one per lithology) from various lithologies at Madziwa

Magnetic susceptibilities (SI x 10^{-3}) and conductivity (S/m) measured for drill core samples of selected lithologies from Madziwa					
Lithology	**Mag sus mean**	**Mag sus min**	**Mag sus max**	**Conductivity Mean**	**Number of readings per sample**
Gneiss	2.05	1.54	2.59	0	4
Leuconorite	1.77	0.79	2.49	0	4
Norite	1.95	0.91	2.88	0	4
Mineralized Pyroxenite (Massive sulphides)	68.03	54.5	97.2	6001 (*7951 max and 4607 min*)	4
Mineralized Pyroxenite (Disseminated sulphides)	1.39	0.8	2.34	0	7
Unmineralized Pyroxenite	1.26	0.85	1.8	0	11
Dolerite	58.02	39.9	69.7	0	4

The selected Madziwa drill core specimens measured for magnetic susceptibility and conductivity were photographed and are displayed in Figures 13 (a) to (g).


a
b
c
PHOTOGRAPHIC SCALE
B/W / COLOUR
GEO EXPLORE STORE
GEO-EXPLORE STORE (PTY) LTD
Cell - 082 744 7594
Fax - 086 580 7392
e-mail: denis@geoexplorestore.co.za
web: www.geoexplorestore.co.za


PHOTOGRAPHIC SCALE
B/W / COLOUR
GEO EXPLORE STORE
GEO-EXPLORE STORE (PTY) LTD
Cell - 082 744 7594
Fax - 086 580 7392
e-mail: denis@geoexplorestore.co.za
web: www.geoexplorestore.co.za

d


PHOTOGRAPHIC SCALE
B/W / COLOUR
GEO EXPLORE STORE
GEO-EXPLORE STORE (PTY) LTD
Cell - 082 744 7594
Fax - 086 580 7392
e-mail: denis@geoexplorestore.co.za
web: www.geoexplorestore.co.za

e


PHOTOGRAPHIC SCALE
B/W / COLOUR
GEO EXPLORE STORE
GEO-EXPLORE STORE (PTY) LTD
Cell - 082 744 7594
Fax - 086 580 7392
e-mail: denis@geoexplorestore.co.za
web: www.geoexplorestore.co.za

f



g

Figure 13: (a) gneiss; (b) norite; (c) mineralised pyroxenite with massive sulphides; (d) mineralised pyroxenite with combination of net textured and disseminated sulphides; (e) unmineralised (barren) pyroxenite; (f) dolerite; and (g) leuconorite.

The dolerite sample also exhibited markedly higher magnetic susceptibility, which is a known and reported property of the Mashonaland Dolerite dikes in Zimbabwe. The relatively low magnetic susceptibility of the unmineralized pyroxenite, compared to the other rocks such as the gneiss and the norite, is surprising. This rock type would be expected to have a comparatively higher magnetic susceptibility due to the paramagnetic properties of pyroxene, and the likely presence of small amounts of interstitial magnetite within the rock matrix. This finding is confounded by the observation that pyroxenite bodies mapped in the field appear to coincide spatially with the magnetic highs in the CIDA and ground magnetic survey results.

4.2 Ground magnetic survey results

The Total Magnetic Intensity results are presented below, followed by presentation of various enhancement products and filters applied to the magnetic data which are intended to emphasize different aspects and features of the magnetic data, and assist in the final interpretation of the magnetic survey maps.

4.2.1 Ely Total Magnetic Intensity (TMI) Results

The Total Magnetic Intensity (TMI) data was diurnally corrected and the gridding was performed using Geosoft Oasis Montaj software. Obvious spikes spanning only a few readings and related to cultural noise (systematically recorded during data collection) were identified and removed from the database. This is true for all cultural noise spikes other than those related to an overhead powerline, running southeast to northwest through the Ely survey grid, which is clearly visible in the TMI image. The regional field International Geomagnetic Reference Grid (IGRF) for May 2021 was calculated and subtracted from the TMI data. Figure 14 shows a profile of the base station data as recorded over the duration of the ground magnetic survey at Ely, with stable diurnal variations of 5nT to 20nT.

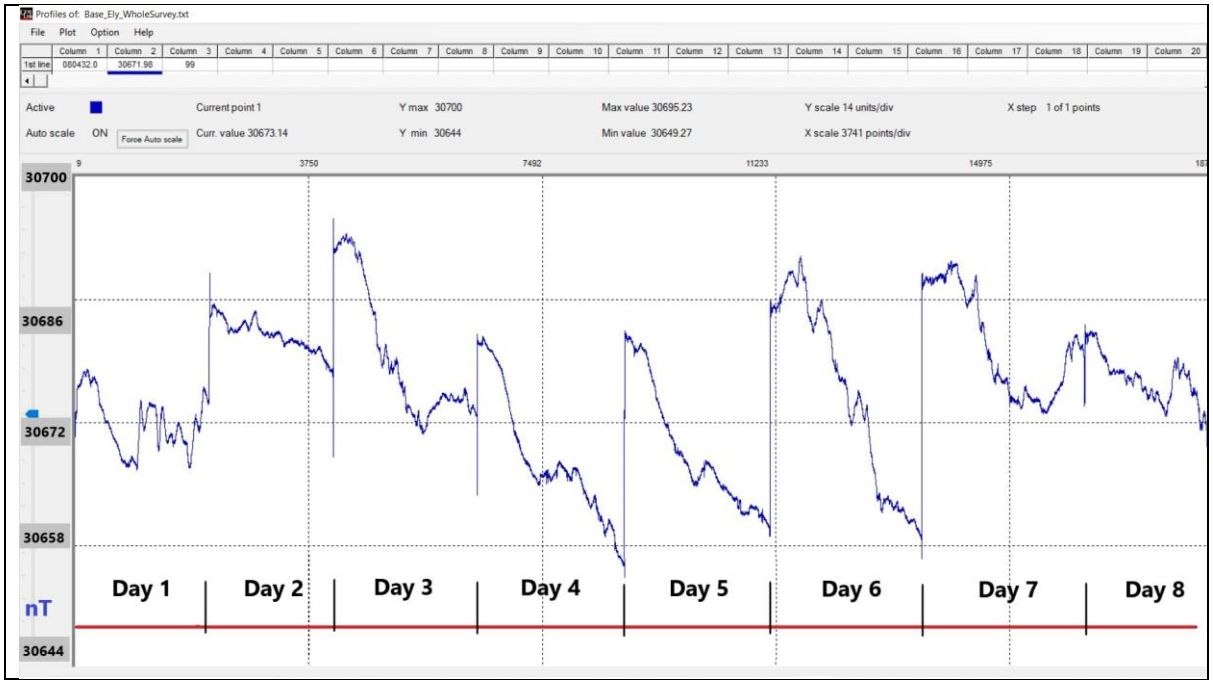

Figure 14: Profile showing base station data over the course of the ground magnetic survey. Note the small range of values on the y-axis showing stable diurnal variations of between 5 nT and 20 nT over the course of a day's survey.

The base station data shows that there were no unusual perturbations in the earth's magnetic field during the acquisition of the ground magnetic survey data.

The map in Figure 15 (a) shows the TMI grid after upward continuation by 15m and decorrugation operations to remove the stripiness associated with high frequency noise typically generated by the sensor being close to the ground. The levelled and smoothed TMI data shown in Figure 15 (a) have a geometric colour stretch applied, while the TMI image in Figure 15 (b) shows the TMI data with a linear colour stretch applied, facilitating comparison of relative anomalies:

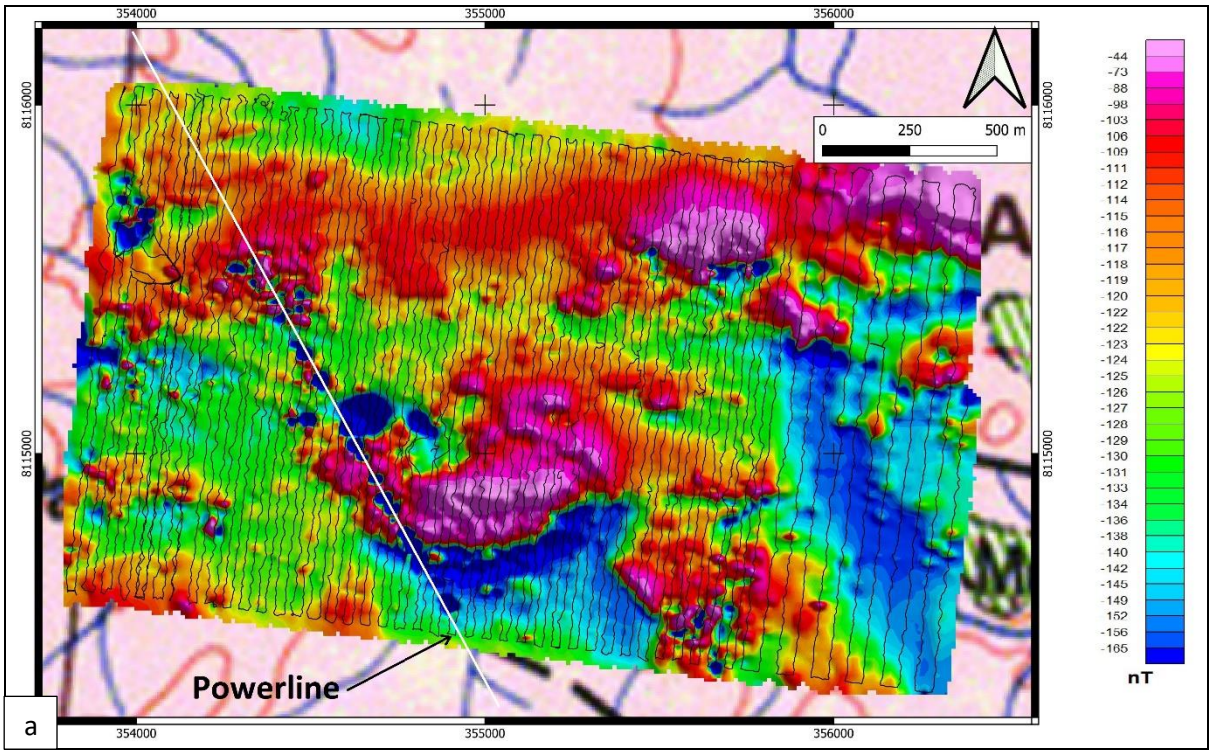

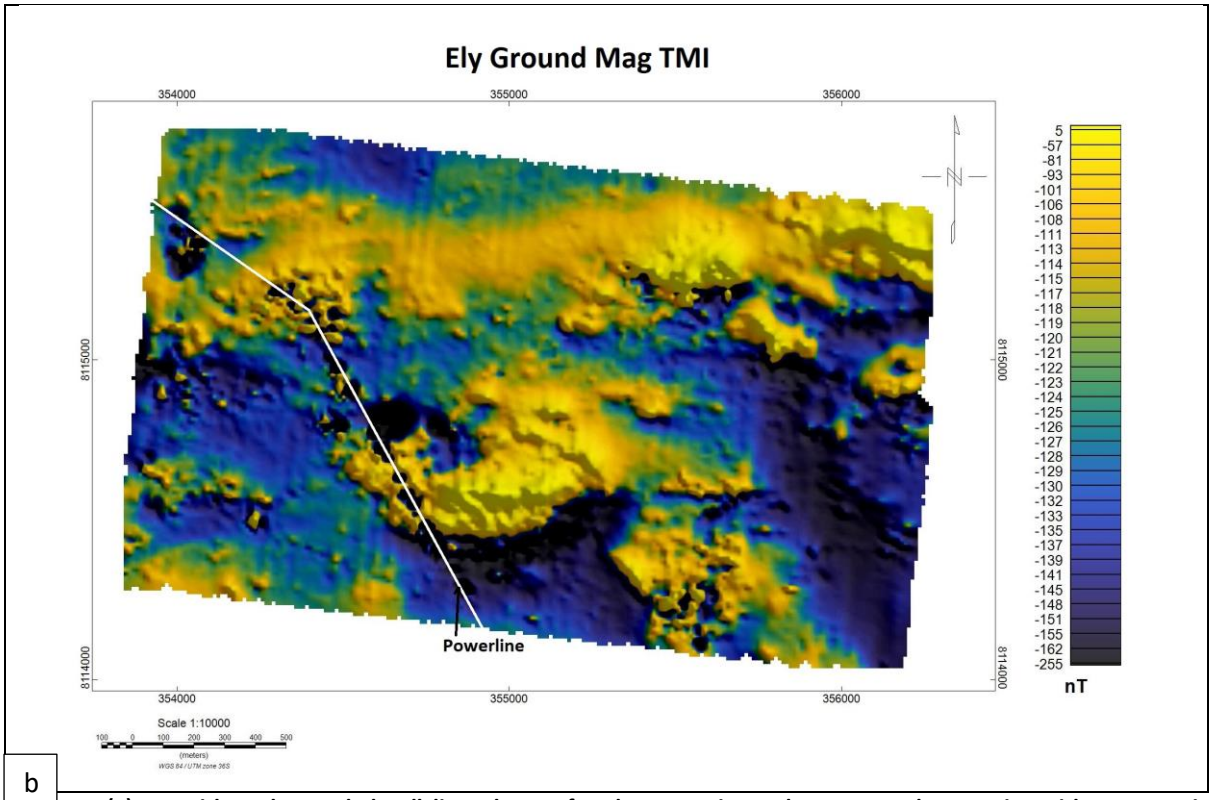

Figure 15: (a) TMI with track recorded walk lines shown after decorrugation and 15m upward contuation with a geometric colour scale applied; (b) the TMI with a perceptually uniform linear colour scale.

The different colour scales applied in Figure 15 (a) and (b) show up the relative intensities of magnetic responses differently. The variations which produce positive and negative (magnetic highs and lows) anomalies and dipoles in the TMI, are indicative of changes in the relative abundance of magnetite and other magnetic minerals present in the subsurface bedrock and unconsolidated regolith. If these variations are consistent for particular lithologies, as one might expect for a suite of intrusive igneous rocks with a common parent magma, the amplitudes of magnetic anomalies relative to the regional background may be used to identify specific rock units by their magnetic signature and enable their approximate extents to be defined.

It is posited that the ultramafic pyroxenites, and to a lesser extent the mafic norites, are producing dipoles with positive magnetic anomalies in the order of 50nT to 400nT relative to background which is characterised by magnetically quiet gneiss with a muted magnetic response. The historically mapped outlines of leuconorite intrusive rocks also appear to be associated with an absence of any distinct magnetic anomalies. Clearly visible in the TMI image is a northwest trending linear feature. This is cultural noise from an overhead powerline, and it has a minor obscuring effect on the expression of magnetic anomalies immediately to either side of it.

4.2.2 Filters and enhancements of TMI

Various filters and enhancements can be applied to the TMI data in order to emphasize particular features. The Reduction to Magnetic Pole (RTP) operator transforms magnetic anomalies from the inclined magnetism of non-polar regions (Madziwa is at latitude 17° south) into their equivalent polar response where a body's magnetism is vertical (Dentith and Mudge, 2014). It effectively replaces the

dipoles appearing in the TMI with monopoles centred directly above their sources. The RTP image for Ely is shown in Figure 16 (b). A drawback of the RTP operator is that it assumes all magnetic sources to be induced by the earth's magnetic field and therefore is prone to distorting the appearance of bodies with remanent magnetism. This may be pronounced for strong remanence and/or where the direction of remnant magnetism is significantly different from the Earth's magnetic field (Dentith and Mudge, 2014).

Another filter commonly applied to the TMI data is the Analytic Signal (AS) filter. Figure 16 (c) shows the AS product of the Ely grid. It performs a transformation which combines the three directional gradients of the magnetic field for a given location. It is effective at delineating geological boundaries and resolving closely spaced bodies to produce more detailed magnetic texture (Dentith and Mudge, 2014). Similar to the RTP operator, it centres the anomalies over their sources but "inverts" negative anomalies since it is dependent on the strength and not direction of a body's magnetism (Dentith and Mudge, 2014). The AS enhancement is thus independent of the inclination of the geomagnetic field, and hence there are no negative values in the AS colour scale.

The first vertical derivative (vertical gradient), or 1VD, is physically equivalent to measuring the magnetic field simultaneously at two points which are vertically above each other, subtracting the data and dividing the result by the vertical spatial separation of the measurement points (Dentith and Mudge, 2014). It emphasizes shallow bodies in preference to deeper seated, broader features that produce small changes or gradients in the magnetic fields and is shown for the Ely grid in Figure 16 (d). The tilt derivative filter (TD) is also effective at enhancing subtle shallow magnetic anomalies which may not otherwise stand out in the TMI image and is shown for the Ely grid in Figure 16 (e).

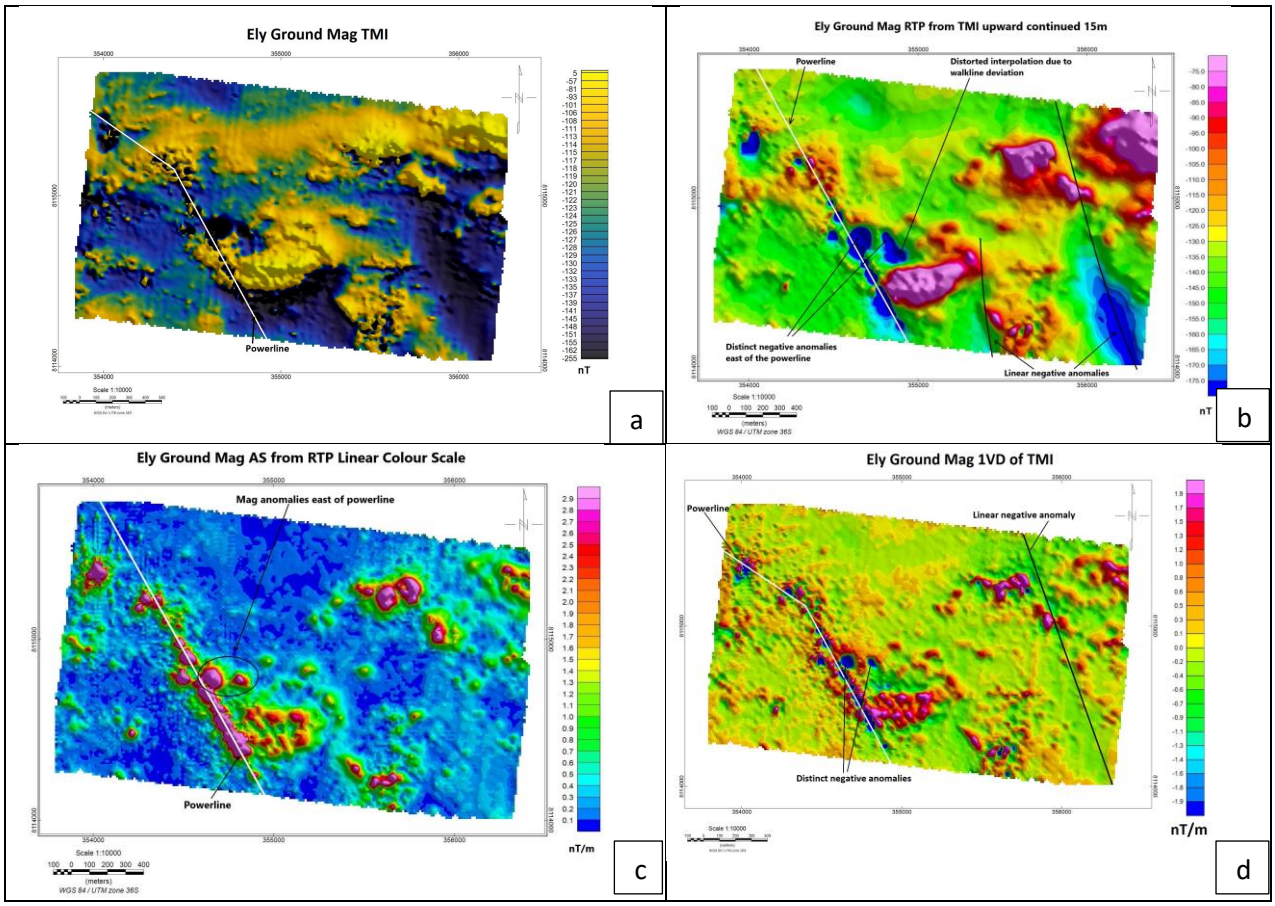

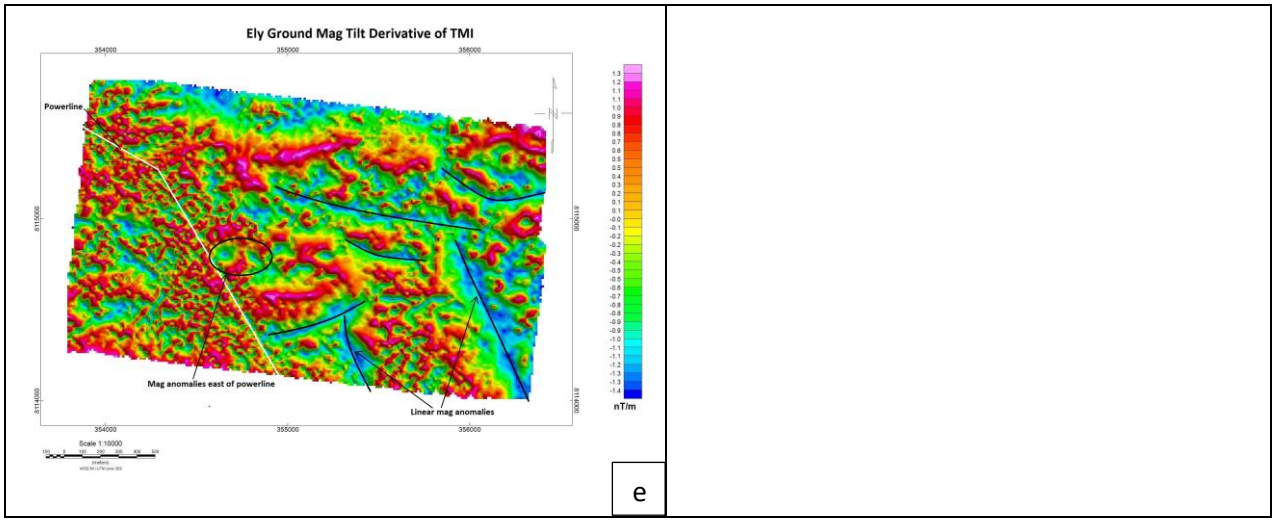

Figure 16: Ely TMI shown in (a), RTP (b), AS (c),1VD (d) and TD (e) filter products or enhancements with annotations showing relevant features.

The RTP map more accurately defines the centres and edges of the positive magnetic anomalies associated with the ultramafic intrusions and resolves negatively anomalous linear features from the adjacent magnetic lows of dipoles shown in the TMI map. This is useful for the mapping of extensive structures such as north-northwest trending faults. Faults are commonly associated with the destruction of magnetisation due to hydrothermal fluids altering the original magnetic fabric of the rock surrounding margins of faults. Distinct, elliptical shaped, negative magnetic anomalies are still apparent immediately to the east of the powerline, though a gap in the data caused by a deviation around a small homestead unfortunately distorts and smears the more eastern negative anomaly.

The AS enhancement of the Ely RTP data clearly shows some internal variation of the magnetic intensity within the magnetic anomalies associated with the pyroxenite bodies. It also helps to spatially define the two distinct anomalies immediately east of the powerline. There is some introduction of artifact in the western portions of the filter product.

The 1 VD filter of Ely TMI enhances higher frequency, near-surface responses over lower frequency, longer wavelength signals. Some “stripiness” oriented in the direction of the walk lines is more pronounced. The two elliptical negative magnetic anomalies immediately east of the powerline are still clearly expressed, as are the linear negative anomalies associated with the NNW trending faults.

The TD filter shows a number of linear to curvilinear structural features, including some which are clearly evident in the other filter products, as well as some that are only apparent in this filter. The edges of the two magnetic anomalies to the east of the powerline are clearly shown up by the zero-value contour of the map’s colour scale, and this is valuable in informing further exploration decisions.

4.3 Magnetic Profile Lines

Three magnetic profile lines are drawn over the magnetic anomalies at Ely with the objective of comparing the magnitude and resolution of the anomalies observed in the CIDA aeromagnetic survey results of 1983 with those of the ground magnetics survey carried out in 2021. The positions of the profiles, oriented on a bearing of 008° east of north, are shown in Figure 17 (a) and (b) depicting the

gridded CIDA magnetic data and ground magnetic data grids respectively with the same three profile lines displayed.

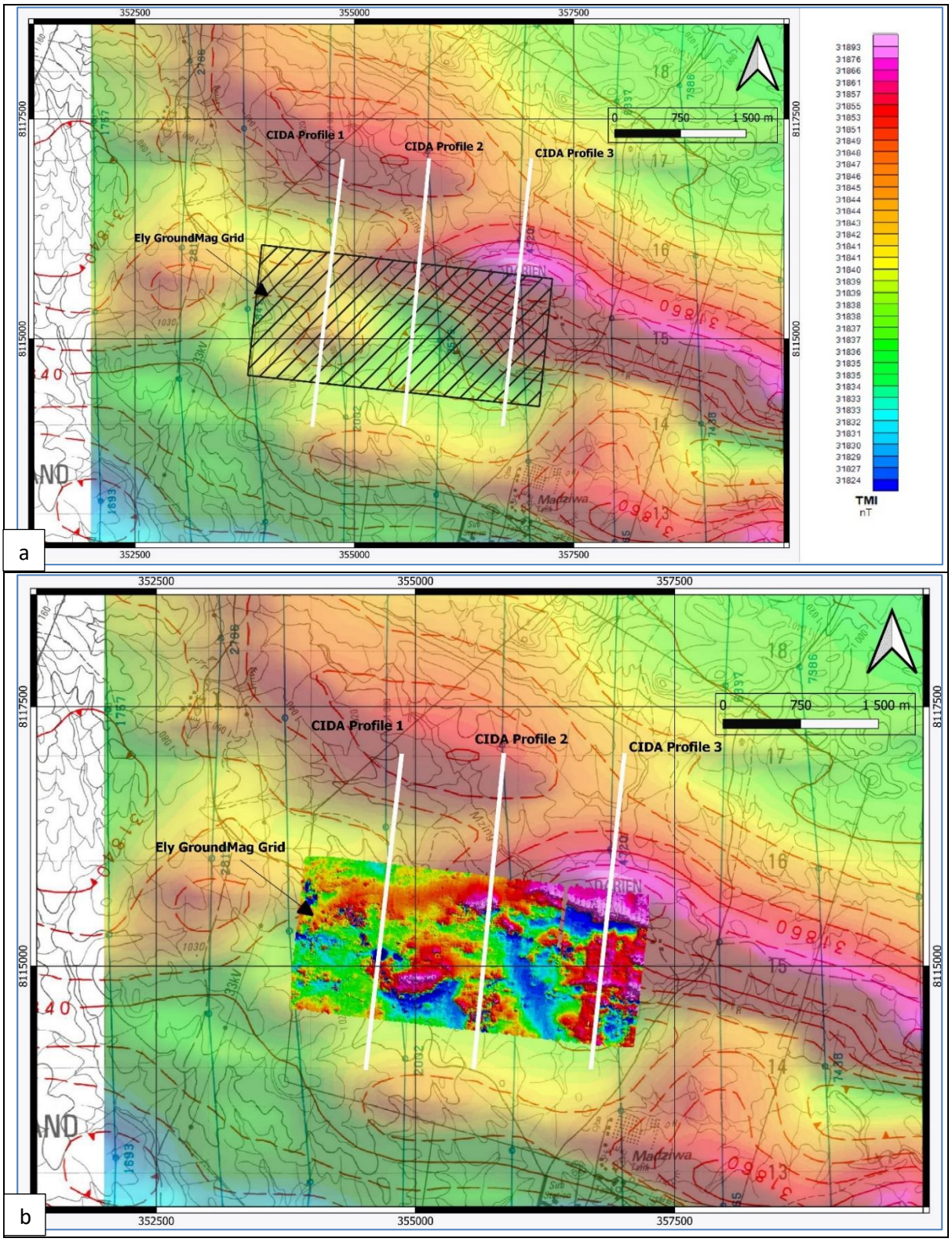

Figure 17: Magnetic profile lines over (a) CIDA aeromagnetic TMI with extent of the ground magnetic survey grid shown; and (b) the same profile lines over CIDA aeromagnetic TMI with the groundmag TMI superimposed for reference.

Profiles 1 to 3 of CIDA TMI were constructed manually in QGIS by generating a profile across digitized TMI contours of the hardcopy 1731 B1 airborne magnetic map. Note that the profiles over the CIDA

TMI at Ely are approximately 3000m in length and are intentionally drawn that length in order to show any noticeable changes in the TMI mapped by the airborne survey. The profiles of the ground magnetic data, while oriented along the same profile lines as for the CIDA TMI map, are approximately half that length at only 1450m long. The start and end of overlapping sections of the profile lines are indicated by red arrows in Figures 18 (a), 19 (a) and 20 (a). TMI profiles for Profile line 1 are displayed in Figures 18 (a) to (c) below.

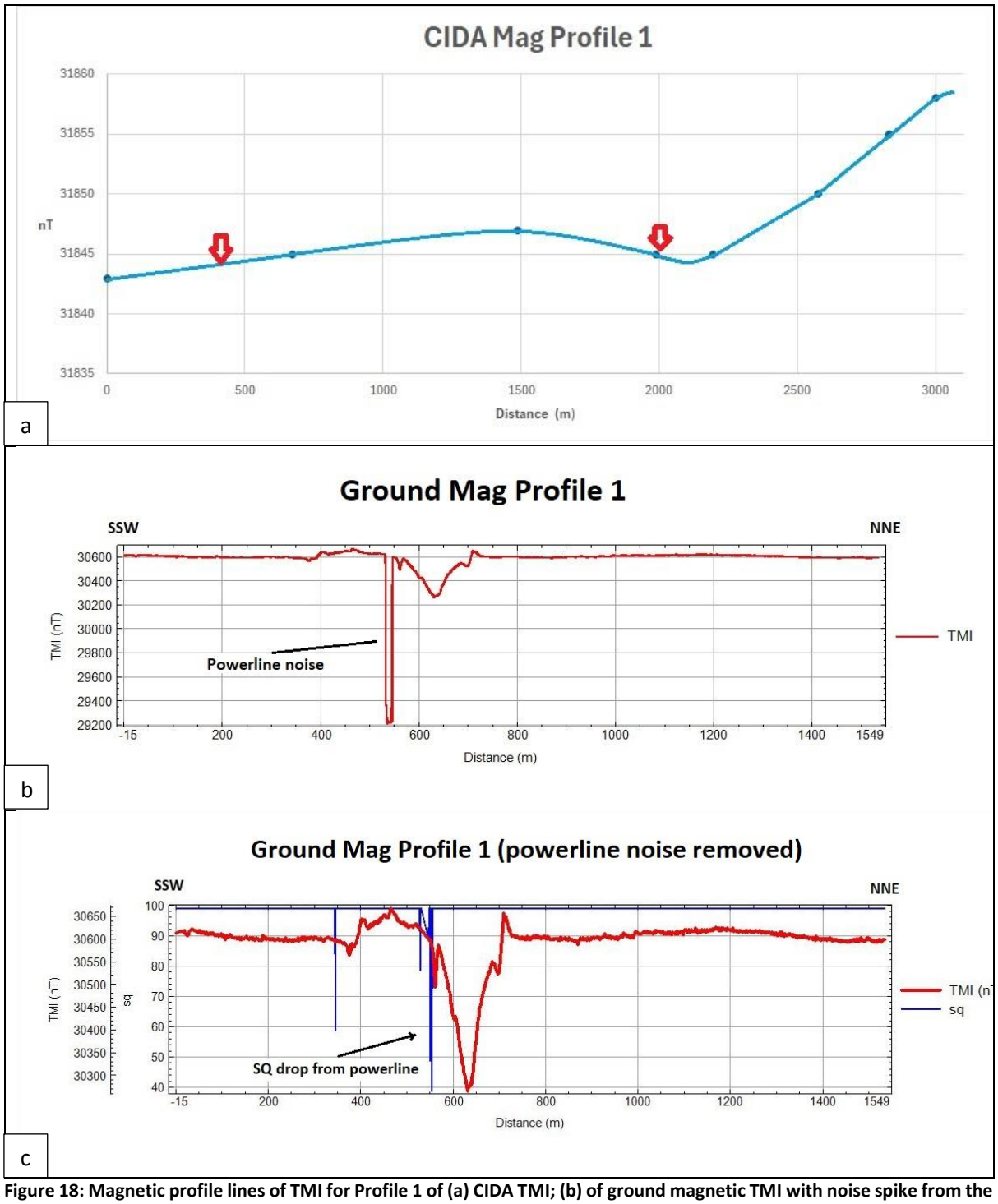

Figure 18: Magnetic profile lines of TMI for Profile 1 of (a) CIDA TMI; (b) of ground magnetic TMI with noise spike from the powerline deliberately kept in the data; and (c) of the ground magnetic TMI with the noise spike from the powerline cleaned from the data. Note that the red arrows on (a) indicate the start and end points of the profile extent for the ground magnetic TMI shown in (b) and (c).

CIDA Profile 1 shows a very muted rise and fall in the range of less than 10nT over the 1450m line extent of Ground Mag Profile 1. Ground Magnetic Profile 1 in Figure 18 (b) and (c) shows much more detail with a 400nT range in measured TMI. A pronounced negative magnetic anomaly is observed, flanked by small positive peaks. Figure 18 (b) of Ground Magnetic Profile 1 shows a very large negative spike associated with the powerline in the survey grid. Figure 18 (c) of Ground Magnetic Profile 1 shows the same profile with the spike from the powerline removed from the TMI with the y-axis adjusted accordingly. The SQ curve is shown for reference to indicate the position of the deleted powerline spike. SQ is a parameter that the magnetometer records to indicate signal quality where values below 90 typically indicate interference from proximal cultural noise. The two ground mag profiles illustrate the effect that a powerline (or other similar cultural noise) can have when displaying magnetic data. Figure 19 (a) and (b) shows Profile 2 results for the CIDA TMI and the ground magnetic TMI respectively.

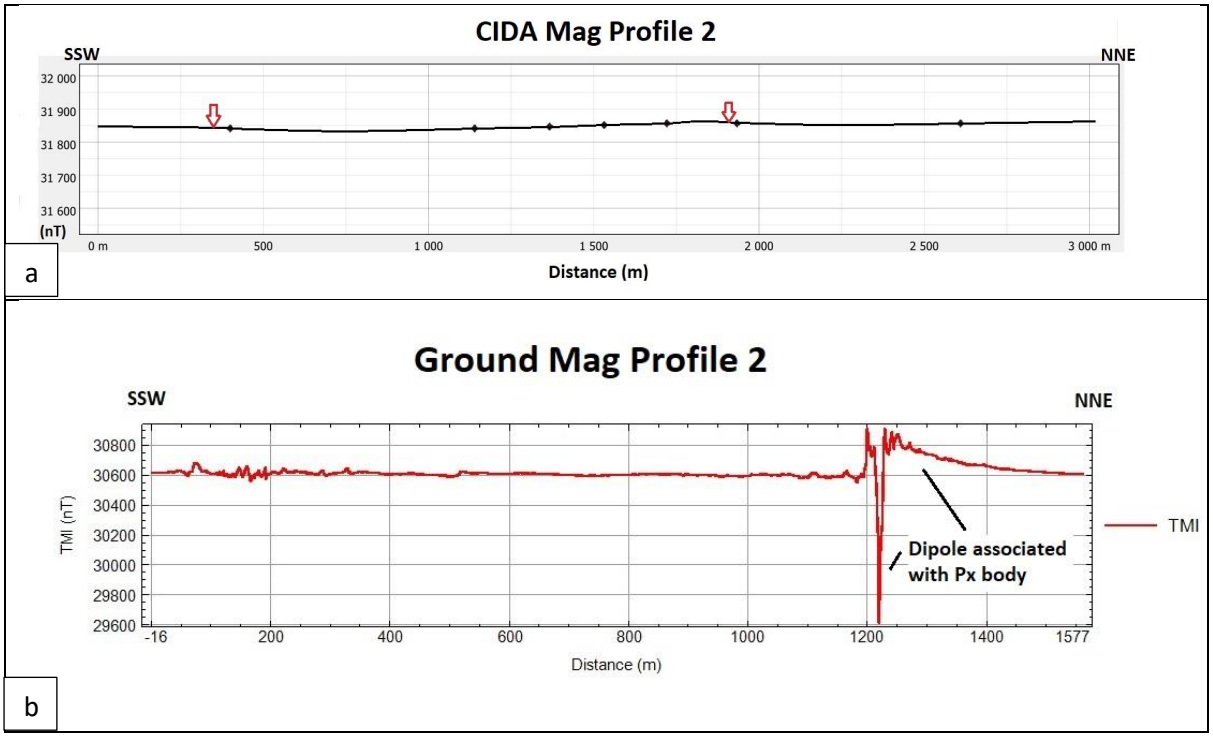

Figure 19: Profile 2 results showing the TMI magnetic profiles for CIDA TMI (a) and ground magnetics TMI (b) at Ely.

CIDA Magnetic Profile 2 shows a muted dip and then rise to a slight peak, with a TMI range of slightly over 15nT. Ground Magnetic Profile 2 shows fairly level TMI measurements around 30600 nT up to 1100m and then a large dipole with a TMI range of greater than 1200nT near the northern end of the profile line. This is inferred to be the response of the magnetic pyroxenite body underneath. This registers as a mere 15nT peak in the CIDA TMI data. Figure 20 (a) and (b) shows the respective TMI profile lines over Profile Line 3 at Ely.

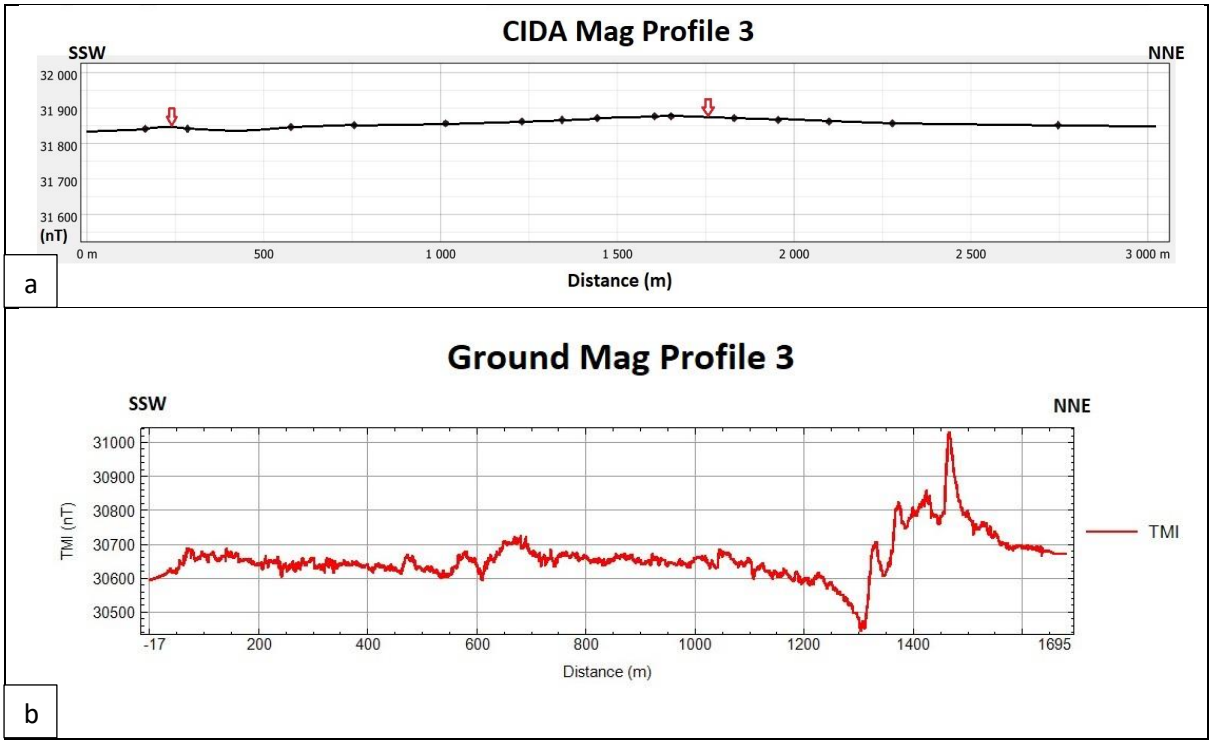

Figure 20: Profile 3 results for TMI magnetic data (a) of the CIDA TMI and (b) of the ground magnetic survey TMI.

CIDA Magnetic Profile 3 shows the largest range of the three airborne mag profiles with a greater than 35nT range, with a distinct peak over the magnetic "high" ridge on the eastern side of the Ely survey area. Ground Magnetic Profile 3 by comparison shows far more detail in the TMI with a 500nT dipole on its northern end over the same positive magnetic ridge, a response considered likely to representative of pyroxenite body underneath.

The magnetic profiles demonstrate the value of a targeted ground magnetic grid in revealing the magnetic character of the geology at Ely and its use for mapping prospect-scale features compared to those that are revealed in the airborne regional survey. Particularly relevant in the context of this exploration programme is the negative anomaly delineated in Ground Magnetic Profile 1. It is worth noting that the flight direction of survey lines for the CIDA airborne survey was sub-parallel to the general strike of the magnetic bodies at Madziwa, and that if the lines had been flown in a north south direction parallel to the ground magnetic survey lines, the CIDA TMI may have shown greater variation. The comparison also demonstrates the importance of noting sources of cultural noise (the powerline in this instance) so that their effects on the TMI data may be considered while analysing and processing the data.

4.4 Moving Loop EM Results

The geology of the area is generally electrically resistive implying very low signal levels for a Time Domain EM survey. However, any sulphide body where the constituent sulphide grains and accumulations are sufficiently interconnected to be conductive, would be expected to produce a distinct response. The mineralisation from known orebodies elsewhere at Madziwa is characterised by steeply dipping to sub-vertical, relatively narrow massive sulphides in veins (not present in all orebodies) and a surrounding halo of net textured and disseminated nickel sulphide ore. Ore body

dimensions vary widely between 50m and 250m in strike length and can exceed 900m in depth extent, as is the case at Sulphide Hill. Ore bodies with these orientations and dimensions are expected to produce relatively low signal levels and require close spacing between survey lines to detect and map the signature of such an orebody. Figure 21 shows the location of the MLEM grid relative to the ground magnetic survey grid.

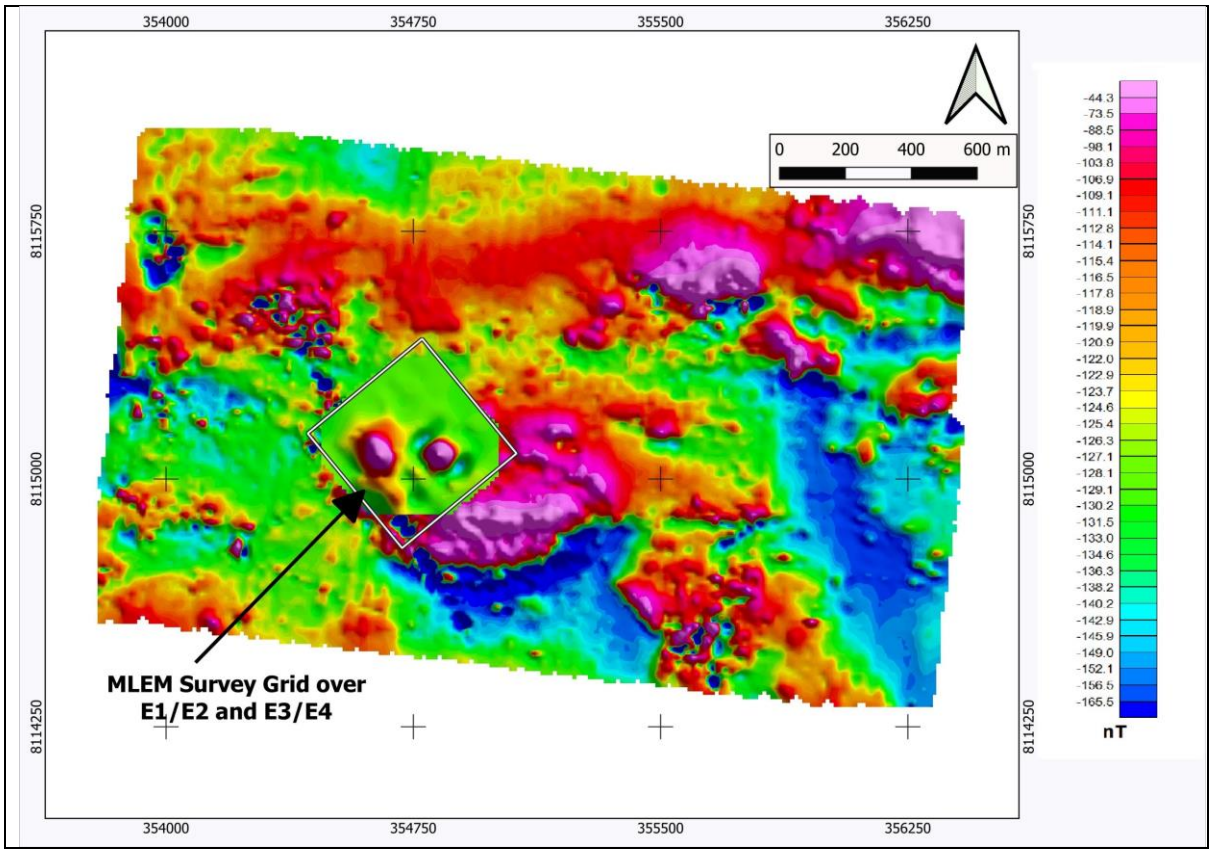

Figure 21: Location map of MLEM survey grid overlaid on the TMI map for reference

The MLEM results over targets E1/E2 and E3/E4 clearly show two conductive zones coincident with the historical geochemical anomalies and drilled mineralization. The results for each channel are summarized in Table 2 alongside the gridded images of each channel.

Table 2: Summary table of EM gridded images for Channels 15Z through 39Z, from early time responses to late time responses of the bedrock conductors at E1/E2 and E3/E4 MLEM survey grid

Channel 15Z The Z component for Channel 15 was gridded in Oasis Montaj. Two highly conductive zones were mapped out which coincide spatially with historical geochemical anomalies and drilling carried out on E1/E2 and E3/E4 mineralised zones. The E1/E2 anomaly also coincides with a mapped gossan outcrop and abundant float.	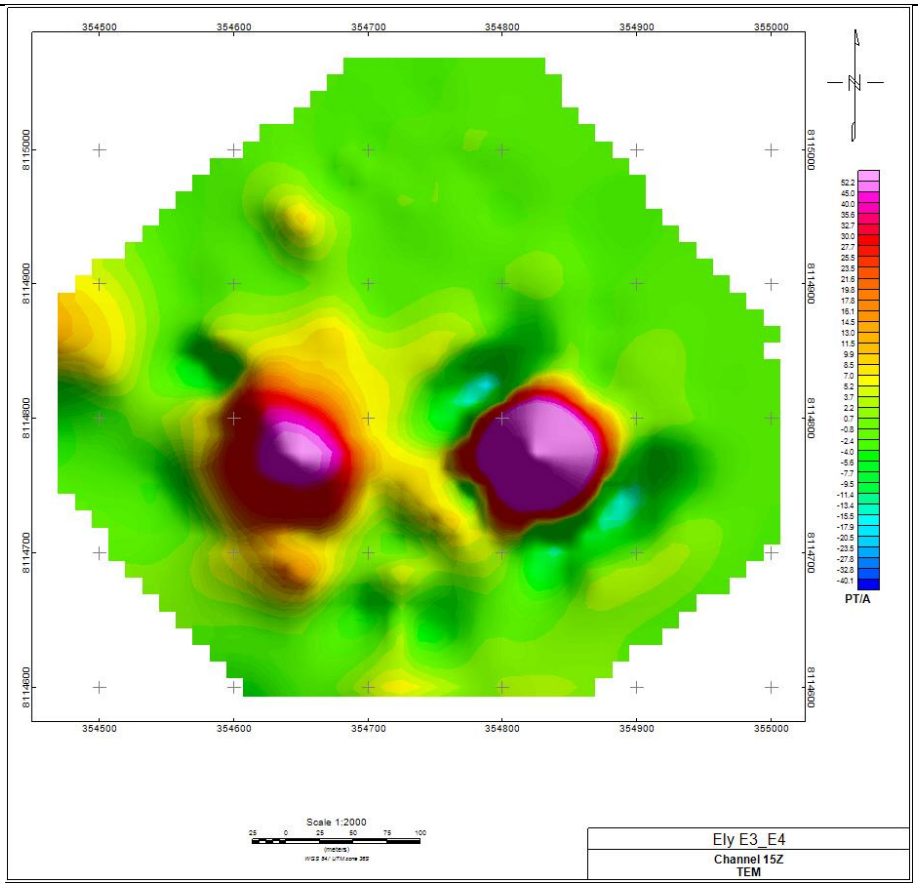
Channel 20Z Channel 20 Z-component, which shows mid-time responses, was also gridded. The two conductive zones were similarly mapped out in this channel.	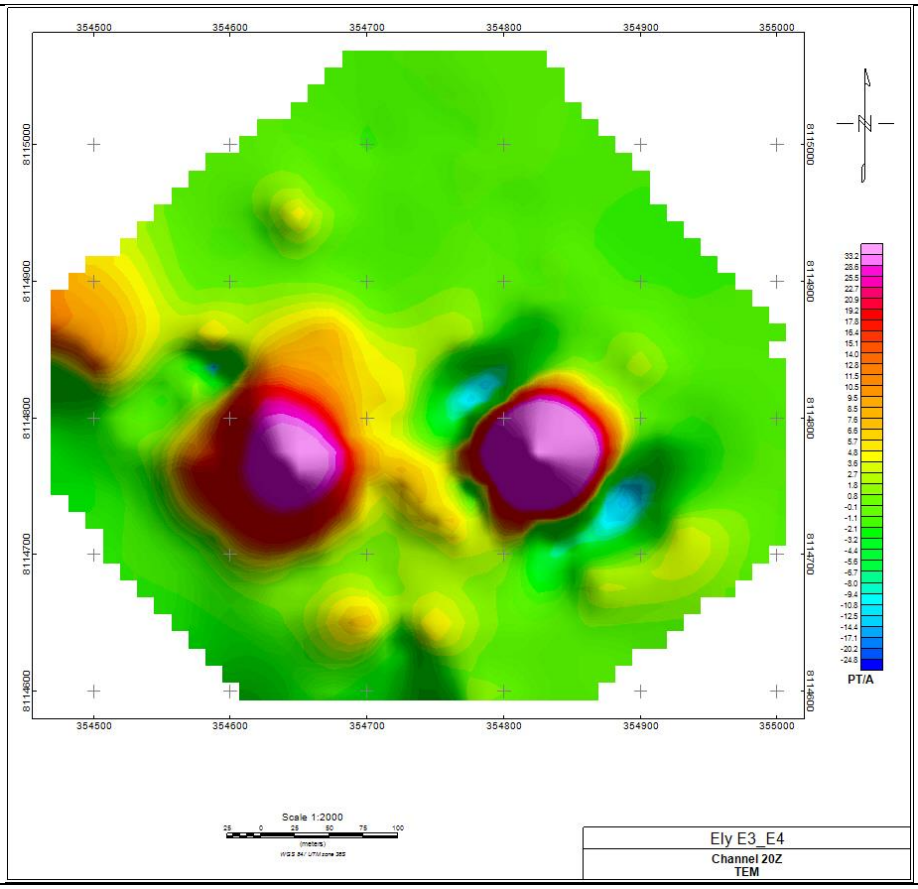

Channel 25Z

Channel 25Z, which falls within the mid to late times category, was gridded. The two mapped conductive zones are still apparent.

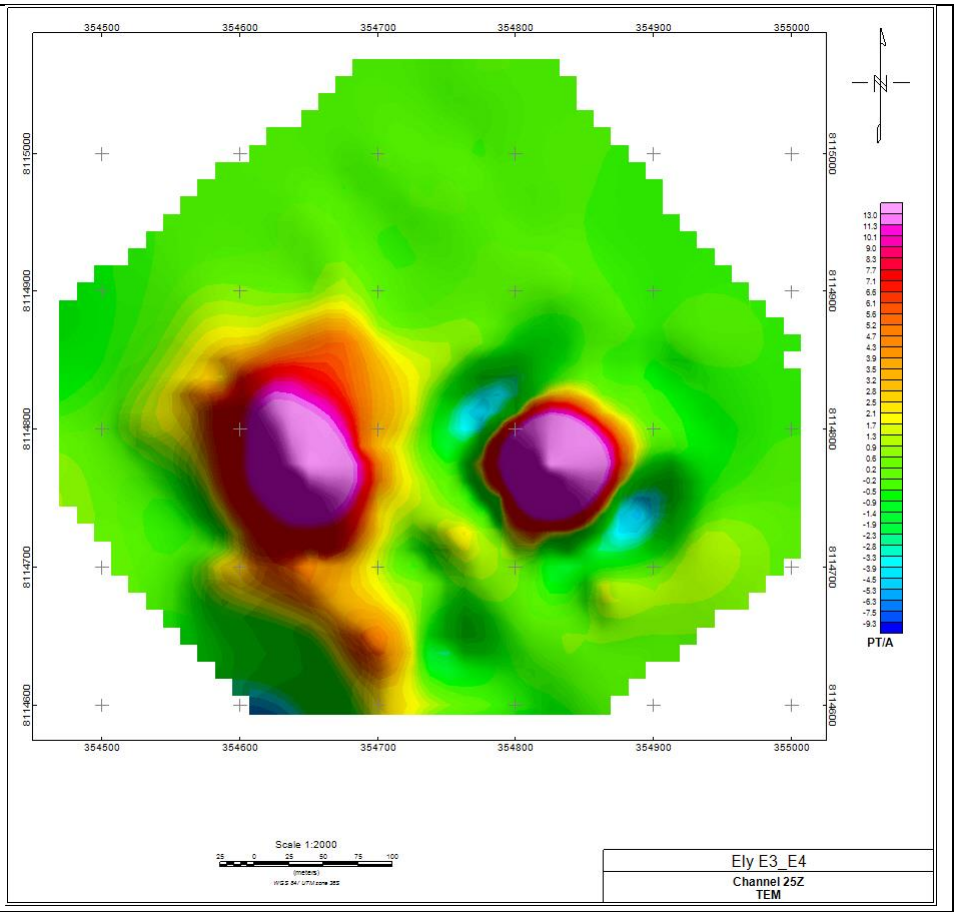

Channel 30Z

Channel 30 Z-component which falls within the late times category, was gridded. The two mapped conductive zones are still observed, though the eastern zone is less pronounced, while the western conductive zone is more pronounced.

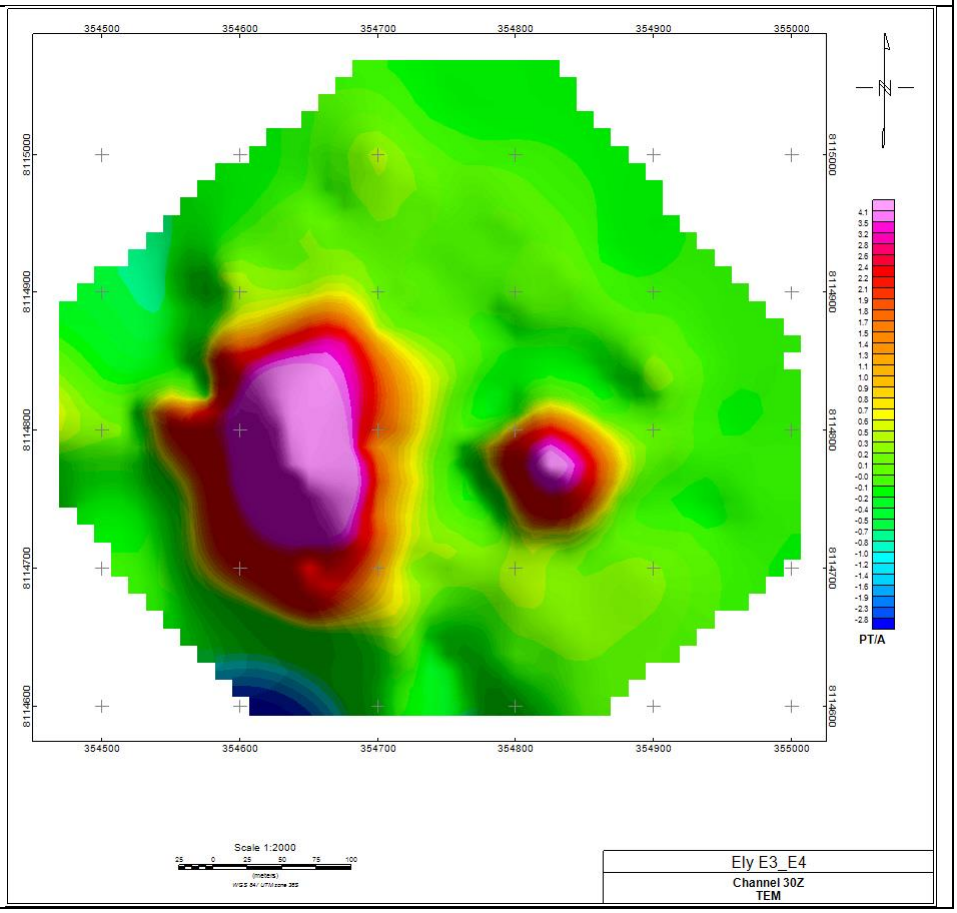

Channel 35Z

Channel 35 Z-component, reflecting the very late time responses, was gridded. The eastern conductive zone over E3/E4 is no longer expressed, but the western zone over E1/E2 is strongly pronounced, indicating that the western zone may be more conductive than the eastern zone.

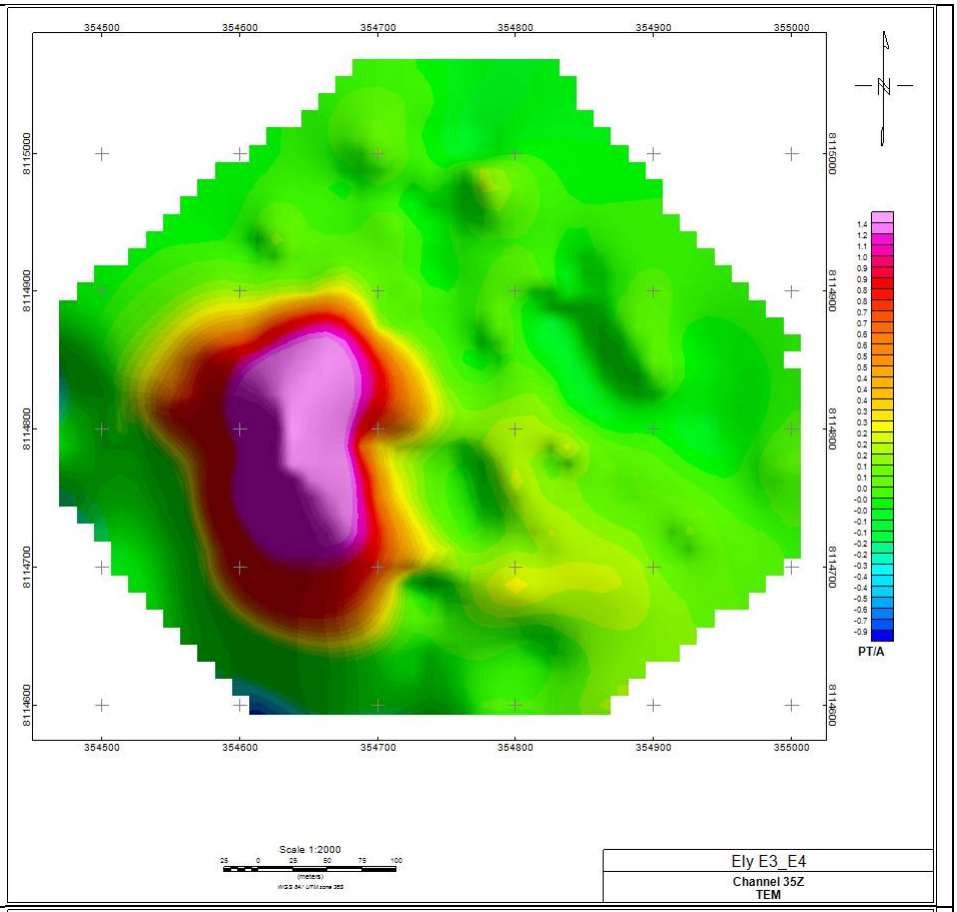

Channel 39Z

Channel 39 Z-component, the last channel, was gridded. The conductive zone on the eastern side is no longer evident. The western conductive zone is still clearly expressed, indicating a strong conductor potentially reflecting a massive sulphide accumulation beneath the E1/E2 anomaly.

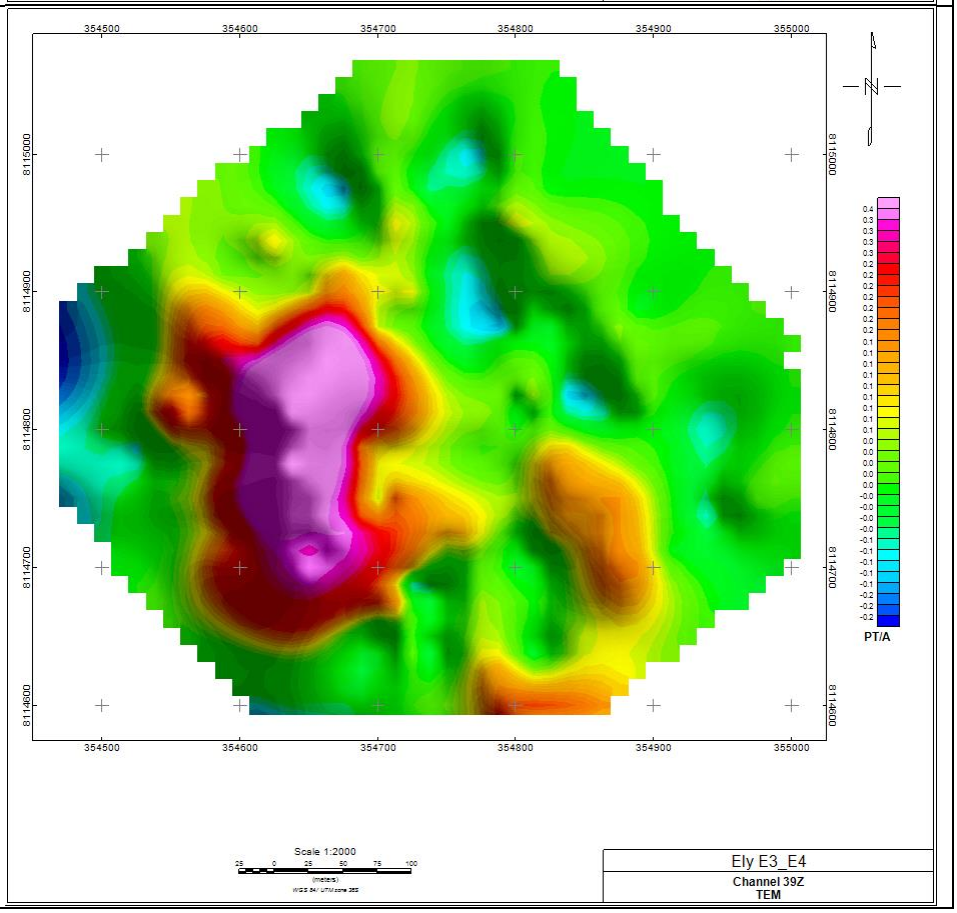

4.5 EM Plate Modelling in Maxwell Software

Two lines of the MLEM survey were selected for modelling using Maxwell Software developed by EMIT. These were Line 1150 and Line 1250, which transect the western E1/E2 and eastern E3/E4 conductive zones respectively. Modelling of these lines show plates dipping steeply to the northeast at between 58° and 67° from the horizontal. Figure 22 shows the location map of the modelled lines 1150 and 1250 plotted over the Channel 25Z gridded image at Ely.

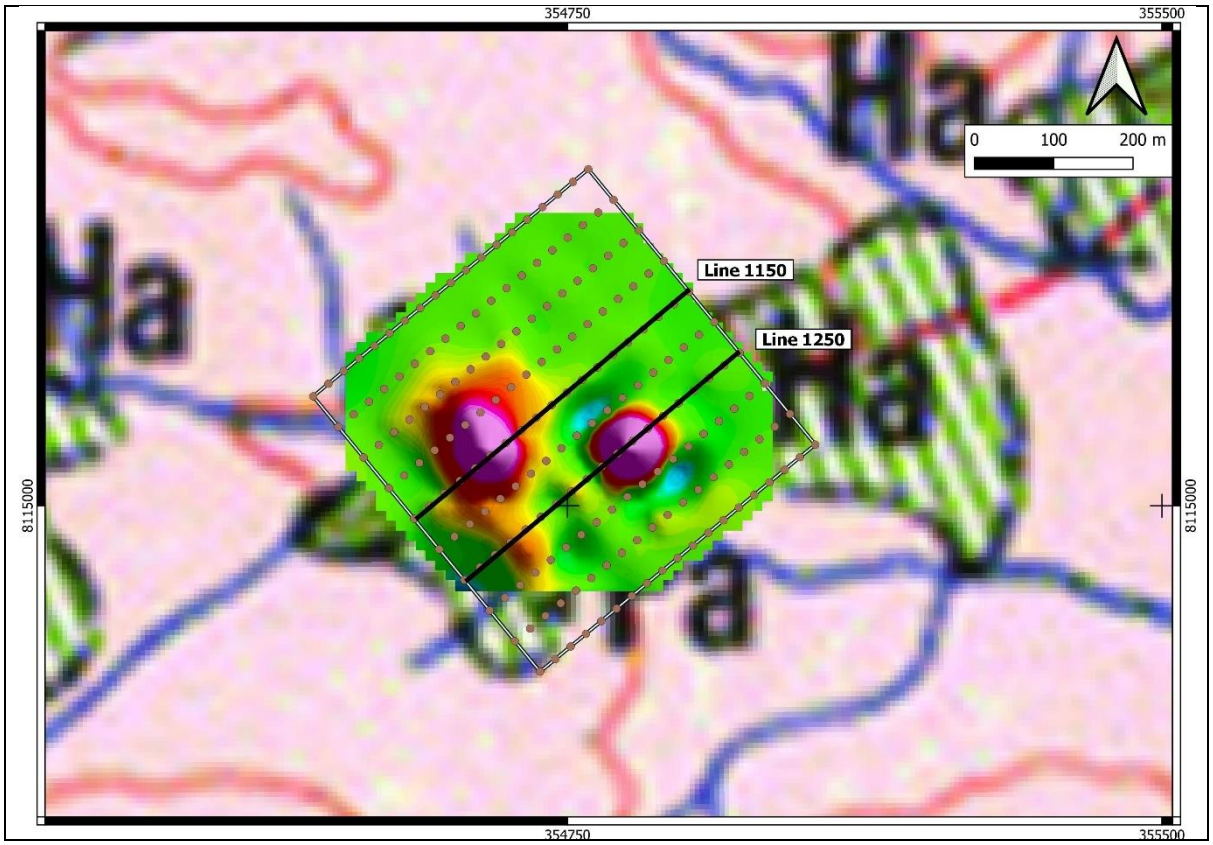

Figure 22: Location map showing the positions of the two modelled lines of MLEM data at the Ely survey grid.

4.5.1 Line 1150 Modelling over E1/E2 zone

Modelling of Line 1150, which is aligned northeast southwest over the E1/E2 conductive zone, shows a thin EM plate dipping steeply to the northeast at 67°. The depth to the top of the bedrock conductor is modelled at 26m. Channels 20 to 29, recording the mid to late time responses, were modelled. A conductivity thickness of 300S was calculated. Figure 23 compares the TMI magnetic profile (a) over the E1/E2 negative magnetic anomaly, with (b) and (c) displaying the modelled MLEM results from Line 1150 over the E1/E2 conductive zone.

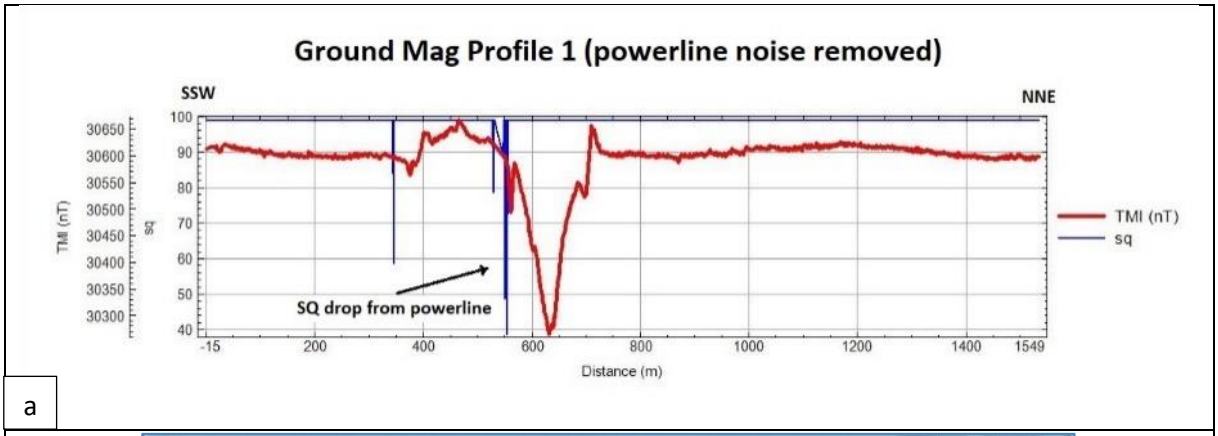
Ground Mag Profile 1 (powerline noise removed)
SSW
NNE
TMI (nT)
sq
SQ drop from powerline
Distance (m)
TMI (nT)
sq

a

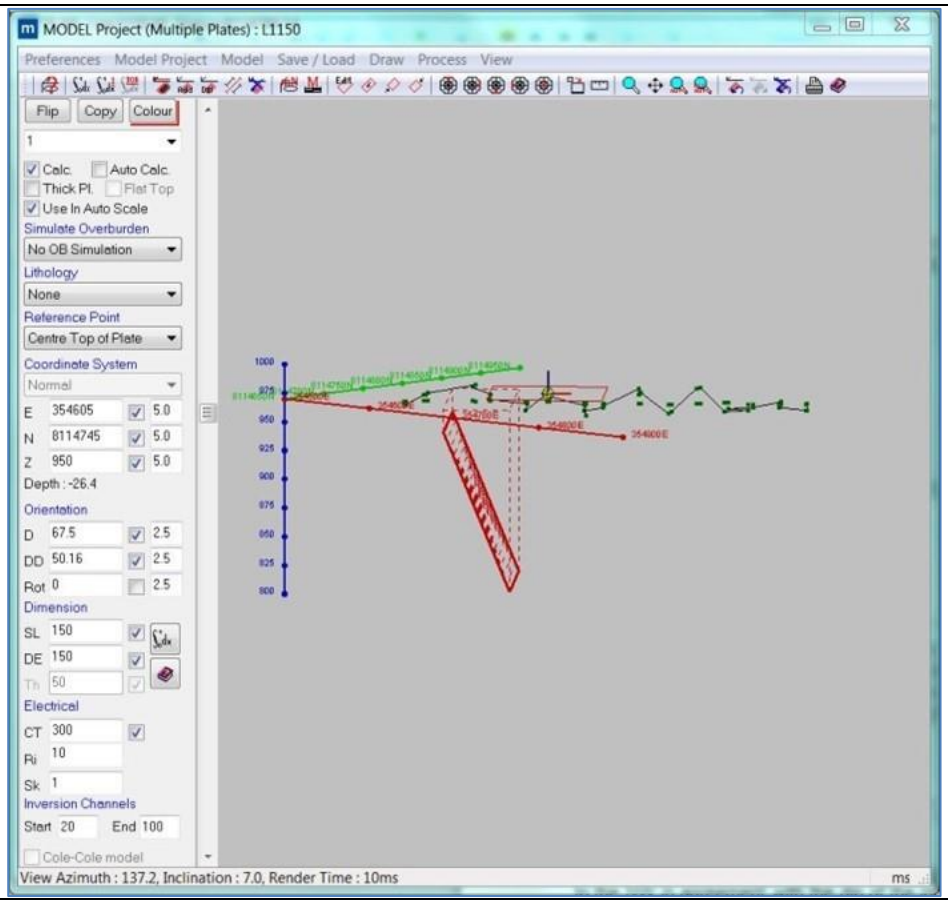
MODEL Project (Multiple Plates) : L1150
Preferences Model Project Model Save / Load Draw Process View
Flip Copy Colour
Calc. Auto Calc.
Thick Pl. Flat Top
Use In Auto Scale
Simulate Overburden
No OB Simulation
Lithology
None
Reference Point
Centre Top of Plate
Coordinate System
Normal
E 354605 5.0
N 8114745 5.0
Z 950 5.0
Depth : -26.4
Orientation
D 67.5 2.5
DD 50.16 2.5
Rot 0 2.5
Dimension
SL 150
DE 150
Th 50
Electrical
CT 300
Ri 10
Sk 1
Inversion Channels
Start 20 End 100
Cole-Cole model
View Azimuth : 137.2, Inclination : 7.0, Render Time : 10ms
ms

b

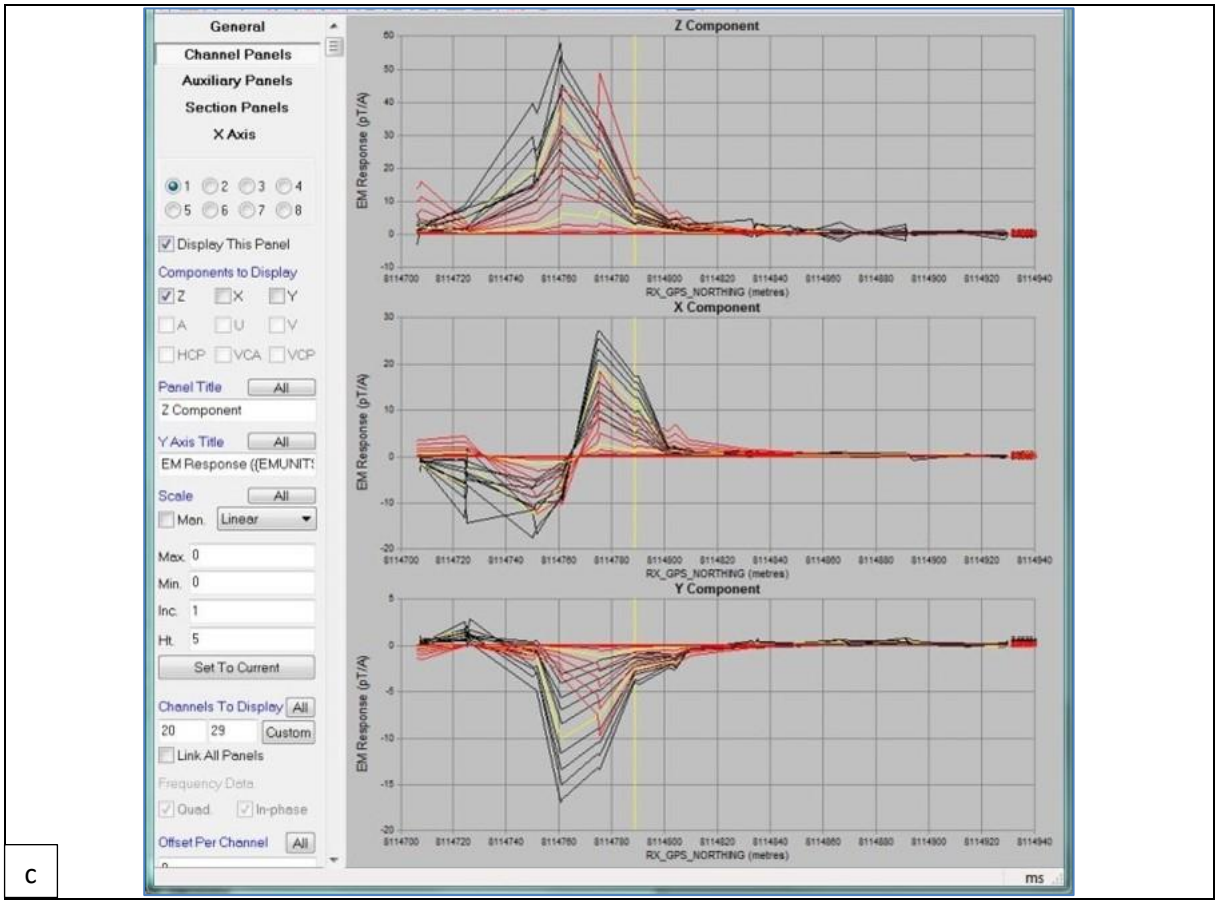

c

Figure 23: Comparison of magnetic Profile 1 with modelling results for Line 1150 and comparison with TMI magnetic profile: (a) shows the TMI magnetic profile over the coincident negative magnetic anomaly at E1/E2; (b) shows the modelled EM plate dipping at 67˚ to the northwest, with the top of the conductor at a depth of about 26m; and (c) shows the measured EM response traces in black and the modelled EM response in red for the three components Z, X and Y respectively. Note the magnetic profile line and the MLEM survey line are not oriented in the same direction.

It is reiterated that the conductor is immediately to the east of an 11kV powerline running northeast to southwest through the Ely area, and that modelled results may be affected to some degree by noise emanating from the powerline. While the modelled plate produces a reasonable fit in the early times, the fit for the E1/E2 conductor in the late times is not particularly good, and the model requires adjustment to produce a better fit. Despite this, the spatial correlation between the negative magnetic anomaly and the strong EM conductor at E1/E2 is clearly evident.

4.5.2 Line 1250 Modelling over E3/E4 zone

Line 1250 passes directly over the eastern conductive zone above the E3/E4 anomaly and was modelled in Maxwell Software. The modelled results show a thin EM plate dipping 58˚ to the northeast. The modelled depth to the top of the bedrock conductor is 24m. Channels 15 to 24 representing the mid to late time responses were modelled. A conductivity thickness of 800S was calculated. Figure 24 compares the TMI magnetic profile (a) over the E3/E4 negative magnetic anomaly to (b) and (c) displaying the modelled results for Line 1250 over the E3/E4 anomaly:

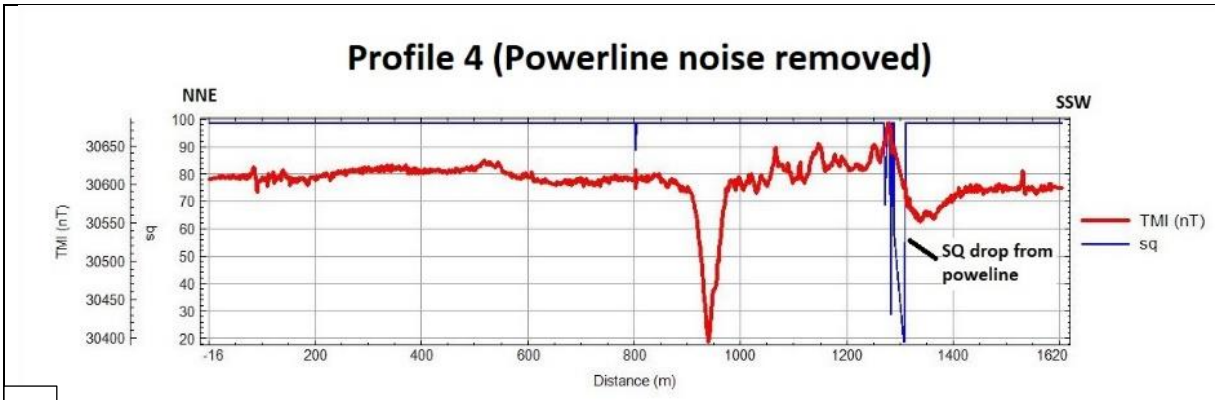
Profile 4 (Powerline noise removed)
NNE
SSW
TMI (nT)
sq
Distance (m)
SQ drop from poweline
TMI (nT)
sq

a

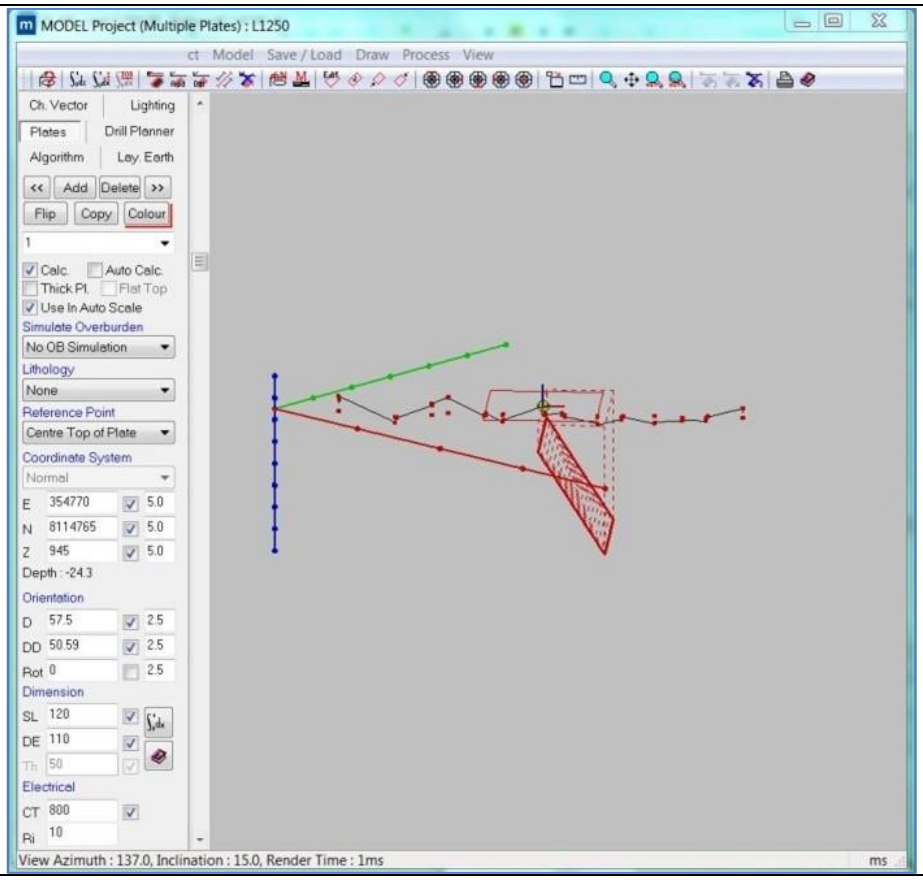
MODEL Project (Multiple Plates) : L1250
ct Model Save / Load Draw Process View
Ch. Vector
Lighting
Plates
Drill Planner
Algorithm
Lay. Earth
Add
Delete
Flip
Copy
Colour
Calc.
Auto Calc.
Thick Pl.
Flat Top
Use In Auto Scale
Simulate Overburden
No OB Simulation
Lithology
None
Reference Point
Centre Top of Plate
Coordinate System
Normal
E 354770
N 8114765
Z 945
Depth : -24.3
Orientation
D 57.5
DD 50.59
Rot 0
Dimension
SL 120
DE 110
Th 50
Electrical
CT 800
Pi 10
View Azimuth : 137.0, Inclination : 15.0, Render Time : 1ms
ms

b

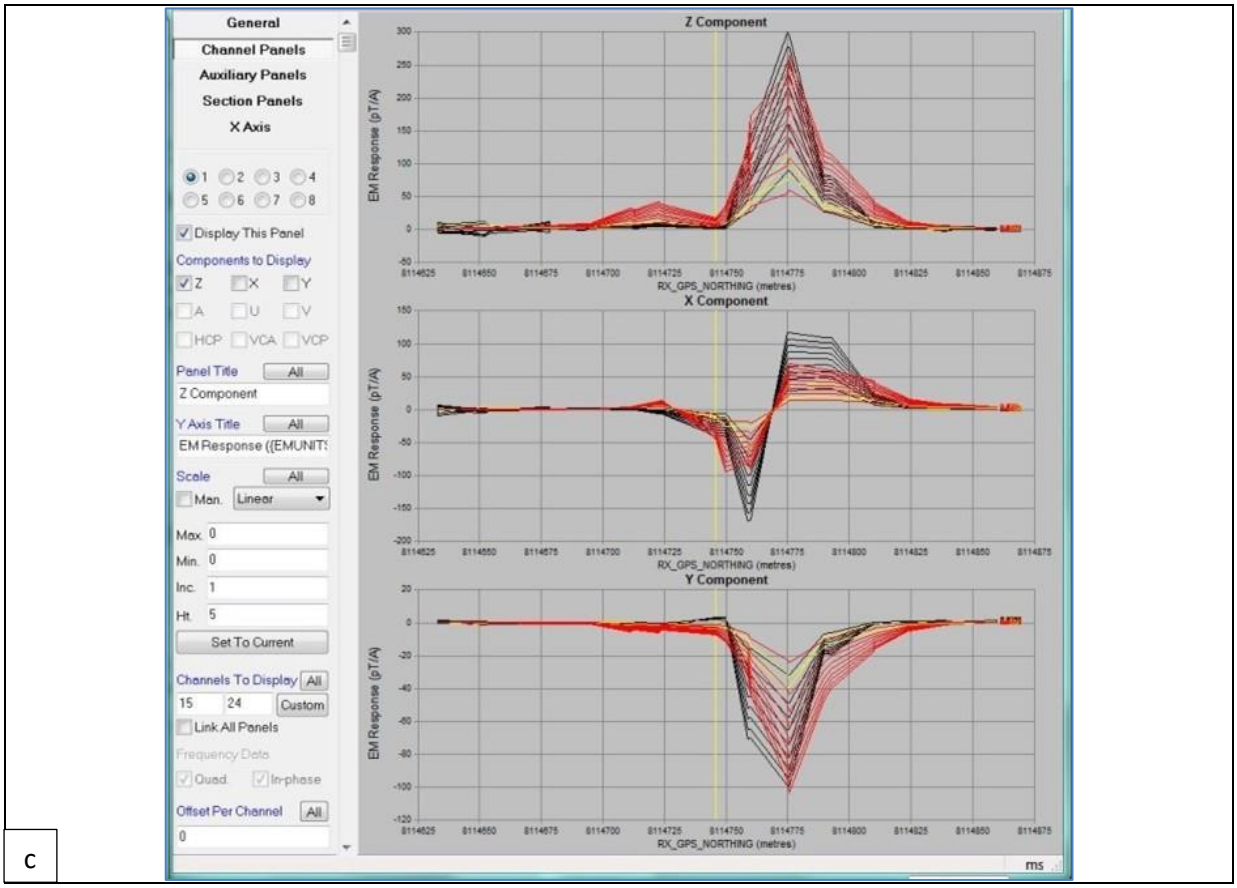

c

Figure 24: Modelling results for Line 1250 and comparison with TMI magnetic profile: (a) shows the TMI magnetic profile over the coincident negative magnetic anomaly at E3/E4; (b) shows the modelled EM plate view from the south; and (c) depicts the measured EM response traces in black and the modelled EM response in red for the three components Z, X and Y.

As is the case for the E1/E2 anomaly, the E3/E4 conductor coincides spatially with the negative magnetic anomaly delineated at E3/E4, as shown in Figure 24 (a) of TMI Profile 4. In both the magnetic and conductivity responses, the E1/E2 anomaly appears to be the more conductive of the two zones, which is an interesting finding considering that the 1960's drilling of the E1/E2 target intersected only weak mineralisation in one drill hole, while the drillholes targeting E3/E4 soil geochemistry anomaly, intersected significant nickel and copper grades.

In summary, the MLEM survey at Ely delineated two highly conductive zones, each coinciding spatially with historical soil geochemical anomalies which were drilled by Anglo American in the 1960s. The two prominent negative magnetic anomalies identified in the recently completed ground magnetic survey over Ely, are located over the same two zones of conductivity and anomalous nickel and copper in soil. The following section of this report examines and discusses these results in greater detail.

5. Discussion and interpretation

The physical property measurements carried out on the drill core samples from Madziwa were intended to assist in characterising the different lithologies at Madziwa and their likely responses in terms of the geophysical surveys executed at the Ely prospect. In general terms, measurable differences in magnetic susceptibility are due to differences in a variety of factors, including but not limited to, the shape and orientation of magnetic minerals, the presence or absence of remnant magnetism, and the volumetric content of magnetic minerals which can exhibit any of three types of magnetic behaviour: diamagnetism, paramagnetism and ferromagnetism (Dentith and Mudge, 2014). The paramagnetic minerals are mineral species which exhibit varying magnitudes of magnetic susceptibility which will affect the magnetic signature of their host rock depending on their relative modal abundance. The two most important mineral species in the Madziwa suite of rocks with significant susceptibility are likely to be magnetite and monoclinic pyrrhotite, both of which are ferromagnetic (Dentith and Mudge, 2014). Importantly, these two minerals often preserve remnant magnetism. Magnetite tends to occur in ultramafic rock compositions as a primary mineral and as a secondary mineral from serpentinization of olivine. It is thus quite likely to be present in a much larger modal abundance in the pyroxenites than in the norites or diorites at Madziwa. Pyrrhotite is the main sulphide species in the Madziwa ore bodies, with the nickel and copper carried in interstitial pentlandite and chalcopyrite (Prendergast and Wilson, 2015). Paramagnetic minerals, including olivine, pyroxene, amphibole, garnet and mica, tend to have weak but still potentially significant, positive susceptibilities, but no remnant magnetism (Dentith and Mudge, 2014).

The gneissic country rock, the norite and leuconorite all produced similar magnetic susceptibility values averaging between 1.7×10^{-3} SI and 2.05×10^{-3} SI. This would suggest that the tonalitic gneissic country rock is largely indistinguishable in terms of its magnetic signature from the norites, diorites and leuconorites of the Madziwa Complex. Since all the known orebodies at Madziwa occur within or very close to the margins of pyroxenite bodies, this may be quite an important and useful characteristic in terms of mapping the pyroxenite bodies and identifying prospective areas for mineralisation. It may serve to narrow the search space for mineralisation from the more extensive combined areas of mafic and ultramafic bodies as currently mapped, to only the magnetically mapped pyroxenites and their immediate surrounds.

The magnetic susceptibility values of the barren and weakly mineralised pyroxenite samples averaged between 1.26×10^{-3} SI and 1.39×10^{-3} SI. These figures are lower than expected, given that pyroxenites tend to have higher, though overlapping, average ranges of susceptibility relative to norites, gabbros and rocks with granitic compositions (Dentith and Mudge, 2014). It apparently also contradicts the observed positive magnetic anomalies that coincide spatially at Ely (and the wider Madziwa area), with the field mapped and ground-truthed pyroxenite bodies. The coherent positive magnetic anomalies identified in the TMI and RTP products agree well with the mapped pyroxenite bodies as presented in Prendergast and Wilson (2015), as shown in Figure 5. It is the author's opinion that the magnetic susceptibility measurements of the barren pyroxenite are therefore not representative, and that the evidence from both the airborne CIDA and ground magnetic survey supports the contention that pyroxenites produce a strong magnetic response and are thus well delineated by magnetic survey results.

Dolerites in the Madziwa area, belonging to the 1.8 Ga Mashonaland Dolerite suite, produce strong magnetic susceptibility values averaging around 58 x 10^{-3} SI. Though none are mapped in the immediate vicinity of the Ely prospect, this is a useful observation for the greater area. The massive sulphide bearing pyroxenite drill core sample produced an average magnetic susceptibility of 68 x 10^{-3} SI, an order of magnitude higher that the other rock types at Ely. This is a significant result with respect to the pronounced negative magnetic anomalies over the known mineralisation and soil geochemical anomalies at E1/E2, E3/E4 and E5 zones.

The massive sulphide sample is also the only sample to exhibit positive conductivity with an average value of 6001 S/m. This conductivity response from a sample of massive sulphide is the enabling property for the successful direct detection of mineralisation using the electromagnetic method. Equally noteworthy is that the sample containing disseminated sulphides produced no measurable conductivity response. This has negative implications for the ability of the electromagnetic method to detect disseminated sulphide concentrations.

It is evident from a comparison of the regional CIDA airborne magnetic survey results with the more detailed ground magnetic survey results, that a well-designed, correctly oriented ground magnetic survey, with adequately spaced lines, is valuable for mapping structure and magnetically prominent bedrock features such as the pyroxenite intrusive bodies at prospect scale. The positions, areal extent and intrusive relationships of the ultramafic igneous bodies are well expressed in the ground magnetic survey plots of TMI, RTP, AS and 1VD. Two major faults, previously mapped and shown in Prendergast and Wilson's (2015) simplified geology in Figure 2 and Figure 5, are also well defined in the TMI and 1VD maps by linear zones of low TMI. Figure 25 shows the interpreted faults, cultural noise from powerline and interpreted lithological boundaries of significant magnetic features on the RTP map of the Ely grid.

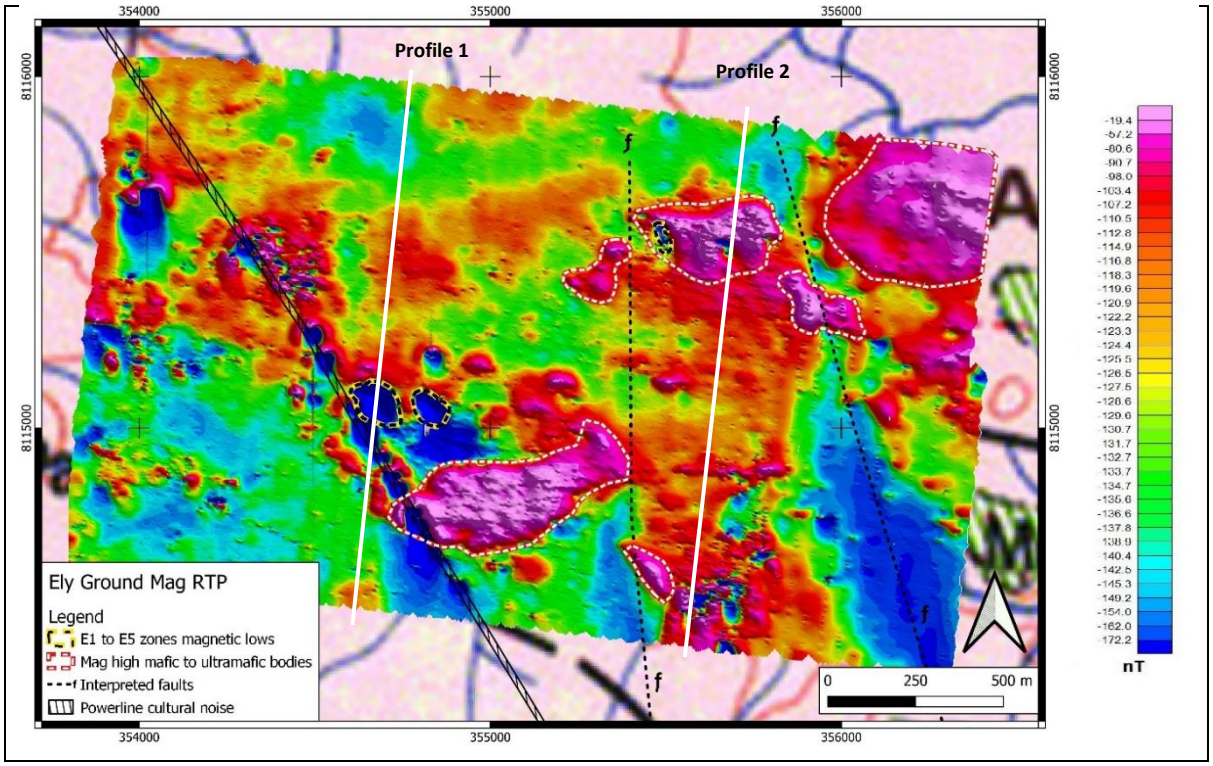

Figure 25: RTP map of Ely with anotations showing the powerline, interpreted faults and outlines of significant magnetic bodies.

The anomalous zones at E1/E2 and E3/E4 show up quite distinctly in the various magnetic enhancements as distinct magnetic “lows”. These negative magnetic anomalies are each consistently registered across multiple lines. The negative magnetic signatures may indicate that the mineralised zones preserve remnant magnetism, a common property for sulphide bodies rich in monoclinic pyrrhotite (Dentith et al., 1994). If present, the remnant magnetism in the sulphide bodies may effectively be cancelling out the induced magnetism of the earth’s magnetic field with differently oriented magnetic field lines, resulting in the observed negative magnetic anomalies.

A much smaller and narrower negative magnetic anomaly, expressed in only a single line of data, appears to be coincident with the historical E5 mineralised zone. It is, by comparison with the E1/E2 and E3/E4 anomalies much smaller in magnitude and spatial extent. Historical grades and drill log descriptions of sulphide mineralisation intersected at E5 by diamond drillholes indicate that the mineralisation is low grade (averaging around 0.47% nickel, with a maximum grade of 0.88% nickel) and disseminated, compared to that intersected at E3/E4. A lower concentration of total sulphides could proportionately influence the magnetic properties of the mineralised zone at E5 and hence its potential to produce a pronounced magnetic anomaly similar to those observed at E1/E2 and E3/E4.

Figure 26 (a) shows the RTP image with black box outline showing the extent of the zoomed in RTP map in Figure 26 (b) of the E1/E2 and E3/E4 anomalies. Figure 26 (b) shows the annotated and georeferenced historical 1:1000 Prospecting Ventures map (previously presented in Figure 5b) overlaid on the RTP map, clearly showing the two negative magnetic anomalies coinciding spatially with the historical soil geochemistry anomalies and drilling E1/E2 and E3/E4 zones.

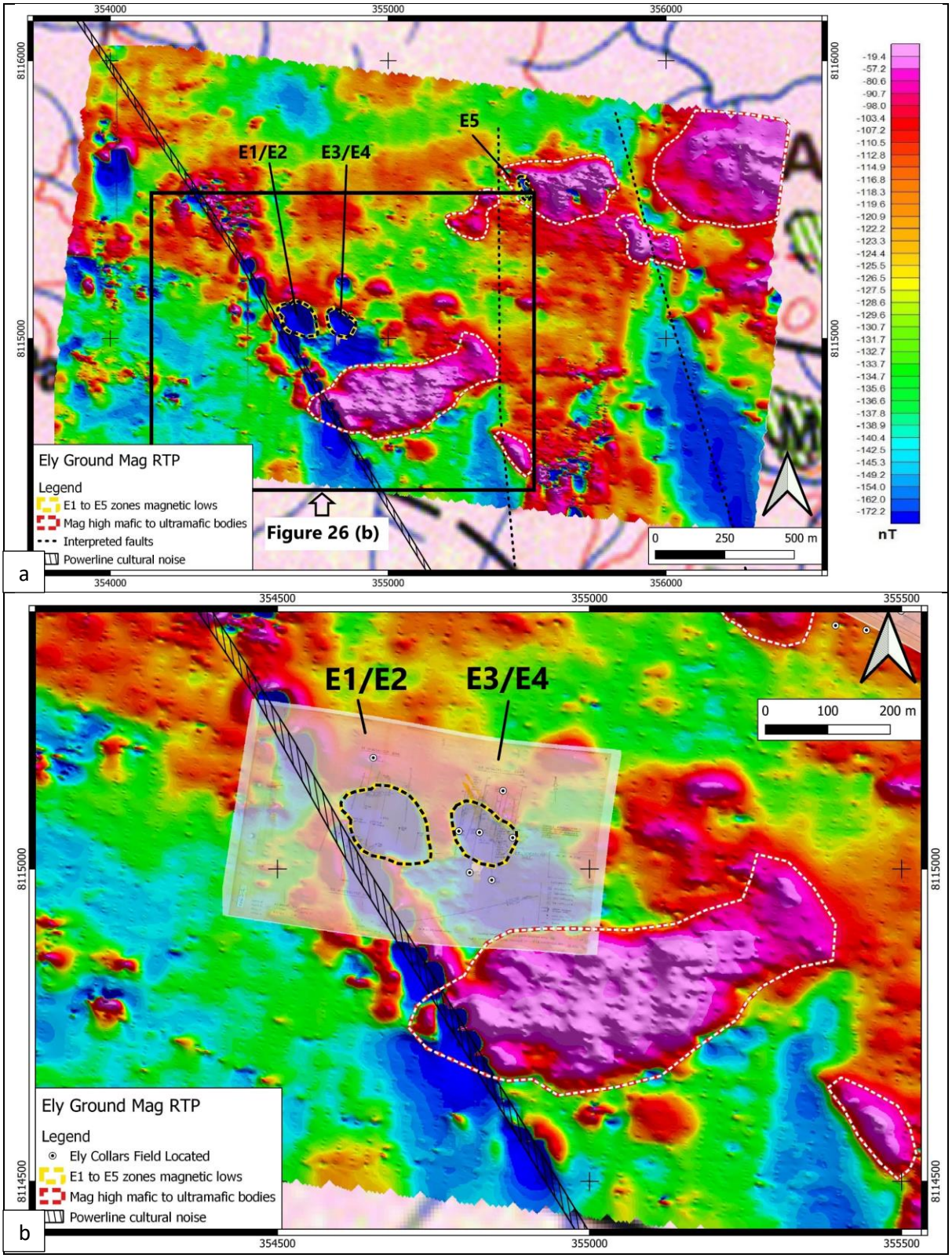

Figure 26: Annotated RTP map (a) showing position of zoomed in area in (b); (b) zoomed in RTP with transparent overlay of georeferenced 1:1000 historical geochemsitry and drilling map from Anglo American reports with anomalies coinciding well with the distinct negative magnetic anomalies registered by the 2021 ground magnetic survey results. Note that the colour scale is the same as for (a).

The E1/E2 negative magnetic anomaly shown in the RTP image is approximately 125m north to south by 115m east to west in its dimensions. The E3/E4 negative magnetic anomaly is smaller with dimensions of 75m north to south by 90m east to west.

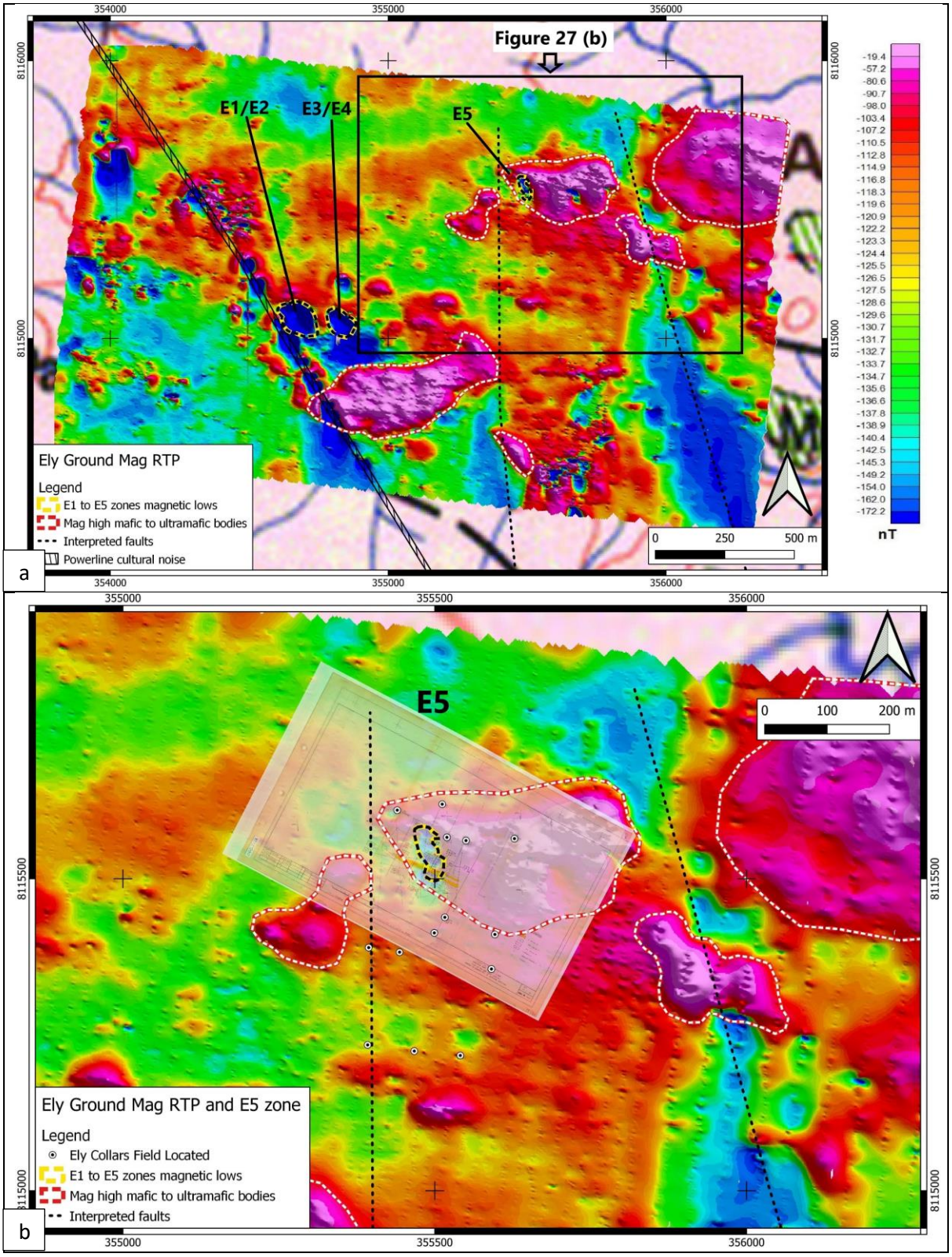

Figure 27: (a) Annotated RTP map with black box outline showing the extent of the RTP map in (b); (b) RTP image zoomed in over E5 zone with georeferenced map of soil geochemistry and drilled mineralisation at E5 from historical Anglo American reports. Note that the RTP colour scale is the same as for Figure 26 (a).

Figure 27 (a) shows the RTP image with black box outline showing the extent of the zoomed-in area depicted in Figure 27 (b). Figure 27 (b) shows the annotated RTP map over the E5 area with the

superimposed, transparent 1:1000 Prospecting Ventures map (first presented in Figure 5c) of soil geochemistry anomaly and historical drilling at E5.

The difference in degree of interconnectedness of the sulphide grains at the E1/E2 and E3/E4 zones, compared to that present at the E5 zone, may account for the difference in magnitude of magnetic signature. In most geological settings favourable to hosting orthomagmatic nickel sulphide deposits, sulphide mineralisation is not usually directly detectable by the magnetic method (Dentith, Francomb and Trench, 1994). The magnetic signature of the sulphide mineralised body is usually too small to be distinguished from that of the surrounding host rock, often featuring highly magnetic ultramafic rocks with abundant magnetite in serpentine, which tend to overwhelm any distinct magnetic signatures emanating from sulphide bodies (Peters and Buck, 2000).

Another factor which may contribute to the difference in observed magnetic signature of the different historical anomalies at Ely is that the mineralised zones at E1/E2 and E3/E4 are located approximately 100m to the north of the magnetic pyroxenite body and are therefore expressed more clearly as discrete anomalies. In contrast, the E5 body is mapped historically as being located within the northeastern pyroxenite body close to its western margin. Its associated magnetic signature may be drowned out by the larger amplitude response of the enveloping pyroxenite body. Regardless, the E5 zone serves as useful reference point for comparison because of the number of historical drillholes drilled there and the potential of the recorded grades and intercept widths to provide insight into the nature of the sulphide mineralisation intersected. Anglo American Prospecting Ventures ultimately decided the E5 mineralised zone to be too small and low grade to justify further development in the mid-1990s (Prospecting Ventures Report, 1996).

The MLEM survey was successful in outlining two zones of strong conductivity at E1/E2 and E3/E4 which very closely overlap the spatial extents of the negative magnetic anomalies identified in the ground magnetic results presented and discussed above. The conductors are expressed from the early time response in Channel 15Z, all the way through the mid-time responses, and into the very late time response of Channel 39Z in the case of the western E1/E2 conductor. The eastern E3/E4 conductor by comparison starts to “fade out” from Channel 35Z onwards. Figure 28 shows the georeferenced MLEM gridded results overlaid on the RTP map at the E1/E2 and E3/E4 anomalies for (a) Channel 25Z, (b) Channel 30Z and (c) Channel 39Z.

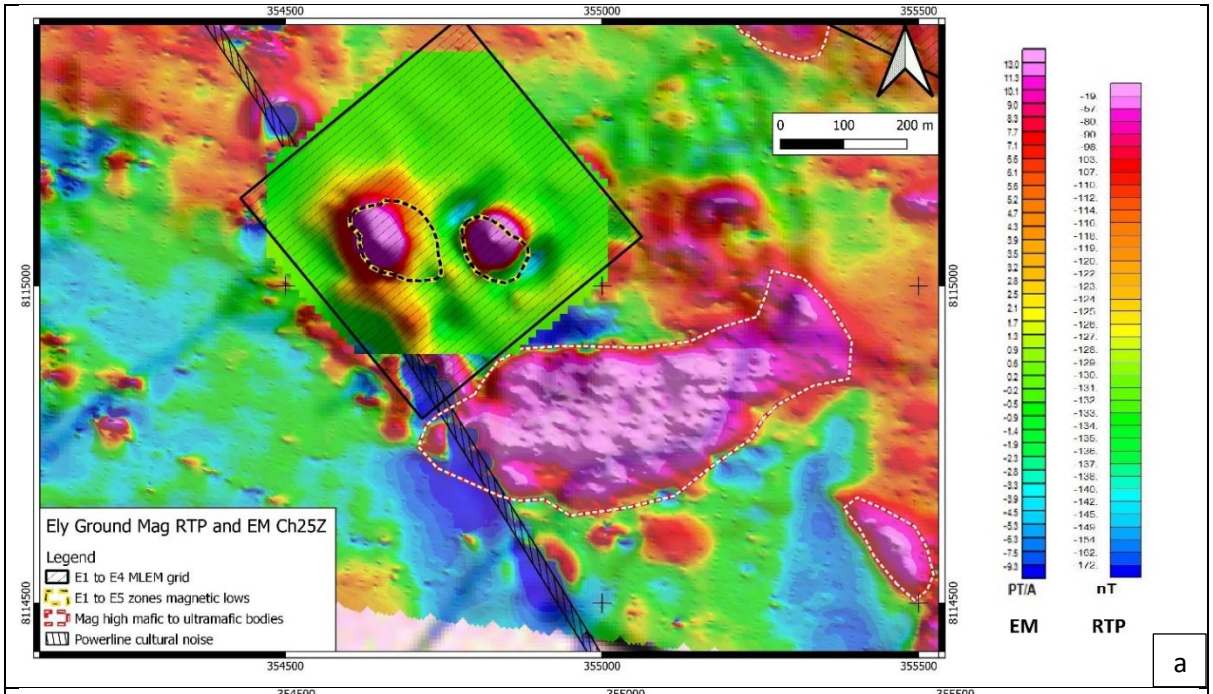
354500
355000
355500
8115000
8114500
0 100 200 m
Ely Ground Mag RTP and EM Ch25Z
Legend
E1 to E4 MLEM grid
E1 to E5 zones magnetic lows
Mag high mafic to ultramafic bodies
Powerline cultural noise
PT/A
nT
EM
RTP
a

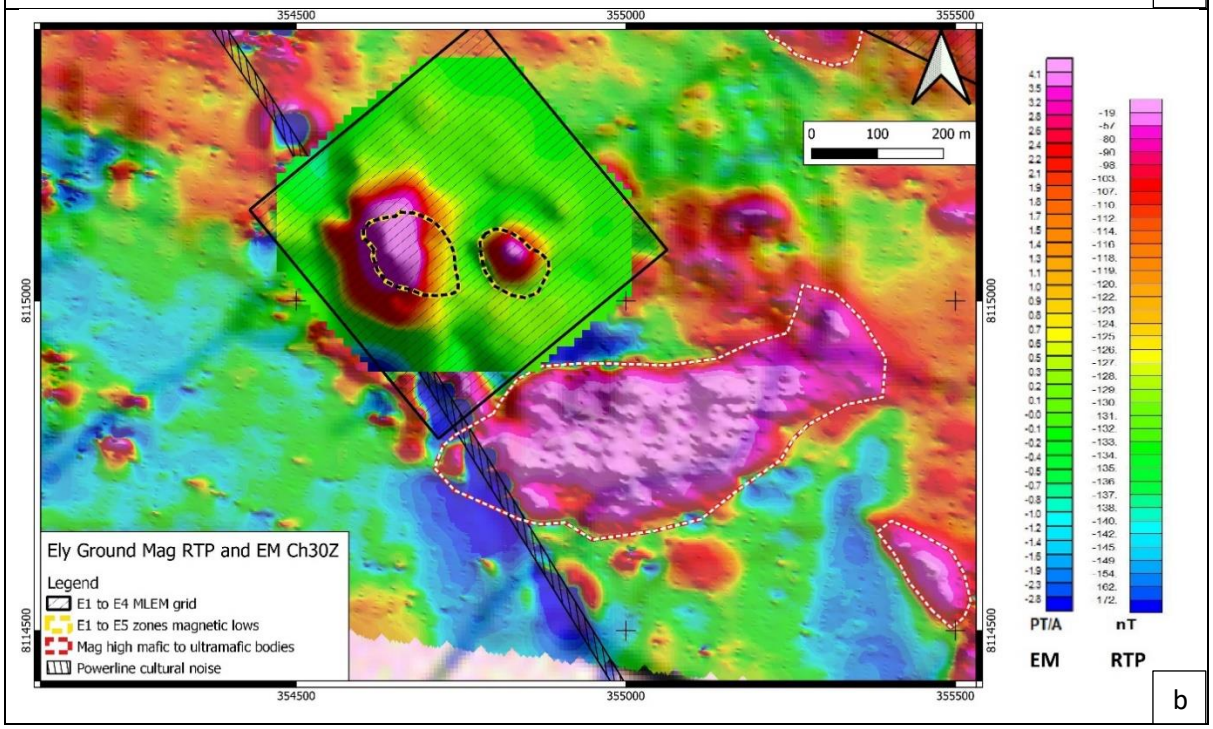
354500
355000
355500
8115000
8114500
0 100 200 m
Ely Ground Mag RTP and EM Ch30Z
Legend
E1 to E4 MLEM grid
E1 to E5 zones magnetic lows
Mag high mafic to ultramafic bodies
Powerline cultural noise
PT/A
nT
EM
RTP
b

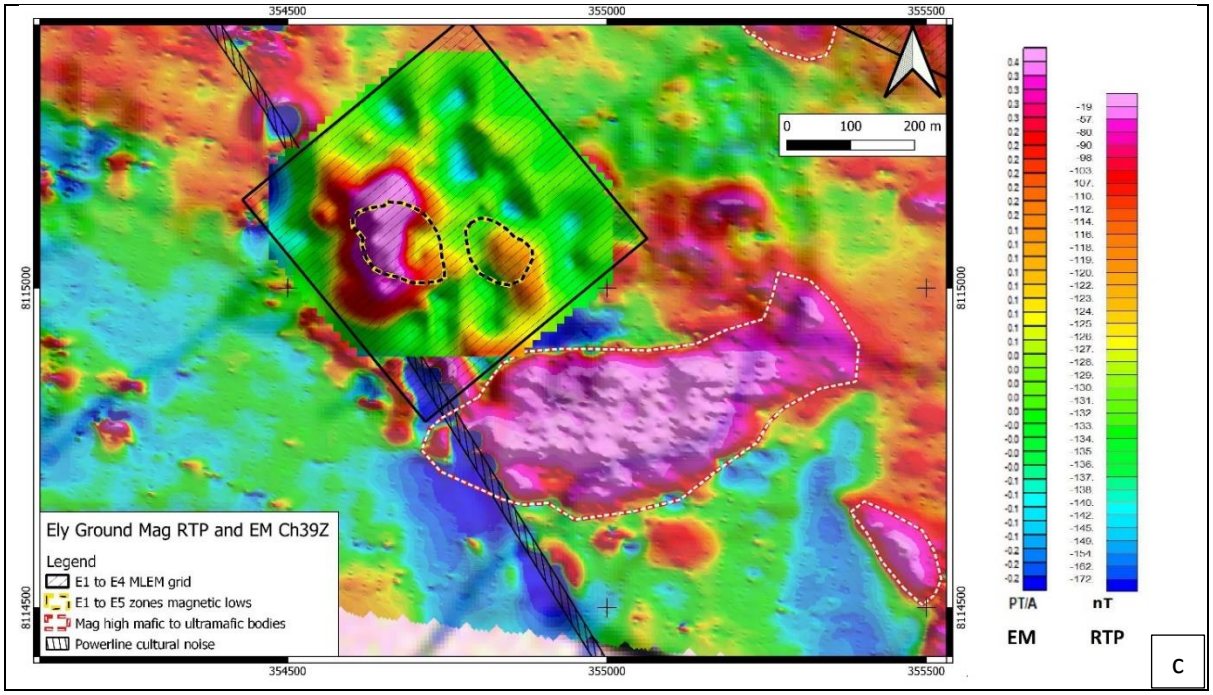

Figure 28: Gridded results of MLEM overlaid on RTP map showing (a) Channel 25Z, (b) Channel 30Z and (c) Channel 39Z. Note the strong spatial correlation of EM conductors with the annotated outlines of negative magnetic anomalies in RTP map.

The MLEM results show that there is a strong spatial correlation between the conductors expressed at both the western E1/E2 and eastern E3/E4 zones, with the annotated outlines of the negative magnetic anomalies delineated by the ground magnetic results. This suggests that the negative magnetic anomalies are indeed associated with sulphides responsible for the conductors observed. Modelling of the E1/E2 and E3/E4 zone conductors produced best fit models of plate conductors dipping moderately to steeply to the northeast. The E1/E2 modelled conductor has a similar strike extent to the original Sulphide Hill orebody. These models will inform future drilling. A MLEM survey remains to be carried out over the E5 zone. However, in view of the muted negative magnetic anomaly observed at E5 compared to those at E1/E2 and E3/E4, and the comparatively low grades and disseminated nature of the sulphides intersected by historical drilling at E5, it may be unlikely that a pronounced conductive response, such as those observed at E1/E2 and E3/E4 anomalies, will be observed.

Future Work on Ely and Madziwa

A limitation of this study was the lack of available drill core for physical property characterization. Lamentably, after mine closure Madziwa's core yard was looted and fell into severe disrepair, and no drill core logs were available for consultation. While care was taken to select representative samples of different lithologies for this study, it constitutes a very small, and therefore limited, dataset. Any future geophysical work on Ely and Madziwa should include a substantially larger selection of samples from each lithology and mineralisation style for petrography and the measurement of physical properties. This will allow a more robust characterisation of the different rock types and sulphide abundances in them, to inform the interpretation of the magnetic and electromagnetic datasets.

In addition, magnetic modelling of the high-quality ground magnetic data may prove useful in enhancing the EM modelling. It may assist in improving the modelling of EM data over Line 1150 where

the fit between modelled and measured data is not good in the late channels. Further modelling should be undertaken to try to resolve this misfit.

6. Conclusion

The physical property contrasts of the lithologies constituting the Madziwa Igneous Complex make it a favourable prospect for exploration using geophysical methods. There is no deep surficial cover, thick saprolitic profile or conductive saline ground water layer which typify prospective terrains in Western Australia and interfere with the ability to obtain clear geophysical signals from the bedrock lithologies. A detailed ground magnetic survey with closely spaced lines was able to map the extents of the ultramafic pyroxenites clearly. This alone would constitute a successful outcome for the geophysical exploration since the known orebodies at Madziwa all occur close to the margins of the pyroxenites, whether in contact with surrounding norites or enveloping gneisses.

The ground magnetic results from the Ely survey grid indicate that sulphide accumulations may be directly detectable in some instances using the magnetic method, characteristically showing up as distinct, circular to ellipse shaped, negative magnetic anomalies. Evidence is presented that the negative magnetic anomalies are spatially correlated to nickel copper sulphide mineralisation at Ely in the form of mapped historical soil geochemical anomalies, gossan occurrences, trenching and drilling results at the E1/E2 and E3/E4 magnetic anomalies. This correlation is further supported by the subsequent results of the moving loop EM survey, which identified two highly conductive zones spatially coincident with the negative magnetic anomalies. Drilling of these two modelled conductors remains to be carried out to confirm conclusively the presence of nickel copper sulphide bodies as the source of these conductors and negative magnetic anomalies. Further research would include a more extensive sample base for physical property measurements, as well as an attempt at magnetic modelling and refinement of the EM modelling, as these efforts would contribute to a better understanding of the source of the geophysical signatures in the Madziwa area.

7. Bibliography

Birch, G. J., 1985. Petrology of the Madziwa Mafic Intrusion Zimbabwe. Unpublished PhD Thesis. Imperial College of Science and Technology, University of London.

Chimimba, L. R., 1986. The Madziwa nickel-copper deposits, Zimbabwe, in Anheusser, C. R., and Maske, S., (eds)., Mineral deposits of Southern Africa, vol. 1.: Johannesburg, Geological Society of South Africa, pp. 237–241.

Craven, B., Rovira, T., Grammer, T., and Styles, M., 2000. *Exploration Geophysics*. **31**, pp. 201-209.

Davies, R.S., Davies, M.J., Groves, D., Davids, K., Brymer, E., Trench, A., Sykes, J. P., and Dentith, M., 2021. Learning and Expertise in Mineral Exploration Decision-Making: An Ecological Dynamics Perspective. *International Journal of Environmental Research and Public Health*. 18, 9752.

Dentith, M. C., Francombe, K. F., and Trench, A. 1994. Geophysical Signatures of Western Australian Mineral Deposits: An Overview. Exploration Geophysics, **25**, pp. 103.

Dentith, M. C., and Mudge, S. T., 2014. *Geophysics for the Mineral Exploration Geoscientist*, Cambridge University Press, Cambridge.

Gewald, H., 1974. The Mineralization at Madziwa Mines Rhodesia. Unpublished PhD Thesis. University of London.

GDD Instruments, 2024. MPP Probe. Available at https://www.gddinstruments.com/mpp-probe. (Accessed: October 2024)

King, A., 2007. 'Review of Geophysical Technology for Ni-Cu-PGE deposits', in B Milkereit (ed.), *Plenary Session: Ore Deposits and Exploration Technology.* In "Proceedings of Exploration 07: Fifth Decennial International Conference on Mineral Exploration", pp. 647-665.

McCall, L. M., Dentith, M. C., Li, Z. X., and Trench, A. 1995. The magnetic signature of komatiitic peridotite-hosted nickel sulphide deposits in the Widgiemooltha area, Western Australia. *Exploration Geophysics*, **26**, pp. 66-77.

Peters, B., and Buck, P., 2000. The Maggie Hays and Emily Ann nickel deposits, Western Australia: A geophysical case study. *Exploration Geophysics*, **31**, pp. 210-221.

Prendergast, M. D, and Wilson, A. H., 2015. The Nickeliferous Archean Madziwa Igneous Complex, Northern Zimbabwe: Petrological Evolution, Magmatic Architecture, and Ore Genesis. *Economic Geology*, 110, pp. 1295-1312.

Prendergast, M. D. (1996). Prospecting Ventures Report. Monthly Progress Report. Anglo American Corporation.

Prospecting Ventures Report, 1968. Internal Company Report. Anglo American Corporation.

Stidolph, P. A., 1977. The geology of the country around Shamva. Geological Survey of Zimbabwe, Bulletin No. 78.

Trench, A., and Williams, P. K., 1994. Nickel: Application of geophysics to nickel sulphide exploration in the Kambalda district, Western Australia. Geophysical Signatures of Western Australian Mineral Deposits, Geology and Geophysics Department and UWA Extension, The University of Western Australia, Publication no. 26, pp. 169-179.

Ushendibaba, M., 2016. Using electromagnetic methods to map and delineate high-grade harzburgite pods within the Ni-Cu mineralised Jacomynspan ultramafic sill, Northen Cape, South Africa. MSc Dissertation. University of Witwatersrand, Johannesburg.